

SUPPORTING INFORMATION

Probing the Existence of a Metastable Binding Site at the β_2 -Adrenergic Receptor with Homobivalent Bitopic Ligands

Birgit I. Gaiser,^{a,†} Mia Danielsen,^{a,†} Emil Marcher-Rørsted,[†] Kira Røpke Jørgensen, Tomasz M. Wróbel,^{†,‡} Mikael Frykman,[†] Henrik Johansson,[†] Hans Bräuner-Osborne,[†] David E. Gloriam,[†] Jesper Mosolff Mathiesen,^{*,b,†} Daniel Sejer Pedersen^{*,b,†}

[†] Department of Drug Design and Pharmacology, University of Copenhagen, Jagtvej 162, 2100 Copenhagen (Denmark)

[‡] Department of Synthesis and Chemical Technology of Pharmaceutical Substances, Faculty of Pharmacy, Medical University of Lublin, 4A Chodźki, 20093 Lublin, Poland

^a These authors contributed equally as first authors.

^b These authors contributed equally as principal investigators.

* Corresponding authors. JMM (pharmacology) jmm@sund.ku.dk. DSP (chemistry) daniel.pedersen@sund.ku.dk.

CONTENTS

1. Design	Page S3
1.1 Molecular Docking	Page S3
1.2 Protein and Ligand Preparation	Page S3
1.3 Ligand Docking	Page S5
1.4 Docking Post-Processing	Page S5
2. Pharmacology	Page S7
2.1 Data results and discussion	Page S7
2.1.1 Correlation between potency and affinity in membrane-based cAMP assay (Figure S1)	Page S7
2.1.2 Linker length and composition (Figure S2)	Page S7
2.1.3 β_2AR-selectivity of bitopic ligands (Figure S3)	Page S9
2.1.4 Kinetic binding experiments (Figure S4)	Page S10
2.2 Experimental methods	Page S13

2.2.1 Cell culturing	Page S13
2.2.2 Membrane preparation	Page S13
2.2.3 Membrane-based cAMP Time-Resolved (TR)-FRET assay	Page S13
2.2.4 Cell-based cAMP biosensor assay	Page S15
2.2.5 Radioligand saturation binding experiments	Page S16
2.2.6 Kinetic binding experiments	Page S17
2.2.7 Competition binding experiments to calculate ligand affinity of unlabeled ligands	Page S18
2.2.8 Competition binding experiments to determine kinetics and affinities of unlabeled ligands	Page S19
3. NMR and HPLC data	Page S20
4. References	Page S62

1 DESIGN

1.1 Molecular Docking

All computational work was performed with the Schrödinger 2015-1 small molecule drug dsi suite for Windows. The β_2 AR-ALP co-crystal structure (PDB file: 3NYA)¹ with a resolution of 3.1 Å was utilized to rationally design potential bitopic ligands.

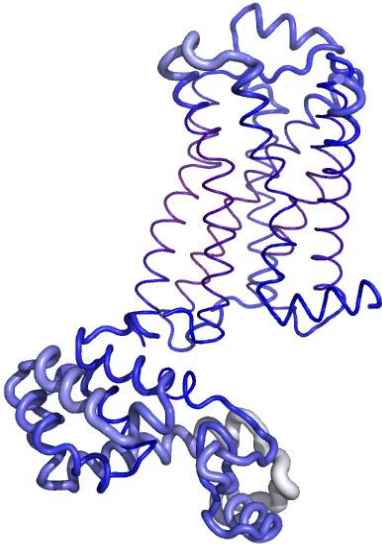
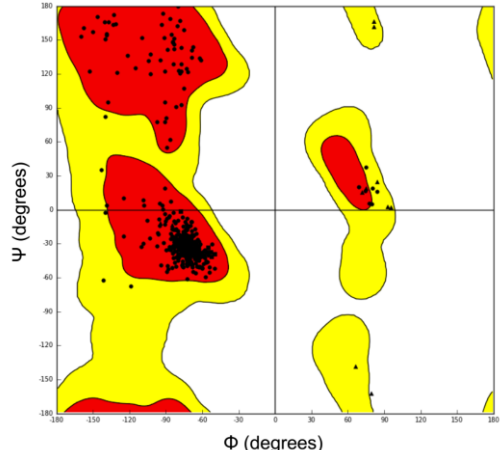
1.2 Protein and Ligand Preparation

Protein validation: Both the R factors and B values as well as the Ramachandran plot statistics reported for the β_2 AR-ALP co-crystal structure (PDB file: 3NYA)¹ were deemed useful for the dockings (Table S1).

Protein preparation: The protein was imported into the Schrödinger 2015-1 small molecule drug dsi suite for Windows and prepared using the Protein Preparation Wizard.² It was pre-processed to assign correct bond orders and add missing hydrogen atoms. Disulfide bonds were allowed to form and water molecules beyond 5 Å from the protein were removed. Hydrogen bonds were assigned after applying the Epik PROPKA function at pH 7.0. From the Asp300 rotamer library the carboxylate with an orientation towards MBS A was chosen (entry no. 3; 12% probability). During restrained minimization with the OPLS_2005 force field, heavy atoms were allowed to converge to a RMSD of 0.30 Å. The thus prepared structure was validated by means of its Ramachandran plot that showed no residues in disallowed regions (Table S1).

Table S1. Structure validation for the published β_2 -adrenergic receptor-alprenolol co-crystal structure (PDB: 3NYA) and the structure as prepared in the present project.

Published 3NYA structure ¹	
Resolution	3.1 Å
R _{work} /R _{free} (%)	23.3 / 28.8

<p>B factor putty</p> <p>(generated with PyMOL, command: spectrum b, red_blue_white, 3NYA)</p>	
<p>Ramachandran plot statistics (%):</p> <p>most favoured</p> <p>allowed</p> <p>disallowed</p>	<p>98.6</p> <p>1.4</p> <p>-</p>
<p>3NYA as prepared in the present project</p>	
<p>Ramachandran plot</p> <p>(generated with the Schrödinger 2015-1 small molecule drug dsi suite for Windows)</p>	

Ligand preparation: The ligand ALP and the bitopic ligands proposed within the present project were drawn in the 2D sketcher, and the corresponding 3D molecular models were generated with the LigPrep tool using the OPLS_2005 force field. The Epik software was used to predict the ligand protonation states at a target pH 7 ± 2 , and chiralities were retained. The thus prepared ligands were minimized.

1.3 Ligand Docking

Docking of ALP into the OBS: For docking into the OBS, a grid box around the crystallized ligand was created allowing ligands of $<8\text{\AA}$ length to dock. All rotational bonds of the receptor were regarded as being rigid. Using the Glide docking tool,³ ALP was docked into the prepared 3NYA structure with standard precision (SP). Ligand sampling was allowed to be flexible and included nitrogen inversions as well as ring conformations. Epik state penalties were included in the docking scores. On the output poses, post-docking minimization was performed. All poses were found to bind to the receptor in the same overall way as the crystallized ligand. Out of the poses with similar docking scores, the best ranked entry that at the same time was the one that matched best with the crystallized ligand as determined by visual inspection was chosen to proceed with.

Docking of ALP into MBS A: For docking into MBS A, a grid was generated from the protein containing the docked ALP in the OBS. A grid box around MBS A and large enough to cover the entire extracellular vestibule (i.e. allowing ligands with a length of $<17\text{\AA}$ to dock) with the coordinates $X = -30$, $Y = 0$ and $Z = 7$ was created. All rotational bonds of the receptor were regarded as being rigid. Using the Glide docking tool, ALP was docked with SP into the prepared 3NYA structure containing ALP in the orthosteric binding site. Ligand sampling was allowed to be flexible and included nitrogen inversions as well as ring conformations. Epik state penalties were included in the docking scores. On the output poses, post-docking minimization was performed.

Docking of bitopic ligands: For docking of the bitopic ligands, a grid box around the crystallized ligand and large enough to cover the entire extracellular half of the receptor (i.e. allowing ligands with a length of $<25\text{\AA}$ to dock) was created. All rotational bonds of the receptor were regarded as being rigid. Using the Glide docking tool, the bitopic ligands were docked with SP into the prepared 3NYA structure. Ligand sampling was allowed to be flexible and included nitrogen inversions as well as ring conformations. Epik state penalties were included in the docking scores. On the output poses, post-docking minimization was performed.

1.4 Docking Post-Processing

Conformational analysis: A conformational search was performed on the ALP output structures in the MBS using MacroModel and the OPLS_2005 force field. Torsional sampling

was applied in water as the solvent allowing for up to 3000 steps with 100 steps per rotatable bond and a maximum of 5000 iterations. For comparison, the conformational energy of the binding pose with the best docking score in the MBS was calculated. From the preferred conformation in water and the conformational energy of the binding conformation the conformational energy penalty of binding was calculated (Table S2) and found to lie within the range of moderately active (i.e. 5-13 kJ/mol). Thus, this docking pose was deemed useful for the design.

Table S2. Conformational energies of alprenolol in water and when docked into the metastable binding site, and the conformational energy penalty of binding, as calculated with MacroModel.

Preferred conformation in water	$E_{\text{pref}} = -178.7 \text{ kJ/mol}$
Conformational energy of binding conformation	$E_{\text{bind}} = -170.0 \text{ kJ/mol}$
Conformational energy penalty of binding	$\Delta E_{\text{conf}} = 8.7 \text{ kJ/mol}$

2 PHARMACOLOGY

2.1 Data results and discussion

2.1.1 Correlation between potency and affinity in membrane-based cAMP assay

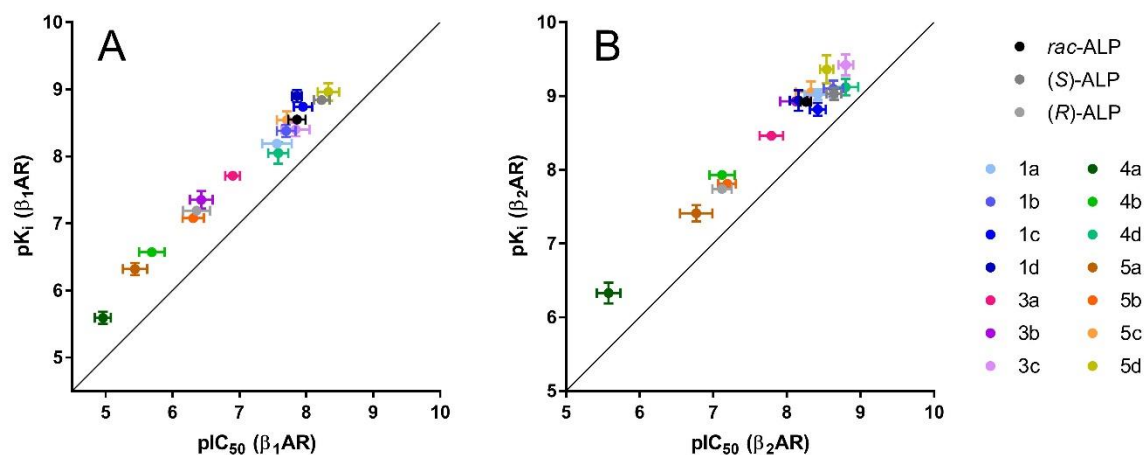


Figure S1. Potency (pIC₅₀) versus affinity (pK_i) plot at the β₁-adrenergic receptor (A) and the β₂-adrenergic receptor (B) for ligands tested at both receptor subtypes in the membrane-based cAMP assay and the radioligand equilibrium binding assay, respectively. There is a good correlation between potency and affinity.

2.1.2 Linker length and composition

Comparison of ligand potencies between the β₁AR and β₂AR in the different assays revealed a similar rank order for the urea (**3a-d**), diamide (**4a-f**) and triazole (**5a-d**) linked bitopic ligands (Figure 4 in main text). For these groups of ligands, a tendency for potency to increase with linker length was observed at both receptors. However, the potency was maintained or decreased with linker lengths longer than 11 atoms for the ureas (**3a-d**) and diamides (**4a-f**), respectively, whereas the triazole-linked ligands (**5a-d**) did not reach a plateau in potency. The most potent triazole linked ligands had 13 and 15 atom linkers (**5c-d**) and were one order of magnitude more potent than the two shortest triazole linked ligands (**5a-b**) that have 9 and 11 atom linkers, respectively. In contrast to the above-mentioned ligand groups, the all-carbon linked ligands (**1a-d**) had similar potencies for the shortest (6 atoms) and the longest (12 atoms) analogue, with potencies slightly below that of (S)-ALP. In preliminary experiments, (S)-ALP and selected bitopic ligands (**3c**, **4d**, **5d**), gave a Schild slope of approximately 1 in Schild plots (Figure S2) demonstrating a competitive mechanism of action. Ligand **1d**, in contrast, had a

Schild slope of around 1.6, which could reflect a different mechanism of action. However, the all-carbon linked ligands appeared to adhere to the plasticware used for the experiments (data not shown) and it is not clear if the lipophilic nature of this class of ligands affects their observed potencies and behavior. The more hydrophilic counterparts of the all-carbon linked ligands, i.e. the PEG linked ligands **2a** to **2b**, showed equipotency on both receptor subtypes, but were approximately one order of magnitude lower in potency than the all-carbon linked ligands.

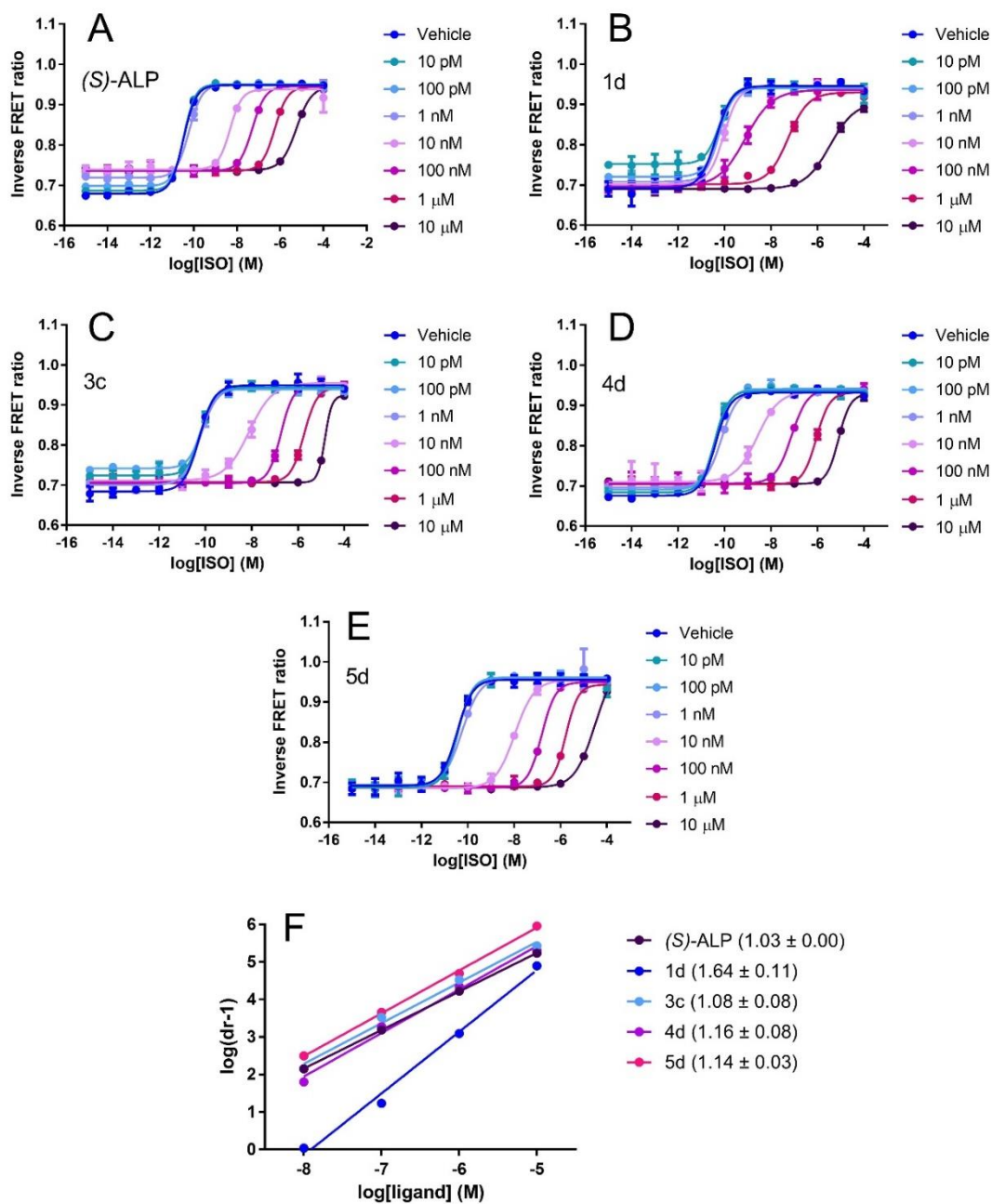


Figure S2. Preliminary data on modulation of the agonist response by (*S*)-ALP and selected bitopic ligands. With increasing concentrations of (*S*)-ALP and selected bitopic ligands, the potency of the agonist isoproterenol decreased in a parallel manner at the β_2 -adrenergic receptor when tested in the cell-based assay (Panels A-E). Conversion of data into Schild plots (Panel F) revealed a Schild slope of ~ 1 for all ligands except the all-carbon ligand **1d**, which had a Schild slope of ~ 1.6 .

As observed for the functional data, there was a tendency for the affinity to increase with increasing linker length (Table 3 in main text) for the urea (**3a-d**), diamide (**4a-f**) and triazole (**5a-d**) linked ligands, whereas no trends were observed for the all-carbon (**1a-d**) linked ligands.

Based on data from the membrane-based cAMP assay, the optimal linker length within each linker class varied from 7-15 atoms (Table 2, Figure 4B in main text). This covers a much broader range of linker lengths than the 9-11 atoms that were proposed during ligand design and could be the consequence of the differing degrees of flexibility of different linker types. In fact, the highly flexible all-carbon and PEG linked ligands (**1a-d**, **2a** and **2b**) were most potent when the linkers were 8 (**1b**) or 7 (**2a**) atoms, respectively. For the more rigid urea, however, potency peaked for a linker of 11 atoms (**3c**), while the most rigid linker classes, i.e. the diamide and triazole ligands, had their most potent representatives at linker lengths of 12 (**4d**) and 15 atoms (**5d**), respectively. The longest triazole ligand **5d** was at the same time the most potent in this linker class, and thus, it needs to be considered that longer triazole analogues could potentially display even higher potencies. When counting the number of rotatable bonds in each linker type as a measure for its flexibility, the most potent representatives of each linker class have nine (**1b**), eight (**2a**), eight (**3c**), eleven (**4d**) and twelve (**5d**) rotatable bonds in the linker. Consequently, data indicate that a minimum of eight rotatable bonds in the linker are required for symmetric bitopic ALP ligands to adopt a conformation that allows good simultaneous binding to the OBS and MBS.

2.1.3 β_2 AR-selectivity of bitopic ligands

A selectivity plot based on ligand affinities in the competition binding assay (Figure S3A) showed that (*S*)-ALP is slightly more selective at the β_2 AR compared to the β_1 AR. This is confirmed by its selectivity ratio (K_i at β_1 AR/ K_i at β_2 AR) of 1.55 corresponding to approximately a 0.5-fold difference (Table 3 in main text). A slight increase in β_2 AR-selectivity

was most pronounced for the urea **3b** followed by the diamide **4b**, the diamide **4d**, and the triazole **5a**. No increased β_2 AR selectivity was apparent for the all-carbon and the PEG linked ligands.

Because of the good correlation between the potencies and affinities of the bitopic ligands, a selectivity plot based on ligand potencies in the membrane-based cAMP assay was generated as well (Figure S3B). From the potency-based selectivity ratios (IC_{50} at β_1 AR/ IC_{50} at β_2 AR) the ligands **3b**, **3c**, **4b-d**, **4f**, and the (*R,R*)-**4d** appeared to be the most β_2 AR-selective ligands.

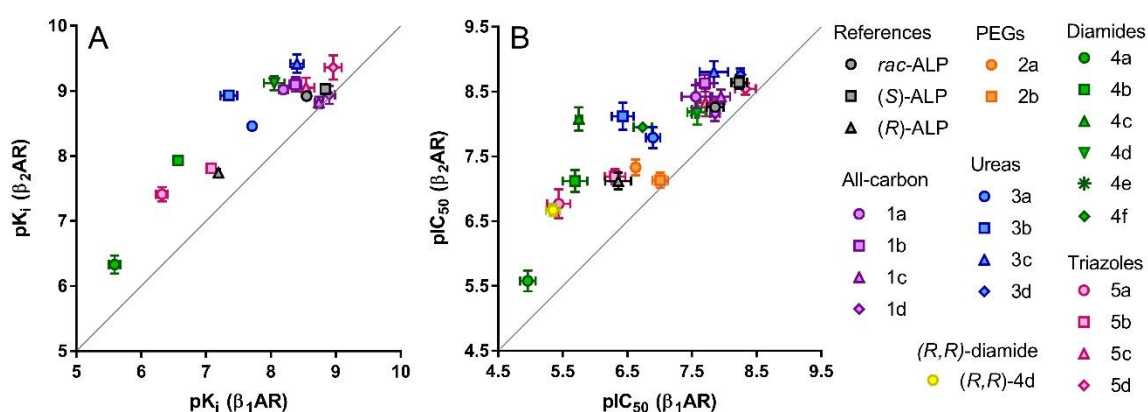


Figure S3. Selectivity plots for (*rac*)-, (*R*)- and (*S*)-ALP and all bitopic ligands tested in the competition binding assay (A) and the cAMP TR-FRET assay (mean potencies) (B). Data represents mean \pm S.E.M. from 3-8 independent experiments carried out in duplicate.

2.1.4 Kinetic binding experiments

Kinetic binding experiments were carried out using 3 H-DHA, and dissociation experiments gave a radioligand dissociation rate (k_{off}) of $0.0588 \pm 0.0042 \text{ min}^{-1}$ (Figure S4A). The observed association rate (k_{obs}) was determined in association experiments and gave an association rate (k_{on}) of $9.95 \pm 0.83 \times 10^7 \text{ M}^{-1} \text{ min}^{-1}$ (Figure S4B). From the k_{on} and k_{off} , an equilibrium binding constant (k_D) was calculated to 0.59 nM. Global fitting of the association data to obtain a single best-fit calculation of the kinetic parameters resulted in a k_{on} of $8.79 \pm 0.45 \times 10^7 \text{ M}^{-1} \text{ min}^{-1}$, a k_{off} of $0.0843 \pm 0.0168 \text{ min}^{-1}$ and a k_D of $0.969 \pm 0.200 \text{ nM}$, which fits well with the values determined using the method originally described by Motulsky *et al.*³⁵ Plotting k_{obs} against the radioligand concentration furthermore confirmed the Law of Mass Action with a $R^2 = 0.9487$ (Figure S4C). The slope of $1.01 \pm 0.01 \times 10^8 \text{ M}^{-1} \text{ min}^{-1}$ and the y-intercept of 0.0217 ± 0.0186

min^{-1} , which optimally equals k_{on} and k_{off} , respectively, resulted in a k_{D} of 0.2148 nM. Finally, the k_{D} of $^3\text{H-DHA}$ determined in saturation experiments used for the equilibrium binding experiments was determined to 0.39 nM (data not shown). Taken together, the determined kinetics for $^3\text{H-DHA}$ are in agreement among the different experiments and calculation methods as well as with values published by others.³⁶⁻³⁸

Optimal $^3\text{H-DHA}$ binding curve separation was achieved at different concentrations of the unlabeled ligands ranging from 1-12 times their K_{i} values (Figure 6 in main text). The complete data set, however, revealed that the degree of binding curve separation had no influence on the calculated kinetic parameters. This is likely due to the use of three concentrations of unlabeled ligand in each experiment. Hence, all data were included in the final data set.

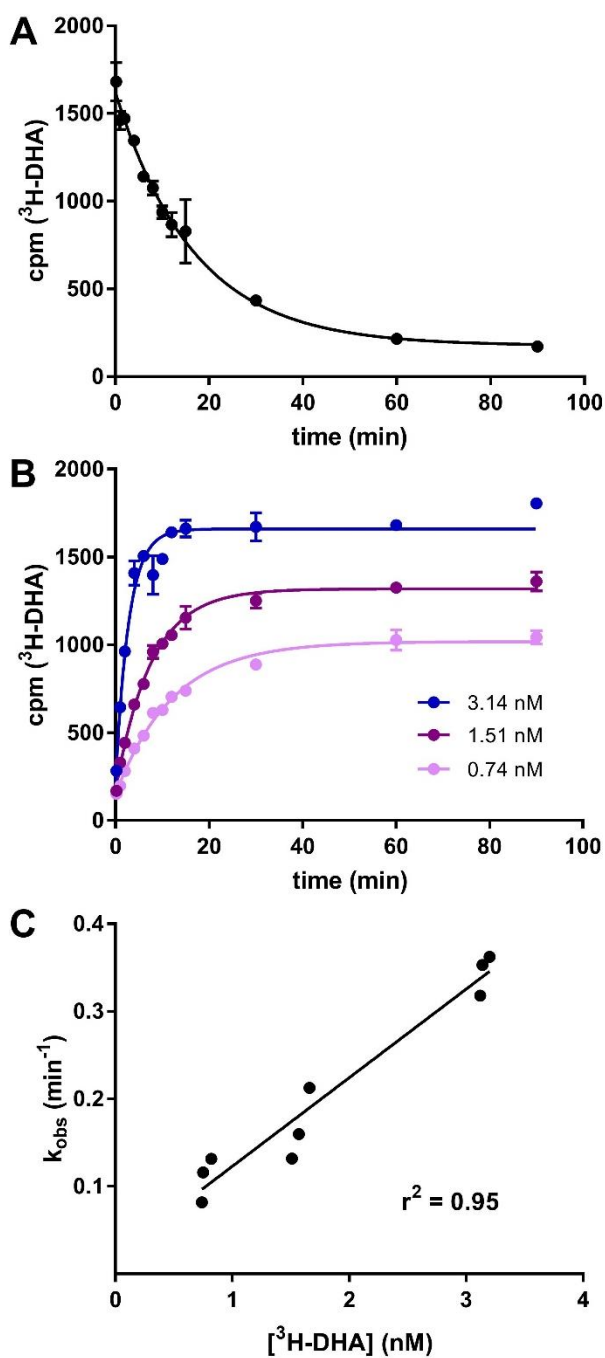


Figure S4. Kinetic binding experiments for ^3H -dihydroalprenolol ($^3\text{H-DHA}$) at the β_2 -adrenergic receptor ($\beta_2\text{AR}$). $^3\text{H-DHA}$ dissociation (A) and association (B). Plotting of k_{obs} as a function of $^3\text{H-DHA}$ concentration confirmed the Law of Mass Action as revealed by the linear correlation with a $r^2 = 0.95$. Data represents mean \pm SD from one representative dissociation (A) and association (B) out of three independent experiments carried out in duplicate, whereas (C) is based on mean values.

2.2 EXPERIMENTAL METHODS

2.2.1 Cell culturing

Two HEK293 cell lines stably overexpressing either the β_1 AR or the β_2 AR^{33,34} were cultured in Dulbecco's Modified Eagle's Medium with 4.5 g/L D-glucose, 1% pyruvate, 5% Fetal Bovine Serum (FBS), 1% Non-Essential Amino Acids, 1% Penicillin/Streptomycin and 1% G418 at 37 °C with 5% CO₂. The medium for the β_2 AR HEK293 cell line also contained 50 μ g/mL Zeocin. All materials were purchased from Gibco®, ThermoFisher.

2.2.2 Membrane preparation

HEK293 cells overexpressing the β_1 AR or the β_2 AR^{33,34} described in *Cell culturing* were grown to near confluence, washed once with phosphate-buffered saline (PBS) (no Ca²⁺, no Mg²⁺) and detached using PBS (no Ca²⁺, no Mg²⁺) supplemented with 2 mM EDTA. The combined cell suspensions were centrifuged at 2,000 rounds per min (rpm) for 5 minutes (5804R, Eppendorf). The resulting cell pellet was re-suspended in lysis buffer (10 mM Tris pH 7.5 supplemented with 1 mM EDTA and protease inhibitors (cOmplete Protease Inhibitor Cocktail Tablets, Roche Diagnostics GmbH)) and left on ice for 5 min to complete cell lysis. The lysate was homogenized by 50 strokes using a tight glass douncer and centrifuged at 1,500 rpm for 10 min (5804R, Eppendorf). The supernatant was isolated and centrifuged at 18,000 rpm for 20 min at 4 °C (Avanti J-25, Beckman). The resulting pellet was re-suspended in membrane buffer (Hank's Buffered Salt Solution (HBSS) with 20 mM 4-(2-hydroxyethyl)piperazine-1-ethanesulfonic acid, *N*-(2-hydroxyethyl)piperazine-*N'*-(2-ethanesulfonic acid) (HEPES) pH 7.4 and protease inhibitors (cOmplete Protease Inhibitor Cocktail Tablets, Roche Diagnostics GmbH)). The membrane suspension was frozen in aliquots of 150 μ L at -80°C.

2.2.3 Membrane-based cAMP Time-Resolved (TR)-FRET assay

Membrane buffer (HBSS supplemented with 1 mM CaCl₂, 1 mM MgCl₂, 20 mM HEPES pH 7.4 and 0.1% Bovine Serum Albumin (BSA)), agonist buffer (membrane buffer supplemented with 0.02% ascorbic acid, 9 mM MgCl₂, 250 μ M 3-isobutyl-1-methylxanthine (IBMX), 100 μ M adenosine-5'-triphosphate (ATP) and 10 μ M guanosine-5'-triphosphate (GTP)) (in 3 \times final concentration) and antagonist buffer (membrane buffer with 0.0025% polyoxyethylene (20) sorbitan monolaurate (Tween-20)) (in 3 \times final concentration) were prepared. All buffer

reagents were purchased from Sigma-Aldrich. ISO ((-)-isoproterenol (+)-bitartrate salt, Sigma-Aldrich) solutions were prepared in agonist buffer (in 3×final concentration). Ligand solutions were prepared in antagonist buffer (in 3×final concentration) with 1% DMSO (3×final concentration). Membranes described in *Membrane preparation* from the β_1 AR- or β_2 AR-overexpressing HEK293 cell lines were thawed and diluted to an appropriate concentration in membrane buffer with 40-50 strokes by use of tight douncer to make a homogeneous membrane suspension. To test for agonistic behavior of the ligands, 5 μ L agonist buffer (no ISO), 5 μ L ligand solution and 5 μ L membrane suspension were incubated for 30 min before terminating the assay and reading the plate on an Envision Multimode Plate Reader. To test for antagonistic behavior of the ligands, an ISO concentration-response curve was prepared in agonist buffer. 5 μ L agonist solution, 5 μ L antagonist buffer (no ligand) and 5 μ L membrane suspension were incubated for 30 min before terminating the assay and reading the plate on an Envision Multimode Plate Reader. Based on the ISO concentration-response curve, an ISO EC₈₀ solution (in 3×final concentration) was prepared. 5 μ L antagonist solution was pre-incubated with 5 μ L membrane suspension for 15 min followed by addition of 5 μ L ISO solution. The plate was incubated for 30 min before terminating the assay and reading the plate on an Envision Multimode Plate Reader. All incubations were carried out at room temperature. Shortly before terminating the assay, cAMP-d2 and anti-cAMP solutions were prepared and added to the plate according to the manufacture's protocol (CisBio cAMP G_s dynamic kit catalogue number 62AM4PEC). To terminate the assay and quantify cAMP levels, 5 μ L cAMP-d2 followed by 5 μ L anti-cAMP were added to the plate, which was incubated for 60 min and then read on an Envision Multimode Plate Reader. The Envision settings were top mirror LANCE/DELFI (barcode 412), excitation filter for Eu³⁺: UV2 (TRF) 340 nm (barcode 101), emission filter for d2: APC 665 nm (barcode 205) and emission filter for Eu³⁺: Europium 615 nm (barcode 203).

Concentration-response curves and inhibition curves from the cAMP TR-FRET assay were fitted using the non-linear regression *log(inhibitor) vs. response - variable slope (four parameters)* function in GraphPad Prism:

$$R = R_{\min} + \frac{(R_{\max} - R_{\min})}{1 + 10^{(\log(\text{IC}_{50} - x) \cdot n_H)}}$$

Where R is the response, R_{min} is the minimum response, R_{max} is the maximum response, IC₅₀ is the ligand concentration that inhibits half of the agonist response, and n_H is the Hill slope corresponding to the steepness of the curve.

Ligand potencies did not differ when ISO was used in concentrations within its EC₄₀-EC₉₀.

2.2.4 Cell-based cAMP biosensor assay

Confluent or nearly confluent β_2 AR-overexpressing HEK293 cells described in *Cell culturing* were washed once with PBS (no Ca²⁺, no Mg²⁺), detached using trypsin-EDTA and diluted in growth medium to a concentration of 300,000 cells/mL. 100 μ L of the cell suspension was added to each well of a Poly-D-Lysine-coated 96 well clear bottom plates (Corning) making the final concentration 30,000 cells/well. The plates were incubated for 16-24 hours at 37 °C with 5% CO₂.

The next day, buffer (HBSS supplemented with 1 mM CaCl₂, 1 mM MgCl₂, 20 mM HEPES pH 7.4 and 0.1% BSA) was prepared. All solutions were prepared in this buffer. The medium was removed from the cells and they were washed once with 100 μ L buffer. Initially, an ISO ((-)-isoproterenol (+)-bitartrate salt, Sigma-Aldrich) concentration-response curve was generated. 100 μ L buffer with 1% DMSO (in 2 \times final concentration) and 100 μ L ISO solution (in 2 \times final concentration) were added to the cells. The plate was incubated for 15 min in dark and read on an Envision Multimode Plate Reader. Next, an ISO EC₈₀ solution (in 2 \times final concentration) and ligand solutions (in 4 \times final concentration) with 1% DMSO (in 4 \times final concentration) were prepared. The cells were washed once with 100 μ L buffer followed by addition of 50 μ L buffer and 50 μ L ligand solution. The plate was incubated at room temperature for 15 min in dark and read on an Envision Multimode Plate Reader to test for agonistic behavior. Next, 100 μ L of the ISO solution was added and the plate was incubated for 15 min at room temperature and read on the Envision Multimode Plate Reader to test for antagonistic behavior. All incubations were carried out at room temperature. The Envision settings were top mirror CFP/YFP (barcode 428), excitation filter for CFP: CFP 430 nm (barcode 138), emission filter for CFP: CFP 470 nm (barcode 240) and emission filter for YFP: YFP 535 nm (barcode 274).

Concentration-response curves and inhibition curves from the cell-based cAMP biosensor assay were fitted similar to data from the cAMP TR-FRET assay. Ligand potencies did not differ when ISO was used in concentrations within its EC₆₀-EC₉₀.

2.2.5 Radioligand saturation binding experiments

All radioligand binding experiments were carried out using membranes described in *Membrane preparation* and binding buffer (HBSS supplemented with 1 mM MgCl₂, 20 mM HEPES pH 7.43 and 0.1% BSA) with a final DMSO concentration of 1% in 96-deep well plates. The radioligand ³H-dihydroalprenolol (³H-DHA) (dihydroalprenolol hydrochloride, Levo-[ring, propyl-³H(N)], 91.3 Ci/mmol or 97.1 Ci/mmol, PerkinElmer) were used in all binding experiments.

Membranes were thawed and diluted to an appropriate concentration in binding buffer with 40-50 strokes by use of a tight douncer to make a homogeneous membrane suspension. 100 μL buffer, 25 μL membrane suspension, and 25 μL ³H-DHA solution in concentrations ranging from 5 pM to 12 nM (in 6× final concentration) were added to 96-well deep well plates in the written order and incubated for 90 min at room temperature on a plate shaker at 500 rpm. Non-specific binding of ³H-DHA was determined in presence of 10 μM ALP. Membrane bound ³H-DHA was separated from unbound ³H-DHA by rapid vacuum filtration onto a 96-well harvester (PerkinElmer) onto GF/B Unifilter 96-well plates (UniFilter® white microplates with bonded GF/B filter, PerkinElmer) followed by 2-3 washes with cold binding buffer (total of 2.5 mL). The plates were dried at 50 °C for 45-60 min followed by addition of 40 μL microscint-0 (PerkinElmer) and measurement of radioactivity on a MicroBeta2 Counter (PerkinElmer). To determine the exact concentration of ³H-DHA used in the experiments, 100 μL ³H-DHA solution was added to pony vials with 3 mL Ultima Gold (PerkinElmer) and counted on a Tri-Carb 2800R Liquid Scintillation Analyzer (PerkinElmer). Data was fitted using the *One site - Total and nonspecific binding* function in GraphPad Prism:

$$\text{Specific binding} = \frac{B_{\max} * X}{X + K_D}$$

$$\text{Non specific binding} = \text{NS} * X + \text{background}$$

Where B_{\max} is the maximum specific binding (cpm), X is the radioactivity of the radioligand (cpm), K_D is the equilibrium binding constant (nM), NS is the slope of non-specific binding (cpm nM⁻¹) and background is the non-specific binding in the absence of radioligand.

2.2.6 Kinetic binding experiments

For ^3H -DHA dissociation experiments 100 μL buffer, 25 μL membrane suspension, and 25 μL ^3H -DHA solution (in 6 \times final concentration), were added to 96-well deep well plates in the written order and incubated for various times up to 90 min at room temperature on a plate shaker at 500 rpm. The assay was terminated and processed as described in *Radioligand saturation binding experiments*.

^3H -DHA dissociation experiments were carried out using approximately 1.6 nM ^3H -DHA and data was fitted using the *Dissociation - One phase exponential decay* function in GraphPad Prism to determine the dissociation rate (k_{off}):

$$Y = (Y_0 - \text{NS}) * e^{-K*X} + \text{NS}$$

Where Y is the binding (cpm), X is the time (min), Y_0 is the binding at time zero (cpm), NS is the non-specific binding (cpm), K is the rate constant (min^{-1}).

For ^3H -DHA association experiments, concentrations of approximately 3.2 nM, 1.6 nM, and 0.8 nM ^3H -DHA were used and incubated for various times up to 90 min. The assay was terminated and processed as described in *Radioligand saturation binding experiments*. ^3H -DHA association data was fitted to a one-phase exponential function using the *One-phase association* function in GraphPad Prism to determine an observed rate constant (k_{obs}):

$$Y = Y_0 * (\text{Plateau} - Y_0) * (1 - e^{(-K*x)})$$

Where Y_0 is binding (cpm) at time X (min), plateau is binding at infinite times (cpm), and K is the rate constant corresponding to k_{obs} (min^{-1}).

From k_{obs} (association experiments) and k_{off} (dissociation experiments), an association rate (k_{on}) of ^3H -DHA was calculated:

$$k_{\text{on}} = \frac{k_{\text{obs}} - k_{\text{off}}}{[3\text{H} - \text{DHA}]}$$

The equilibrium dissociation constant k_{D} was now calculated:

$$K_{\text{D}} = \frac{k_{\text{off}}}{k_{\text{on}}}$$

^3H -DHA association data was also fitted globally using the *Association - Two or more conc. of hot* function in GraphPad Prism to derive a single best-fit calculation of k_{on} and k_{off} :

$$L = \text{Hotnm} * 1e^{-9}$$

$$k_{\text{obs}} = k_{\text{on}} * L + k_{\text{off}}$$

$$\text{Occupancy} = \frac{L}{L + K_D}$$

$$Y_{\text{max}} = \text{Occupancy} * B_{\text{max}}$$

$$Y = Y_{\text{max}} * (1 - e^{(-1 * k_{\text{obs}} * X)})$$

Where k_{on} is the association rate constant ($\text{M}^{-1} \text{min}^{-1}$), k_{off} is the dissociation rate constant (min^{-1}), K_D is the equilibrium binding constant (M), and B_{max} is the maximum binding at equilibrium (cpm).

2.2.7 Competition binding experiments to calculate ligand affinity of unlabeled ligands

25 μL buffer, 25 μL membrane suspension, 25 μL 1 nM ^3H -DHA solution (in $6\times$ final concentration), and 75 μL ligand solution (in $2\times$ final concentration) were added to 96-well deep well plates in the written order and incubated for 90 min at room temperature on a plate shaker at 500 rpm. The assay was terminated and processed as described in *Radioligand saturation binding experiments*.

Displacement curves from the competition binding experiments were fitted using the *one site – fit logEC50* function in GraphPad Prism to determine the IC_{50} value:

$$Y = \frac{\text{Bottom} + (\text{Top} - \text{Bottom})}{1 + 10^{X - \log(\text{IC}_{50})}}$$

Where bottom and top are plateaus of the competition binding curve and $\log(\text{IC}_{50})$ is the log of the concentration of the competitor that gives half the maximum binding at equilibrium. Hereafter, the Cheng-Prusoff equation³⁹ was used to calculate the affinities of the ligands in the form of a K_i value, which is the equilibrium dissociation constant of the nonradioactive ligand:

$$K_i = \frac{\text{IC}_{50}}{1 + \frac{[\text{S}]}{K_D}}$$

Where $[\text{S}]$ is the concentration and K_D the equilibrium dissociation constant of the radioligand.

2.2.8 Competition binding experiments to determine kinetics and affinities of unlabeled ligands

25 μL buffer and 25 μL membrane suspension were added to wells of a 96-well deep well plate. Hereafter, 100 μL solution with 1 nM ^3H -DHA and unlabelled ligand (both in 1.5 \times final concentration) were added and incubated at various times up to 90 min at room temperature on a plate shaker at 500 rpm. The assay was terminated and processed as described in *Radioligand saturation binding experiments*. To determine non-specific binding, 25 μL 10 μM ALP (in 6 \times final concentration), and 25 μL membrane suspension were added to wells of another 96-well deep well plate. Again, 100 μL solution with 1 nM ^3H -DHA and unlabelled ligand (both in 1.5 \times final concentration) were added at various times up to 90 min at room temperature and terminated and processed as described in *Radioligand saturation binding experiments*. Based on the kinetic parameters of ^3H -DHA binding, k_{on} , k_{off} and k_{d} of the unlabelled ligands were calculated using the *Kinetics of competitive binding* function in GraphPad Prism, which is based on the calculation method originally described by Motulsky *et al.*:³⁵

$$K_A = k_1 * [L] + k_2$$

$$K_B = k_3 * [I] + k_4$$

$$K_F = 0.5 * \left(K_A + K_B + \sqrt{((K_A - K_B)^2 + 4 * k_1 * k_3 * L * I * 10^{-18})} \right)$$

$$K_S = 0.5 * \left(K_A + K_B - \sqrt{((K_A - K_B)^2 + 4 * k_1 * k_3 * L * I * 10^{-18})} \right)$$

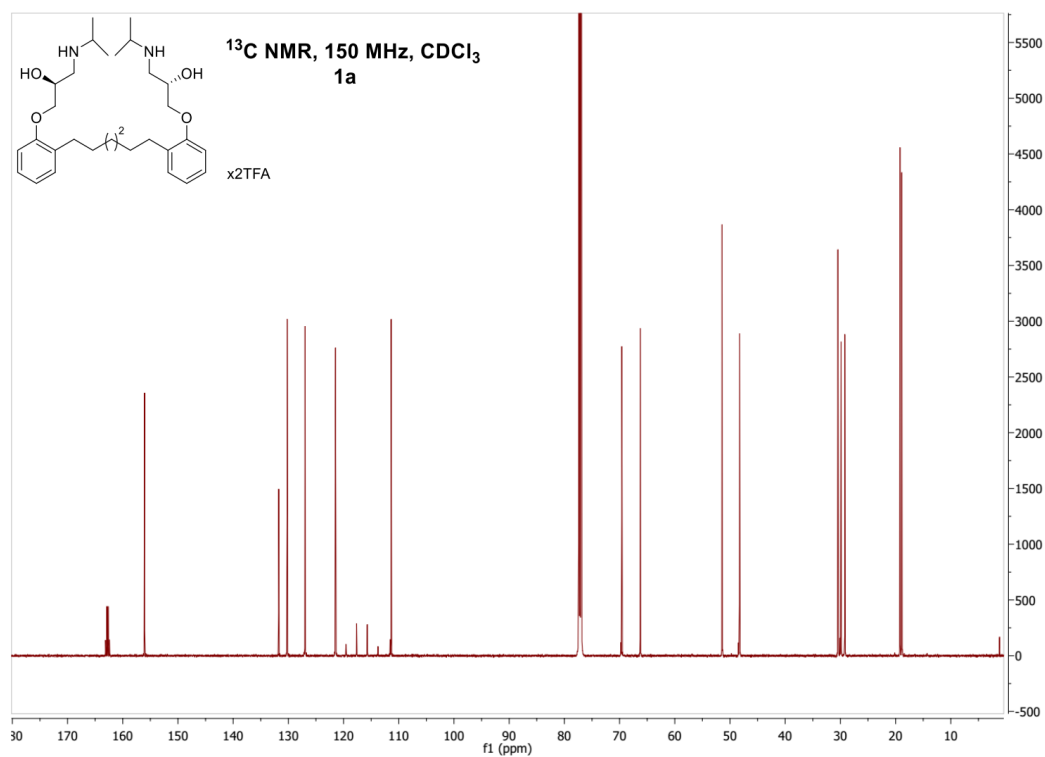
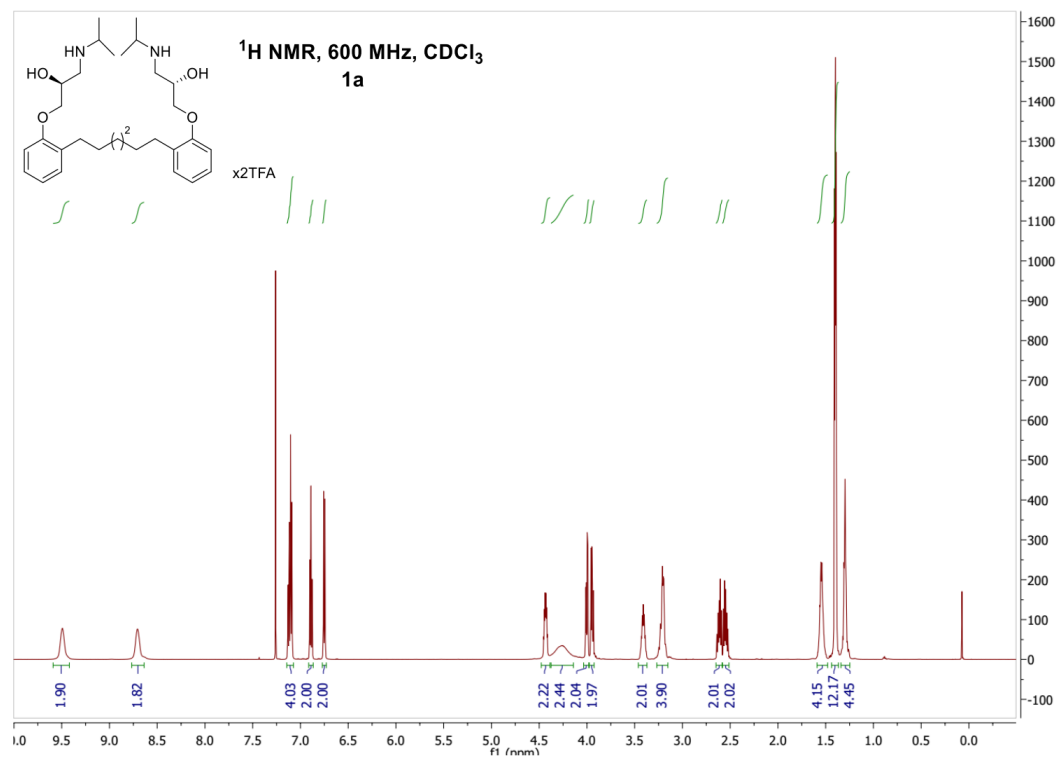
$$Q = \frac{B_{\text{max}} * k_1 * L * 10^{-9}}{K_F - K_S}$$

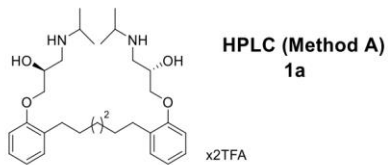
$$Y = Q * \left(\frac{k_4 * (K_F - K_S)}{k_F * K_S} + \frac{k_4 - K_F}{K_F} * e^{(-K_F * X)} - \frac{k_4 - K_S}{K_S} * e^{-K_S * X} \right)$$

Where K_A , K_B , K_F , and K_S are variables defined for the purpose of solving differential equations describing the kinetics of a competitive binding incubation. The two last equations are the result of solving these equations and describe the amount of radioligand bound the receptors as a function of time. Y is the specific ^3H -DHA binding and X is the time (min). $[L]$ and $[I]$ are the concentrations of the radioligand and the unlabelled competing ligand, respectively. Knowing these factors, the maximum binding B_{max} and the association and dissociate rate of the unlabelled ligand, k_1 and k_2 , respectively, can be determined.

3 NMR AND HPLC DATA

^1H and ^{13}C NMR spectra and HPLC chromatograms of final bitopic ligands and truncated analogues



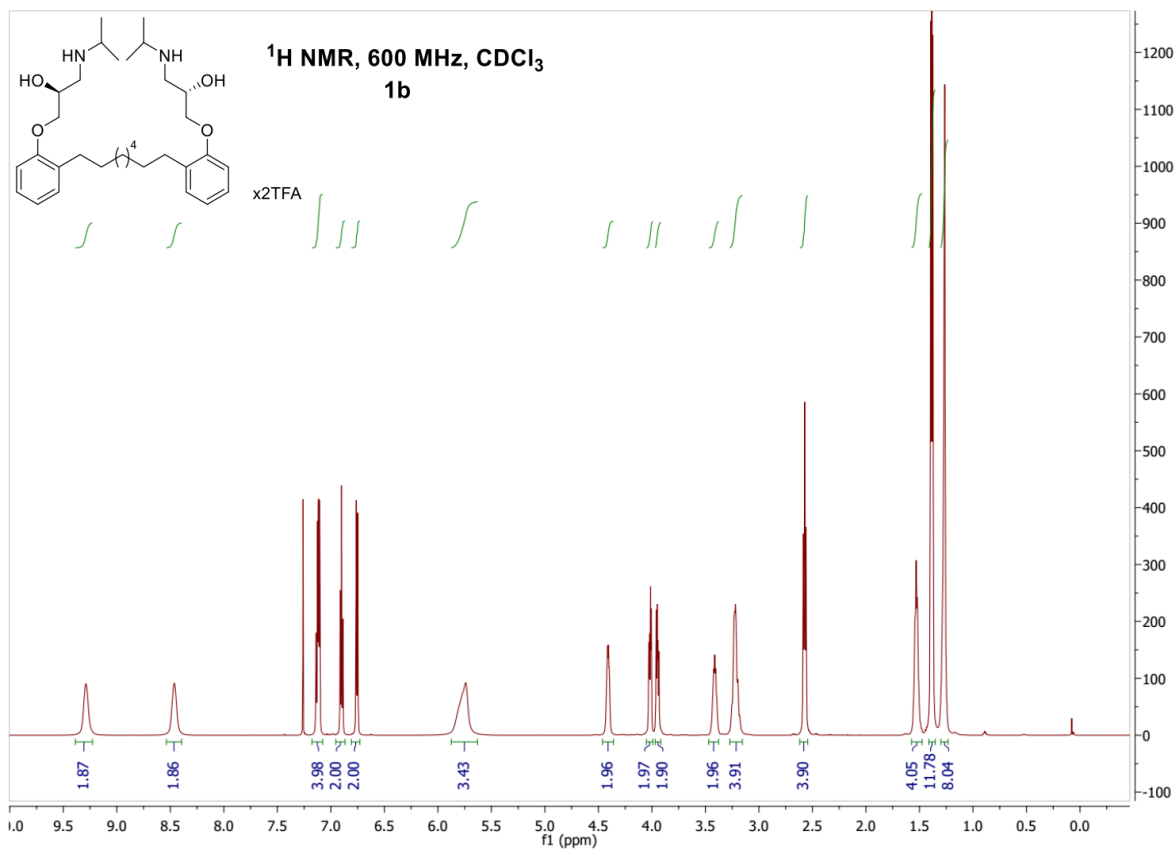
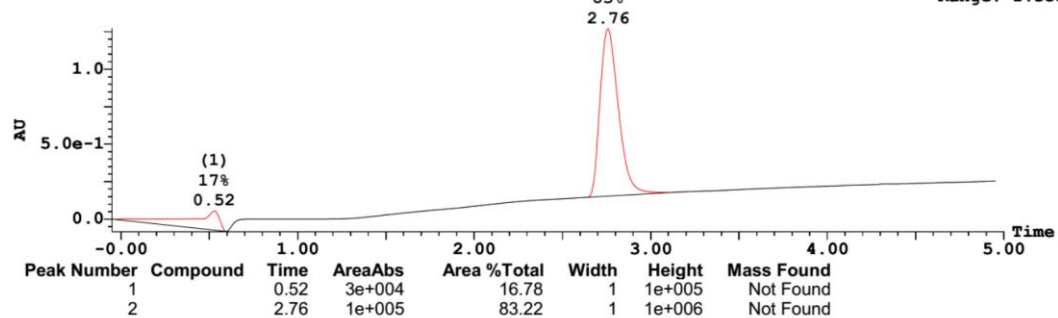


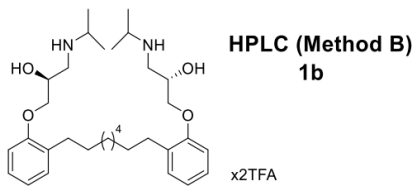
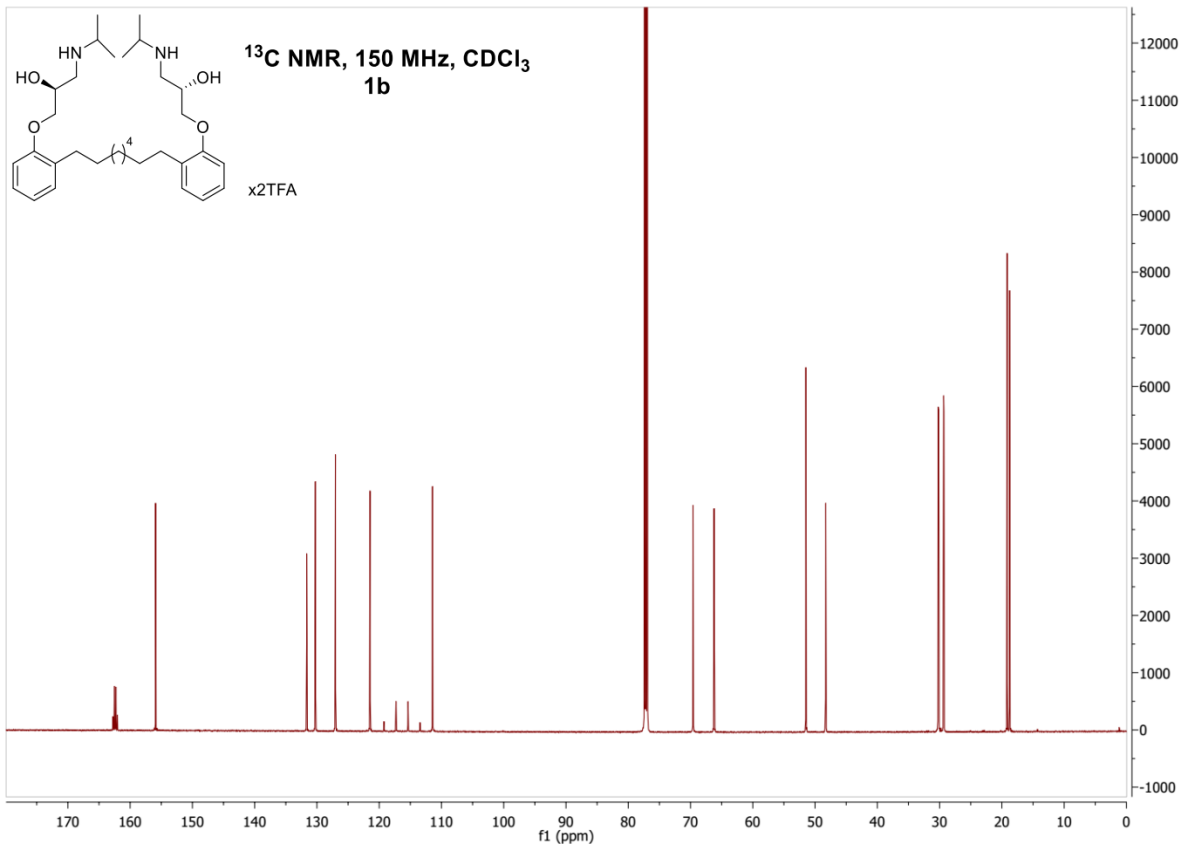
Sample 2 Vial 2:12 ID MCR_BG_151106_BG2-089p48 File MCR_BG_151106_BG2-089p48 Date 06-Nov-2015 Time 14:41:49

2: UV Detector: TAC :Wavelength Range: (215 - 254)

1.272

Range: 1.353

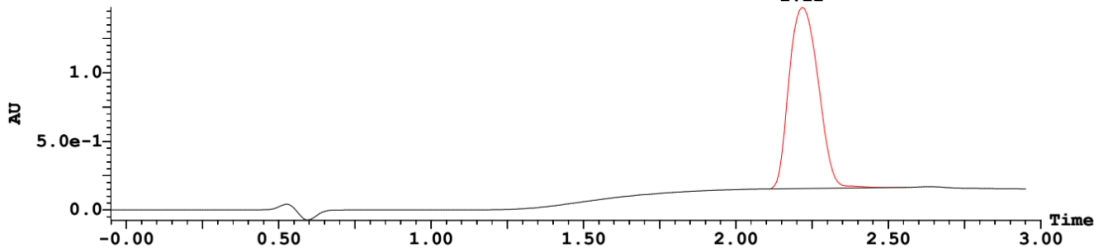


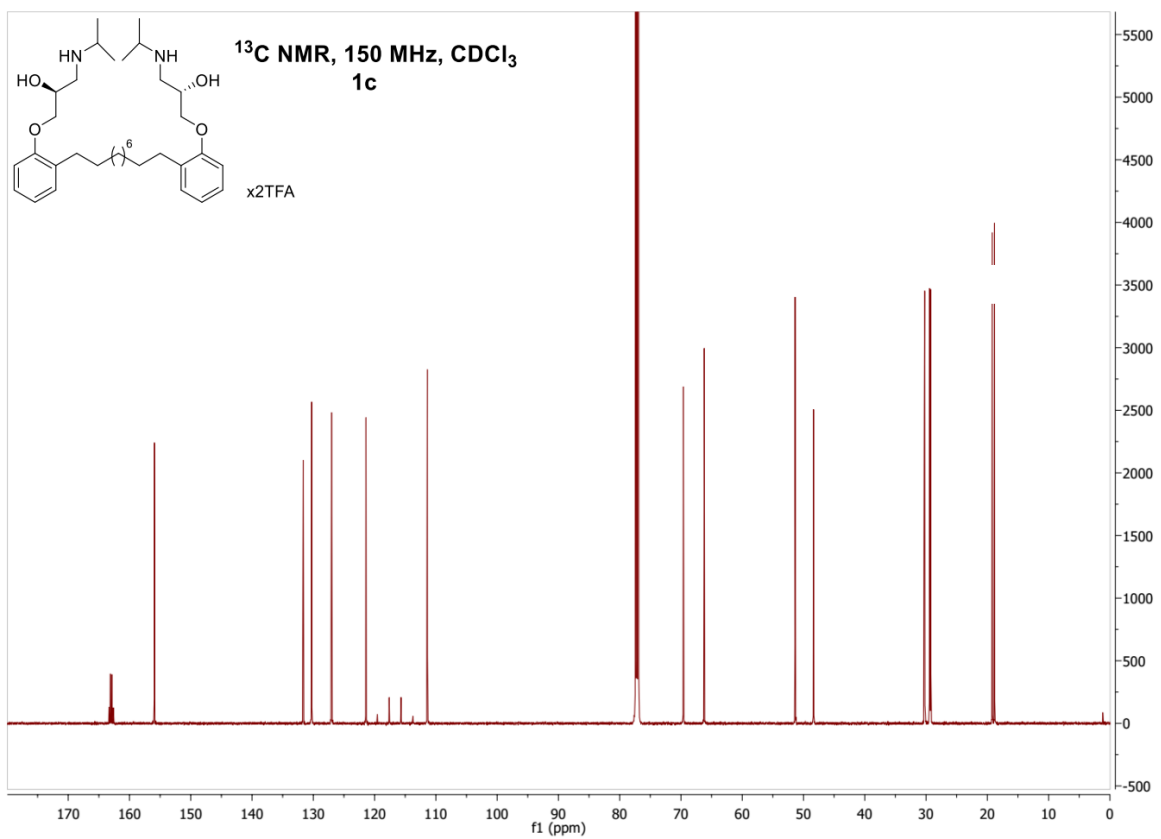
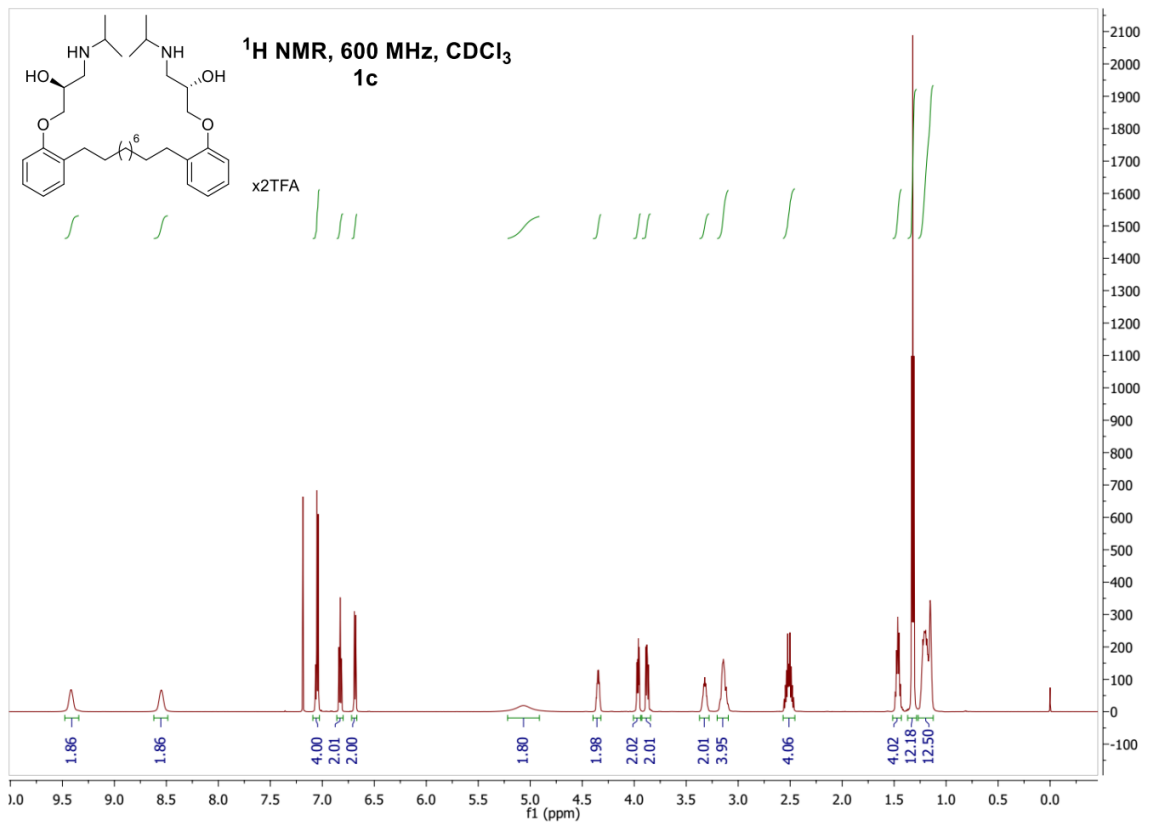


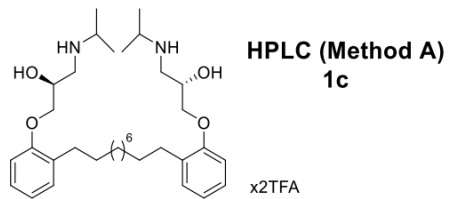
Sample 3 Vial 2:19 ID MCR_BG_151001_BG2-065p21 File MCR_BG_151001_BG2-065p21 Date 01-Oct-2015 Time 16:32:32

2: UV Detector: TAC :Wavelength Range: (215 - 254)

(1) 1.478
100% Range: 1.552
2.22

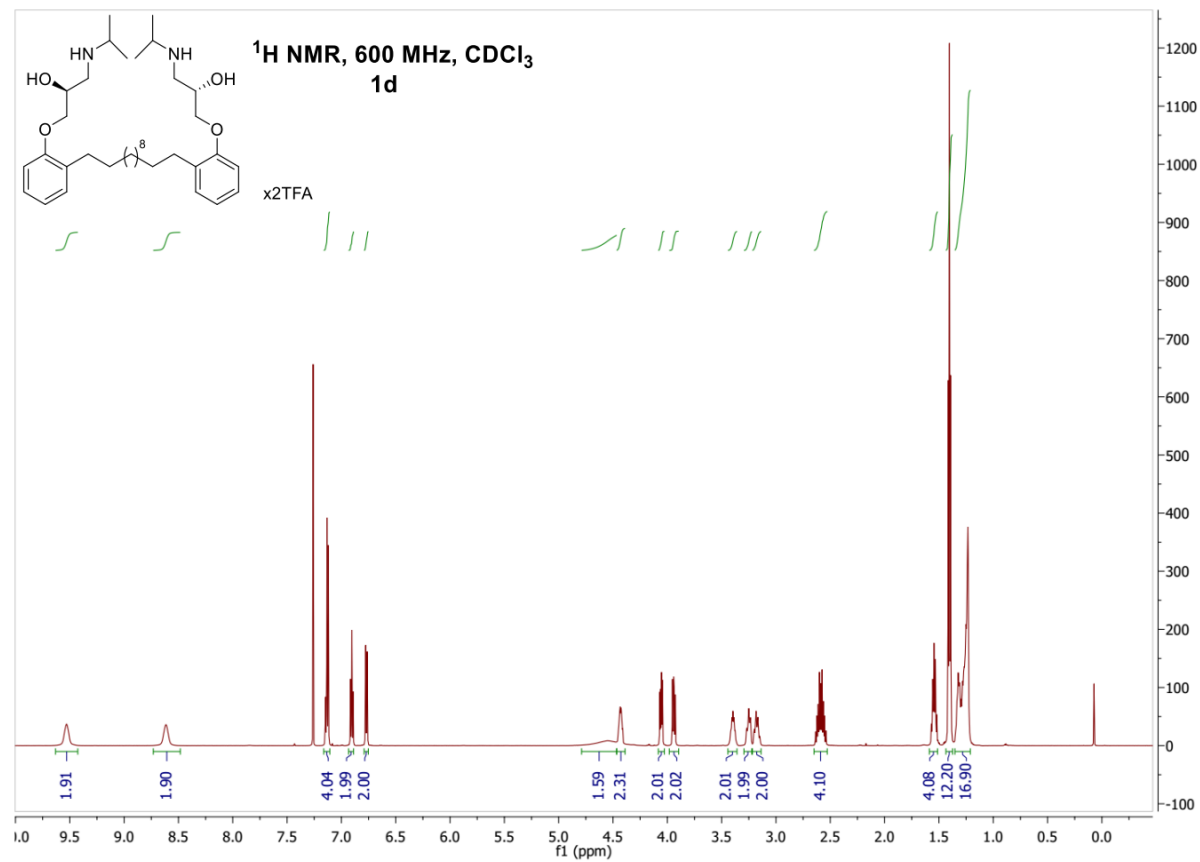
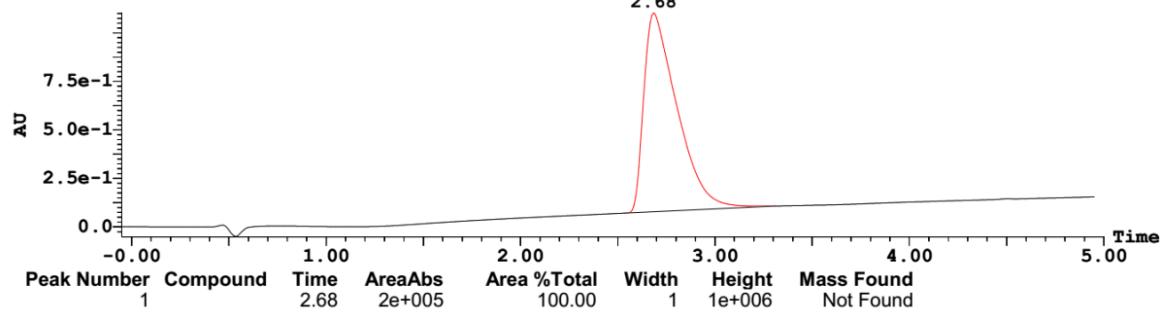


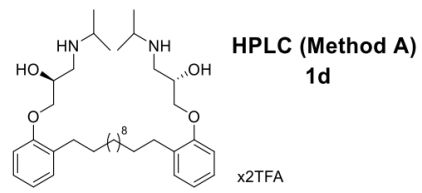
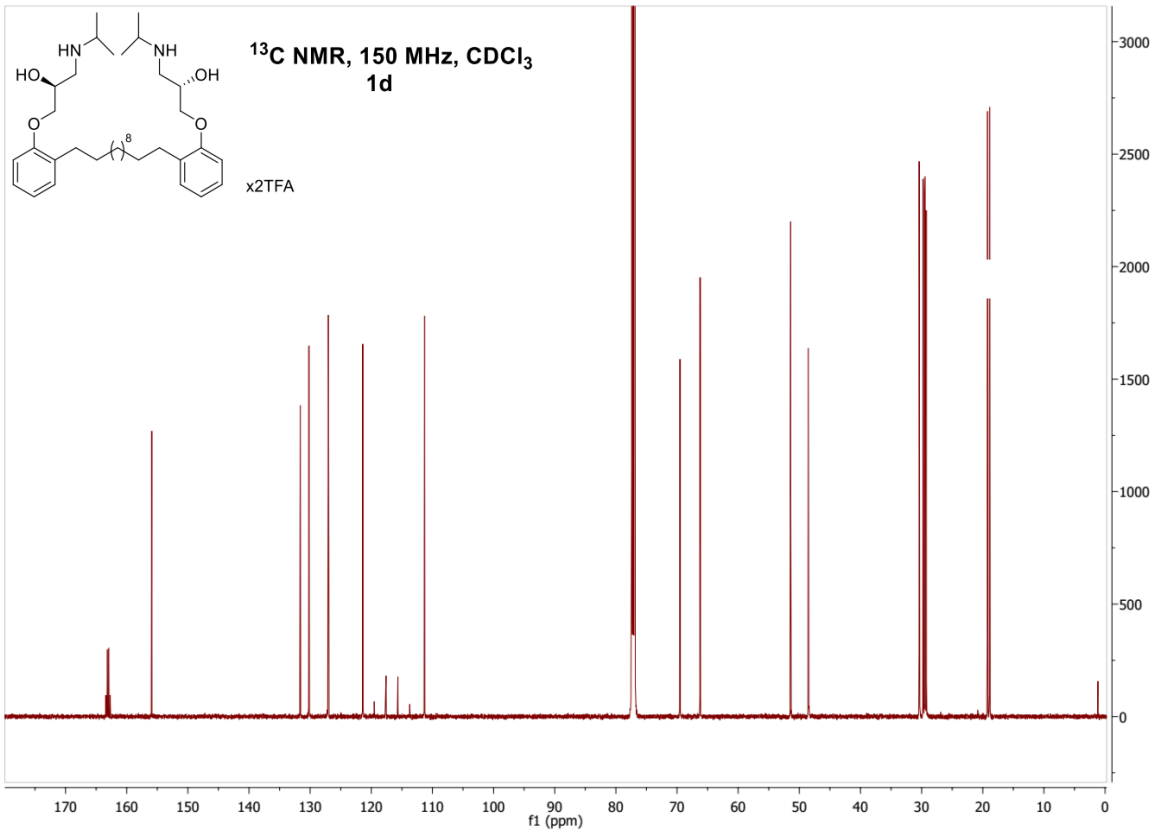




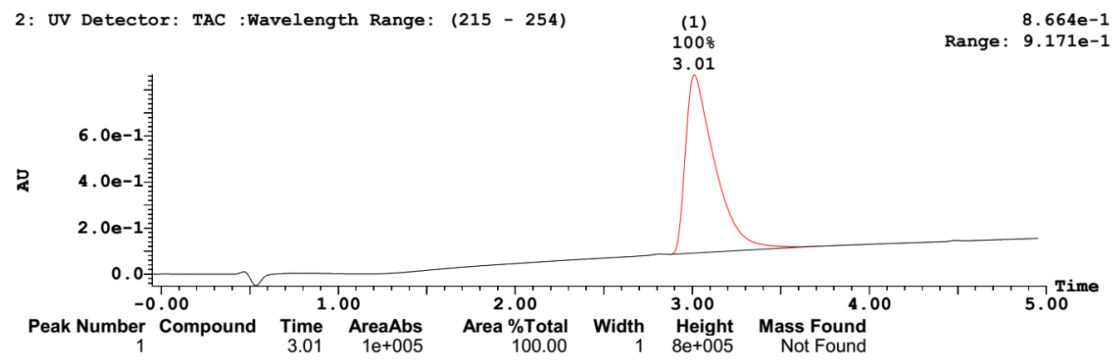
Sample 2 Vial 2:25 ID MCR_BG_151106_BG2-090p55 File MCR_BG_151106_BG2-090p55 Date 06-Nov-2015 Time 17:15:11

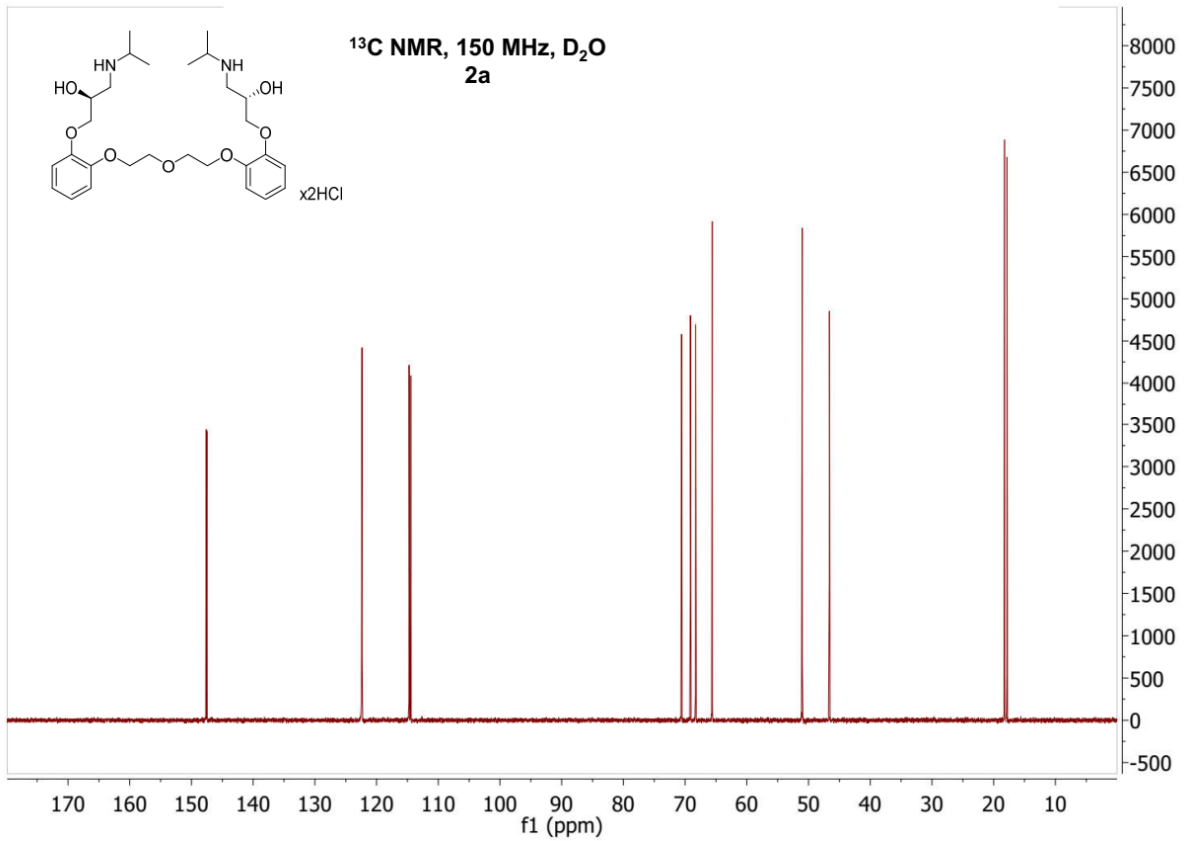
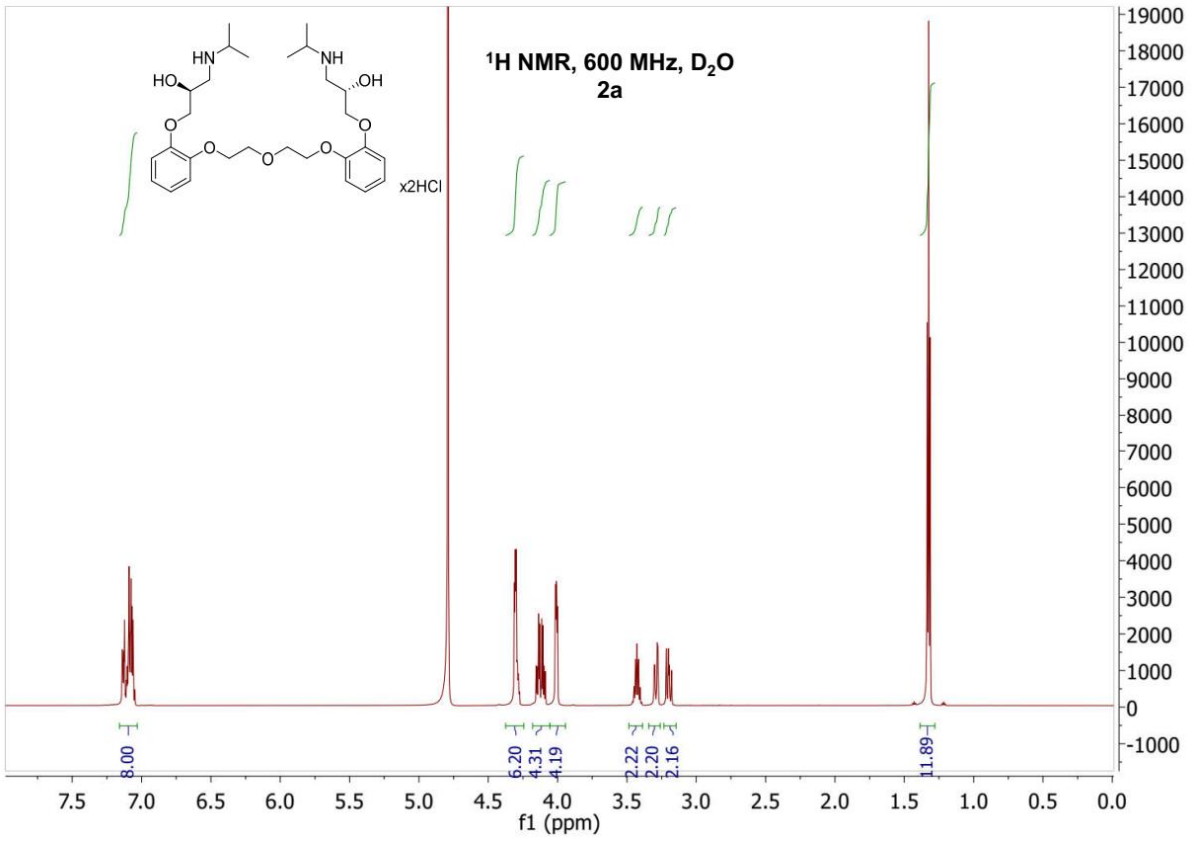
2: UV Detector: TAC :Wavelength Range: (215 - 254) (1) 1.103
Range: 1.152

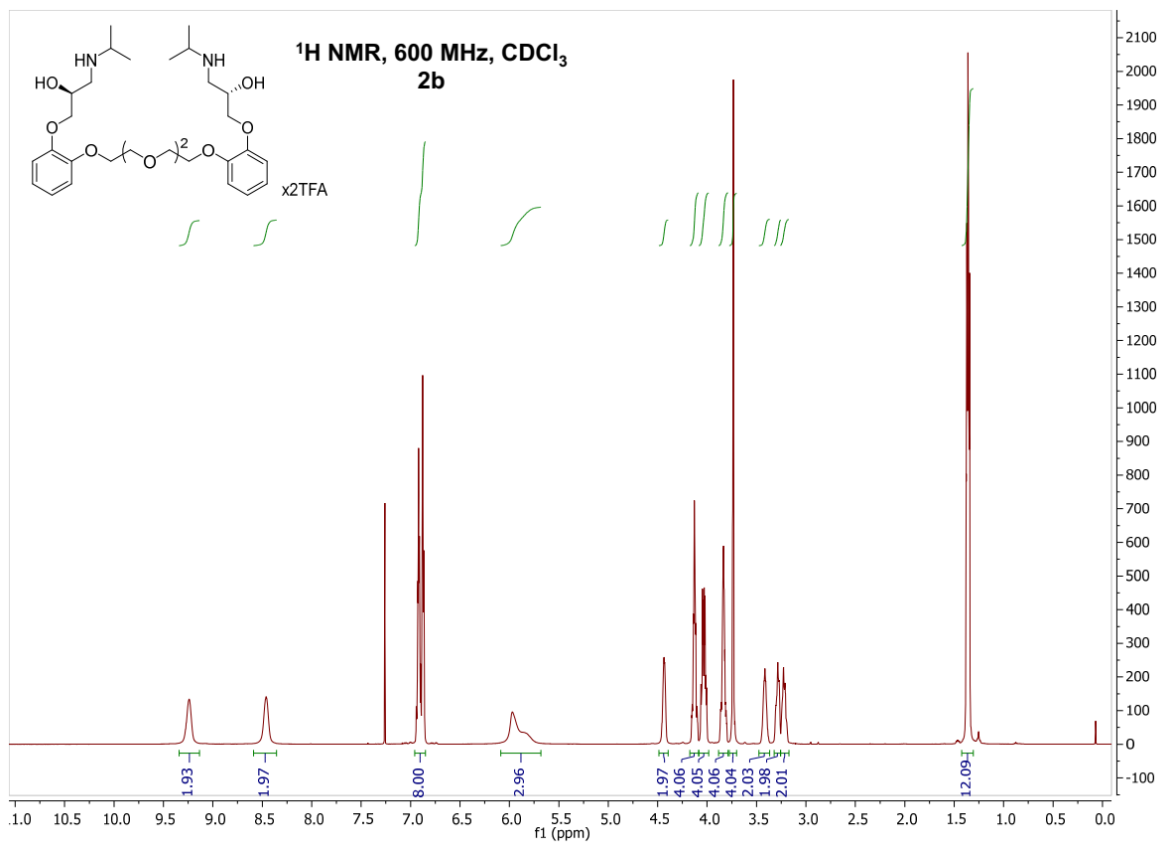
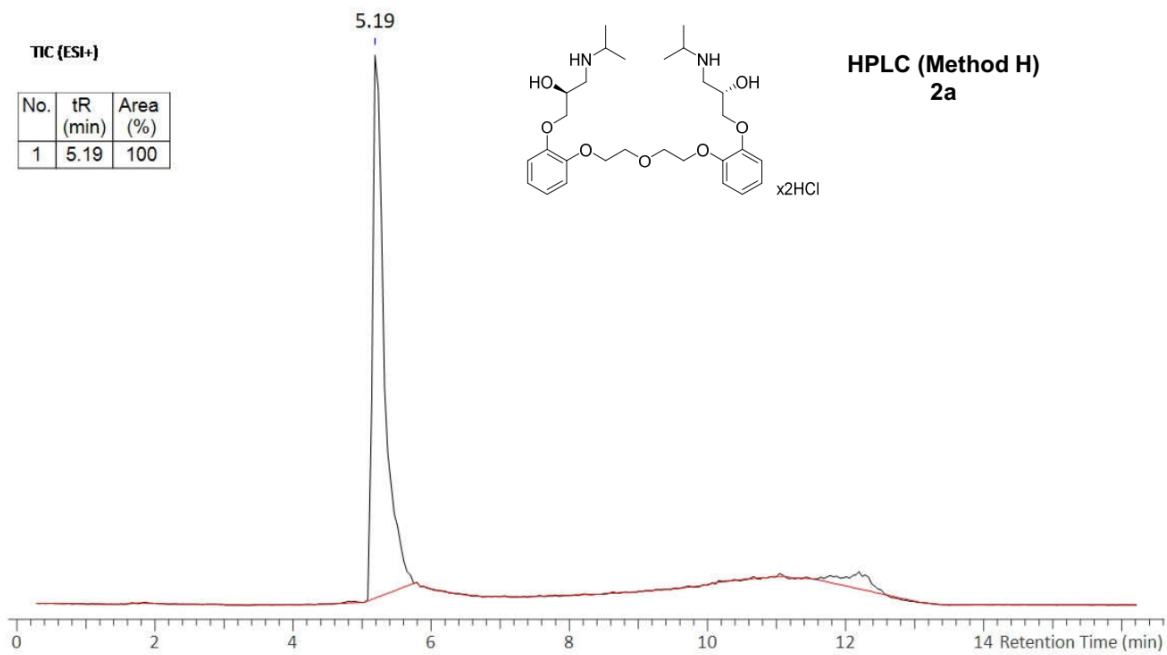


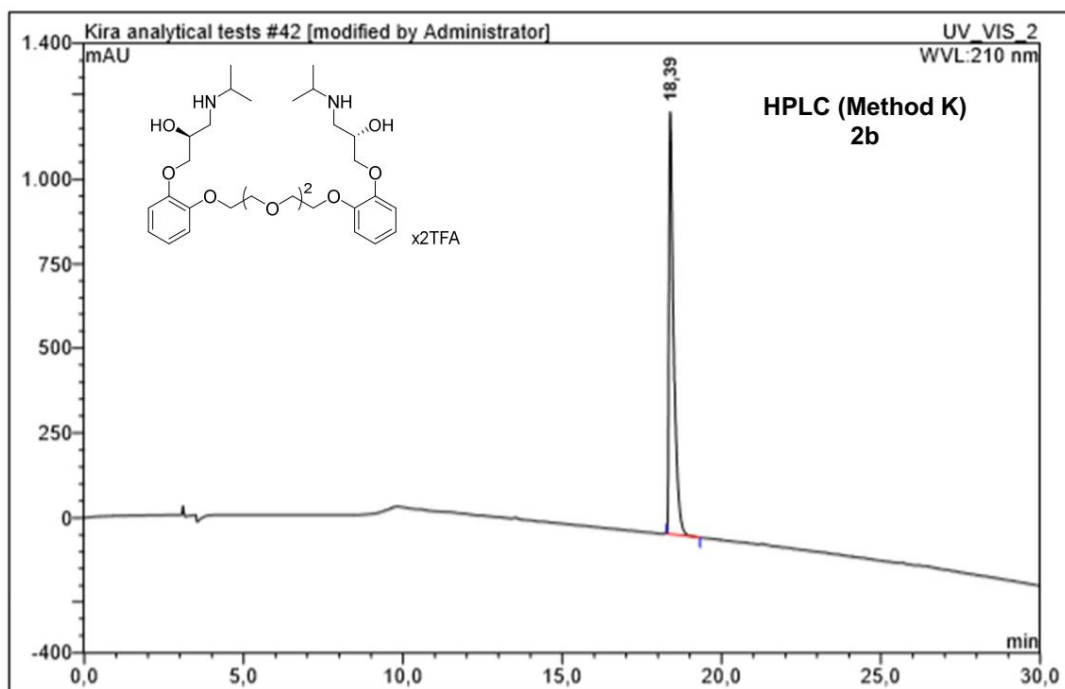
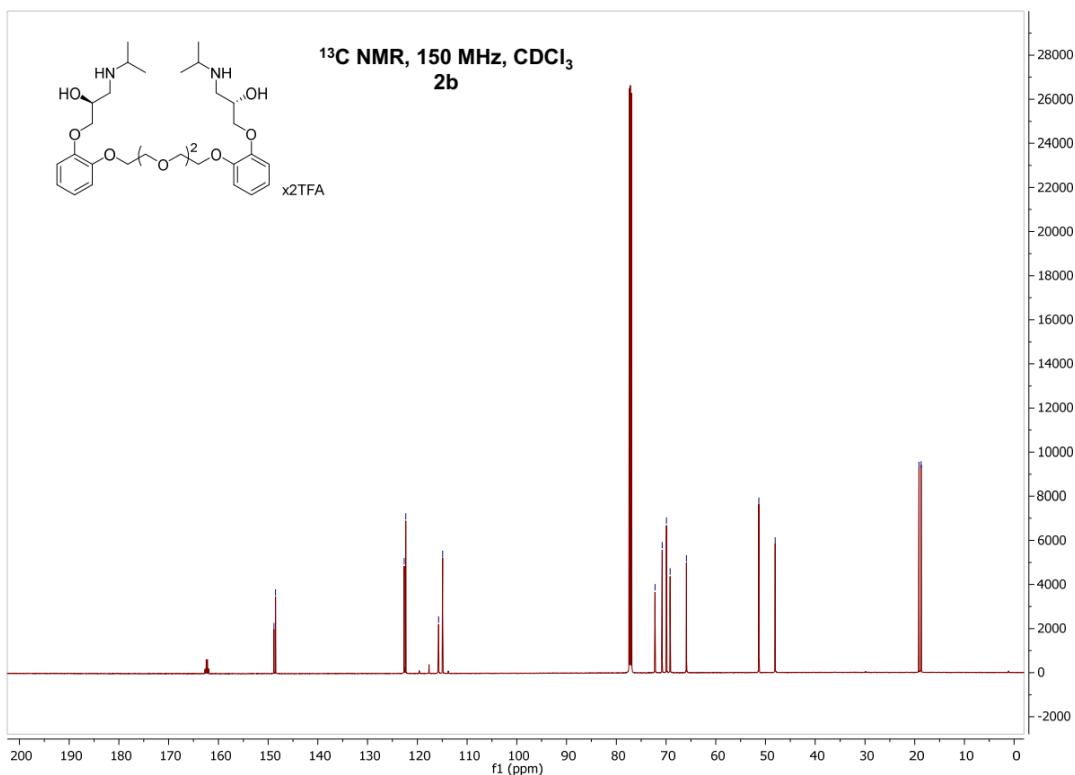


Sample 1 Vial 2:36 ID MCR_BG_151106_BG2-091p59 File MCR_BG_151106_BG2-091p59 Date 06-Nov-2015 Time 18:35:16

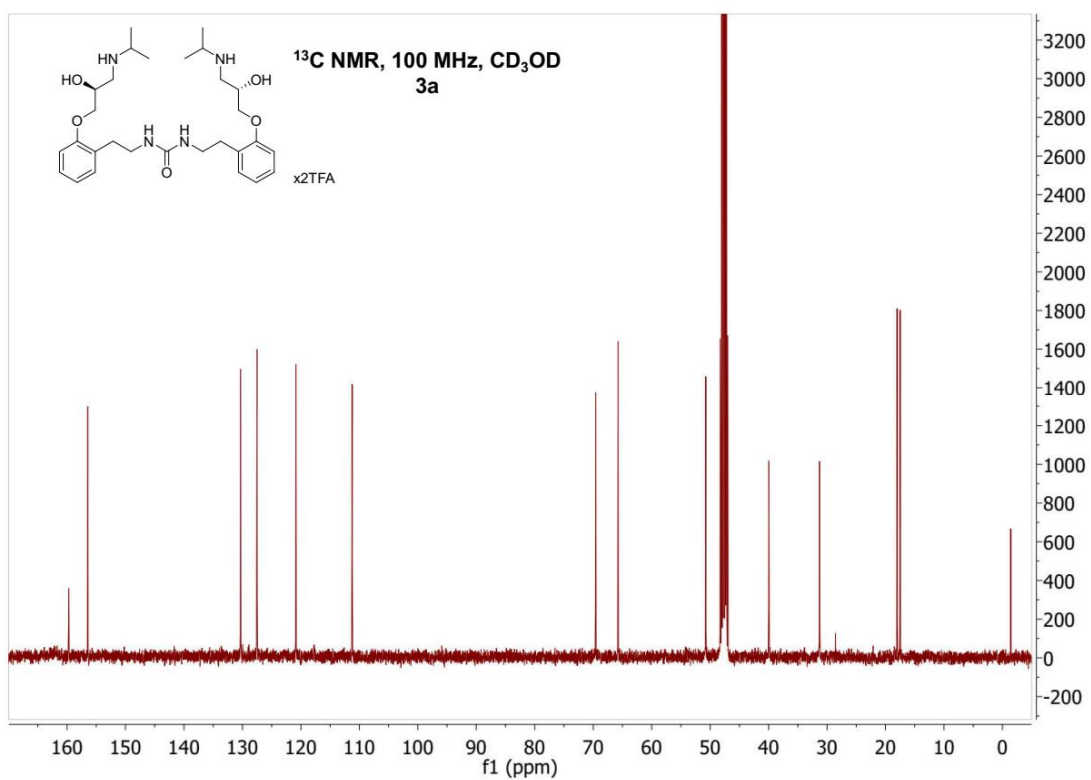
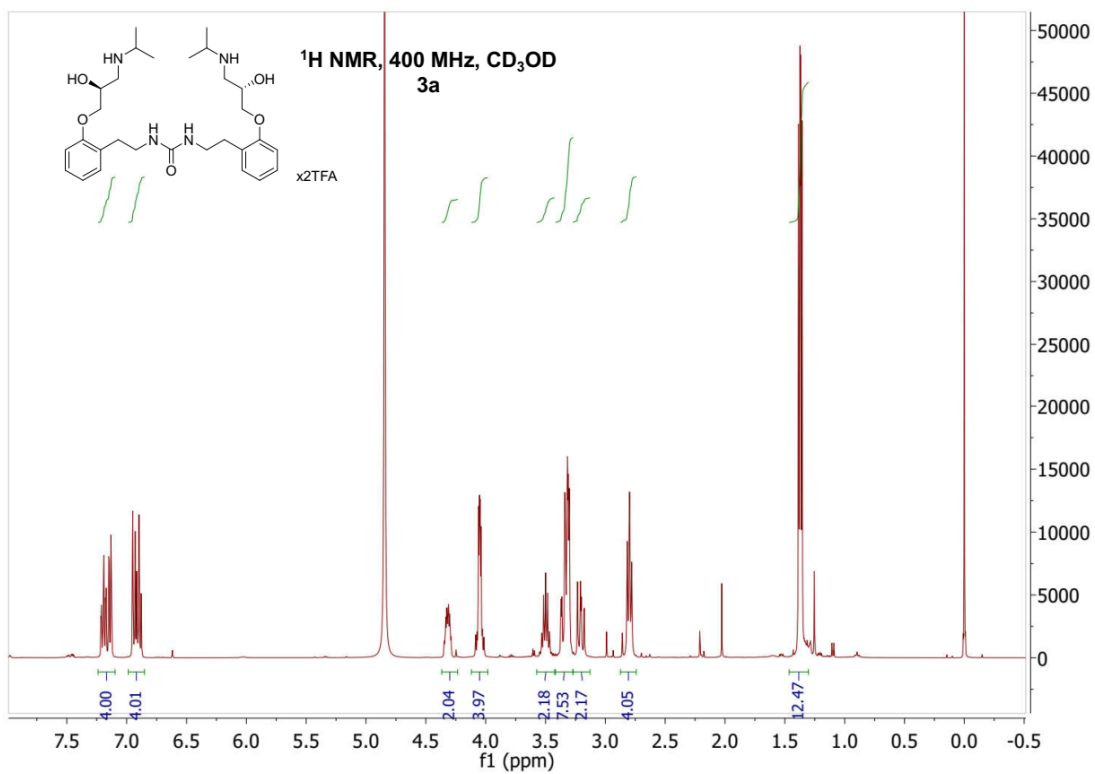


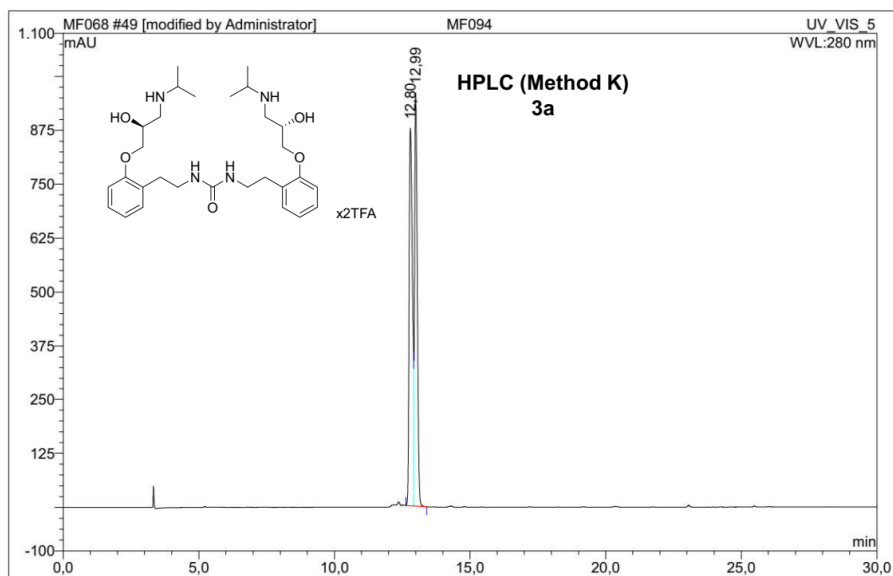






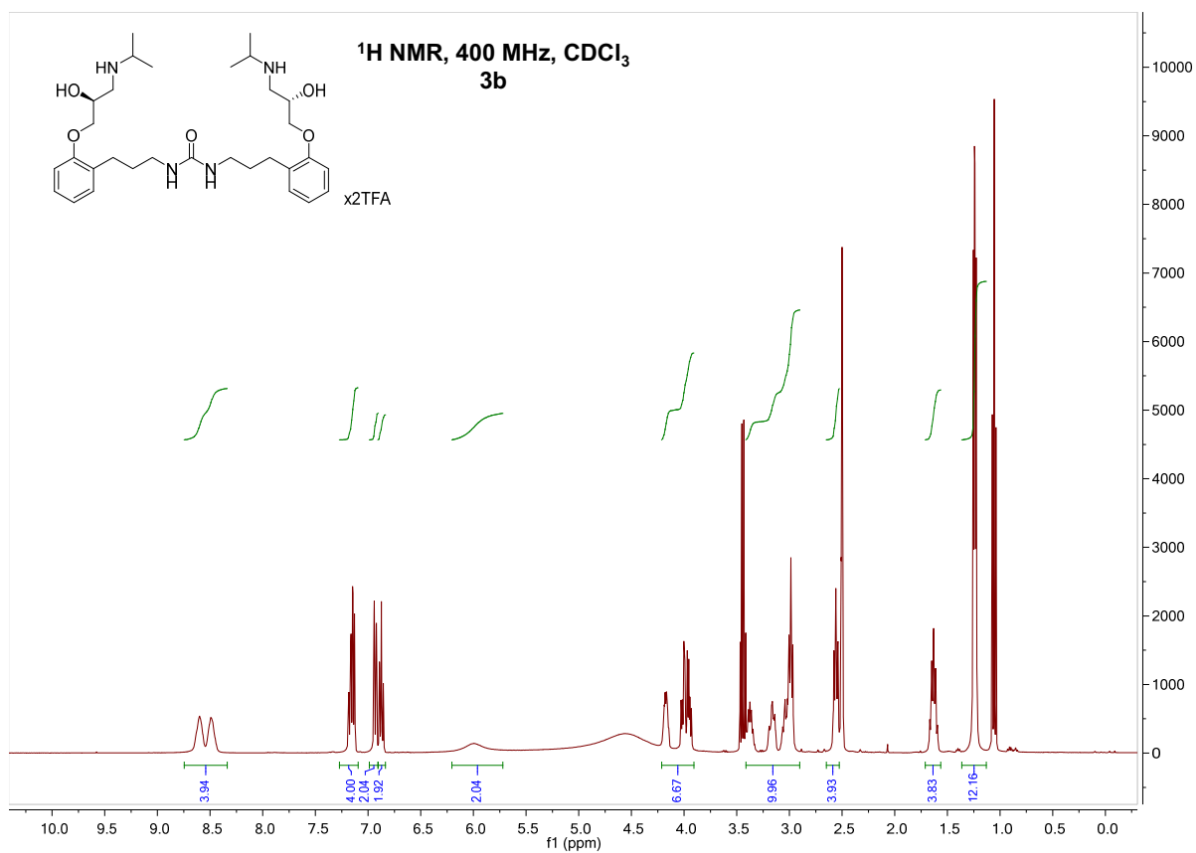
No.	Ret.Time min	Peak Name	Height mAU	Area mAU*min	Rel.Area %	Amount	Resolution(EP)
1	18,39	n.a.	1246,624	214,713	100,00	n.a.	n.a.
Total:			1246,624	214,713	100,00	0,000	

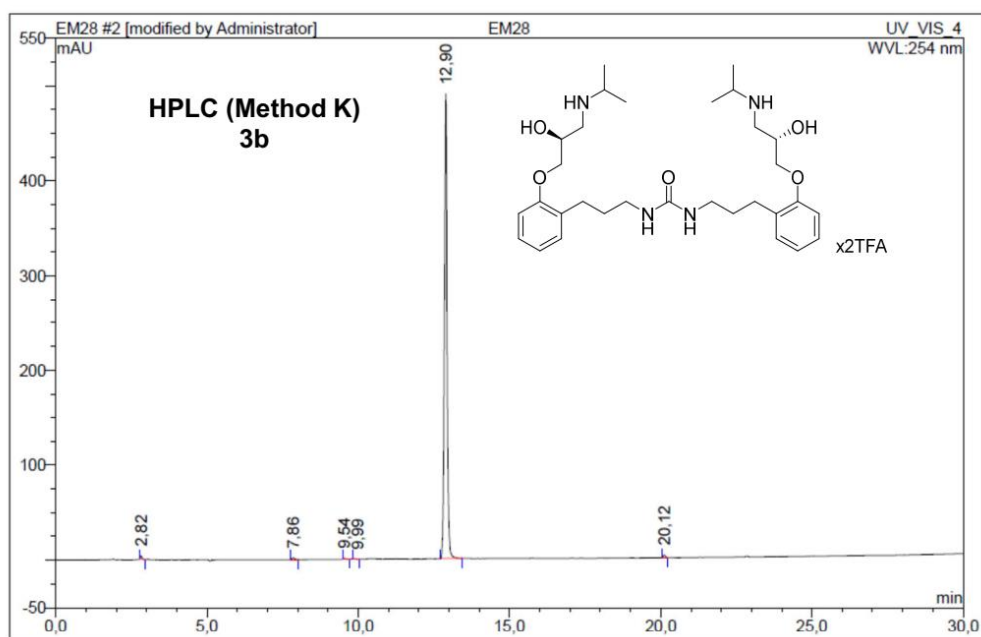
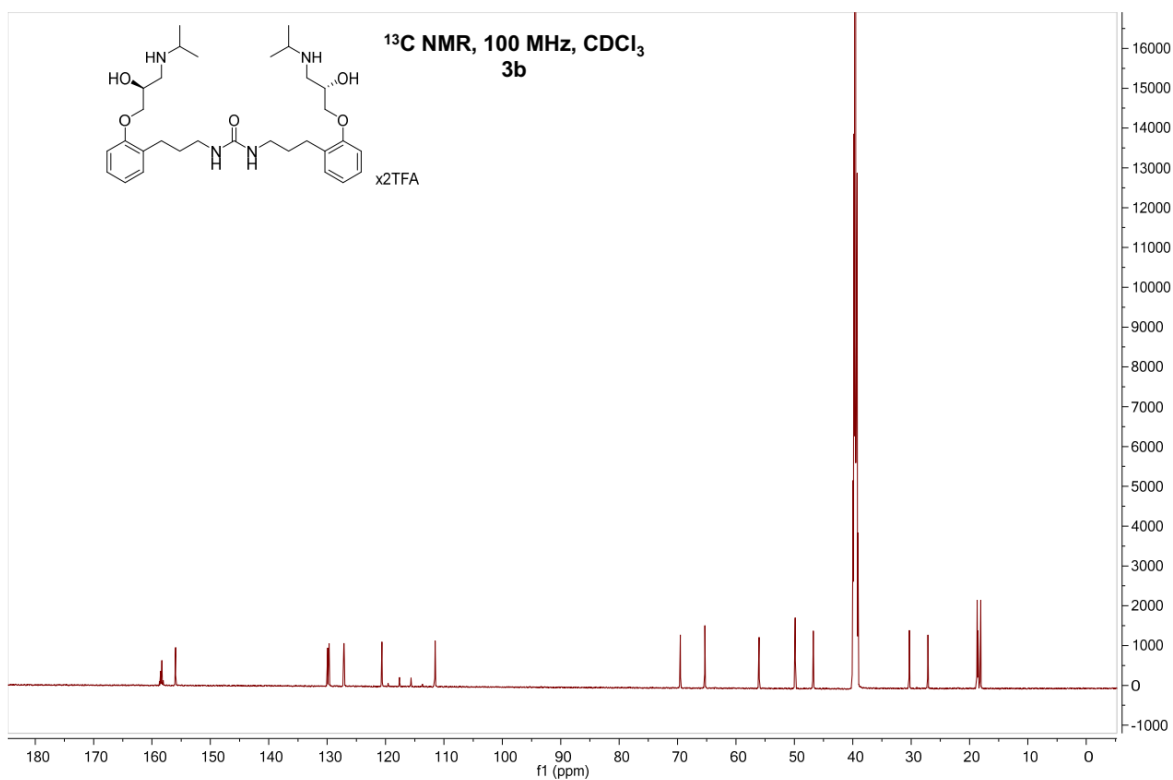




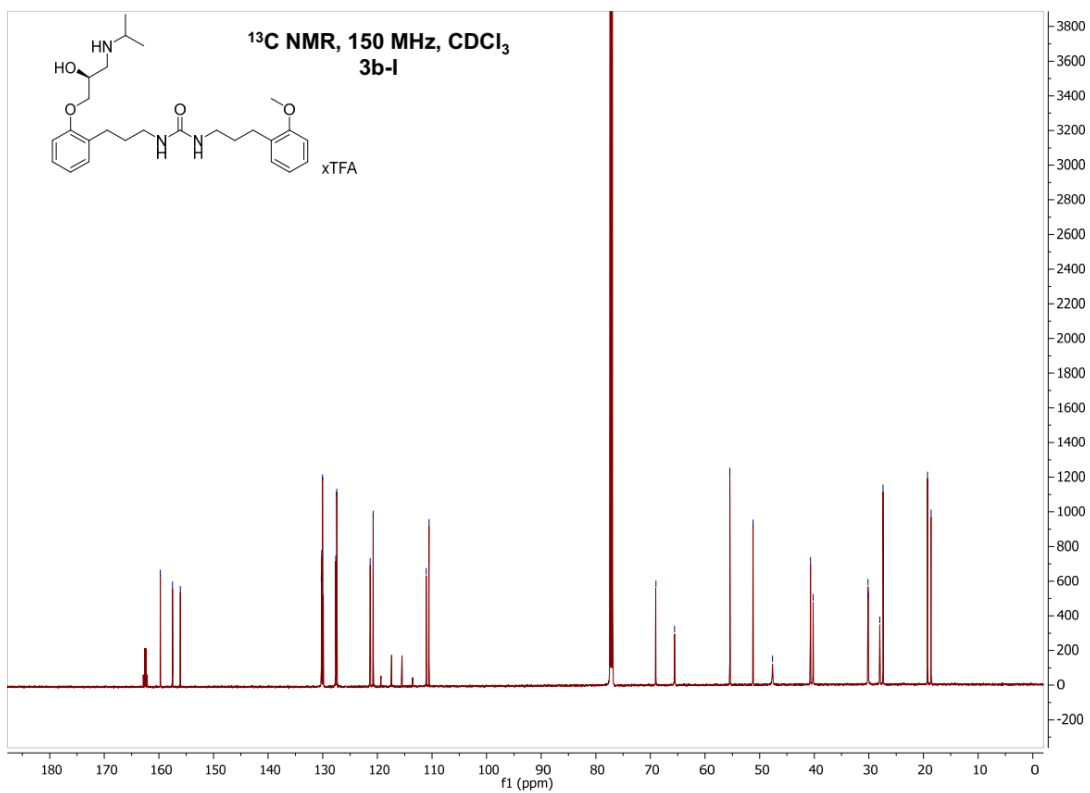
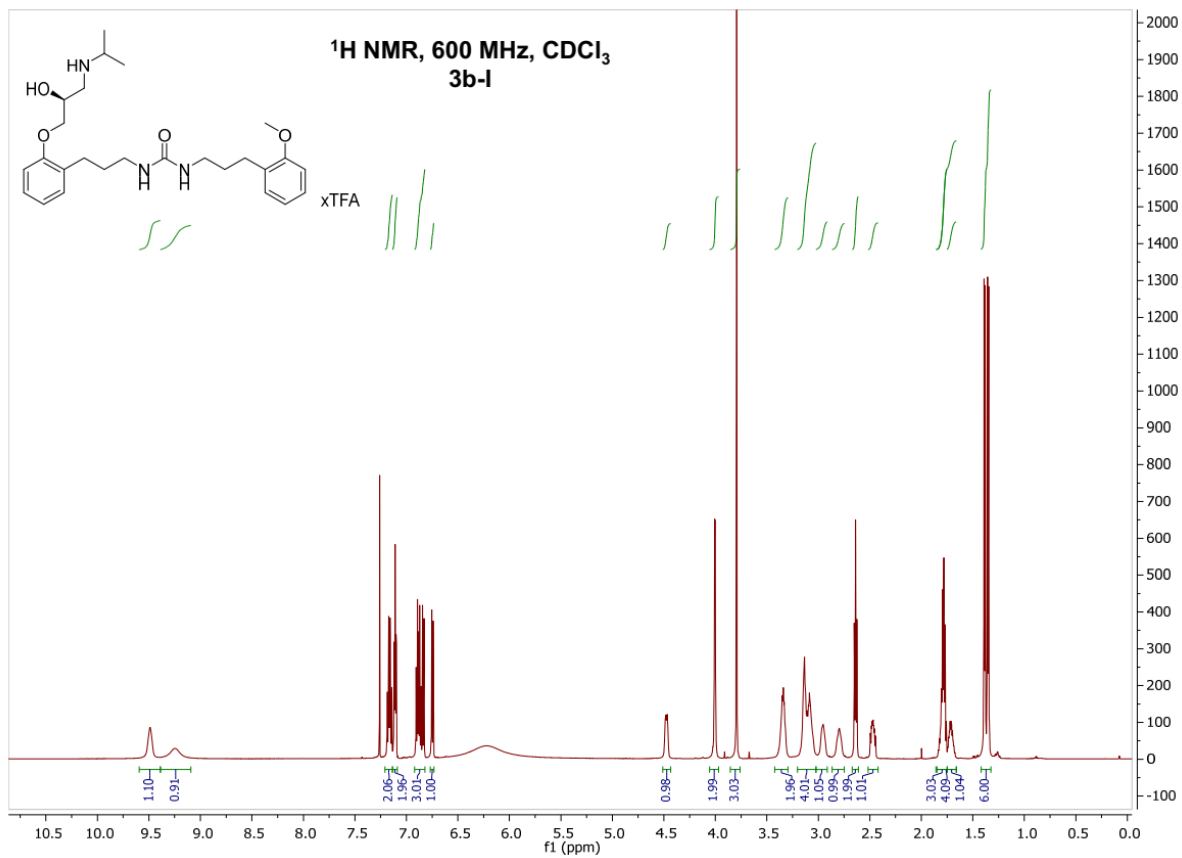
No.	Ret. Time min	Peak Name	Height mAU	Area mAU*min	Rel. Area %	Amount	Resolution(EP)
1	12,80	n.a.	876,315	123,555	51,65	n.a.	0,85
2	12,99	n.a.	958,972	115,654	48,35	n.a.	n.a.
Total:			1835,287	239,209	100,00	0,000	

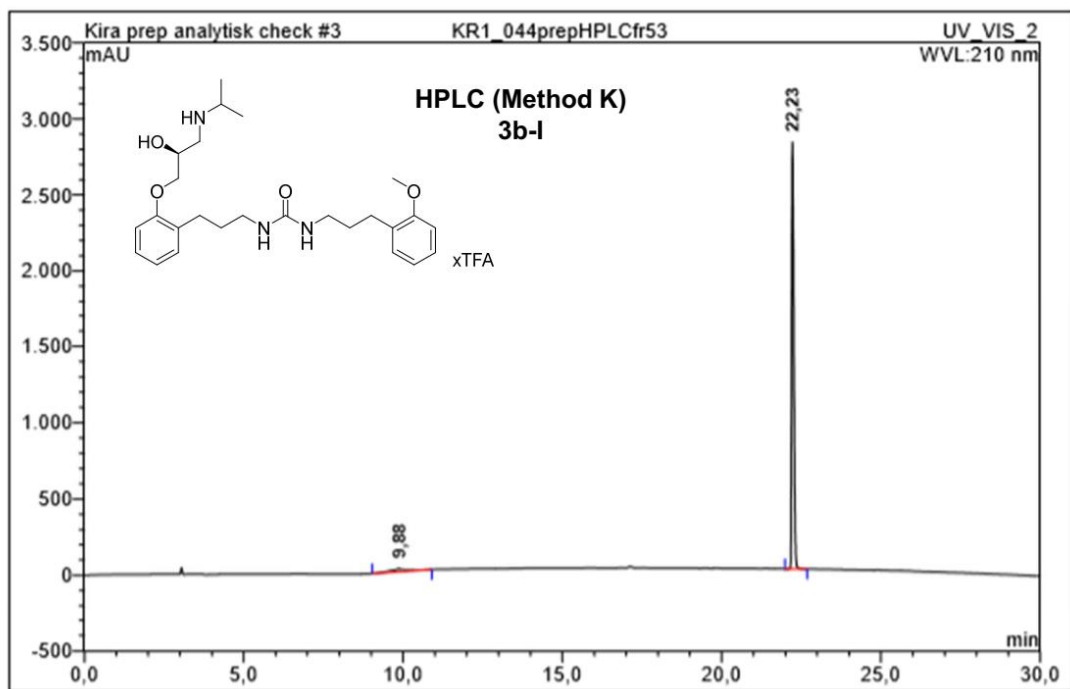
Compound **3a** eluted as the mono- and di-TFA salt, which gave rise to two close peaks.



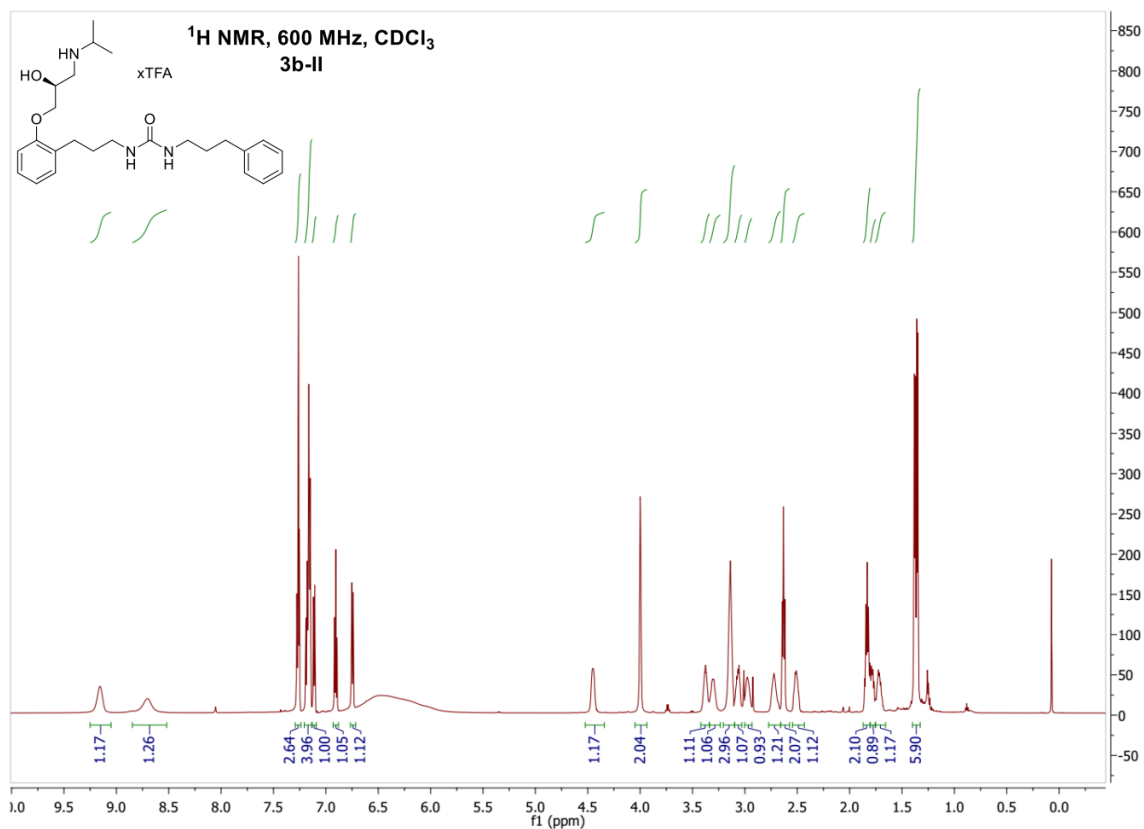


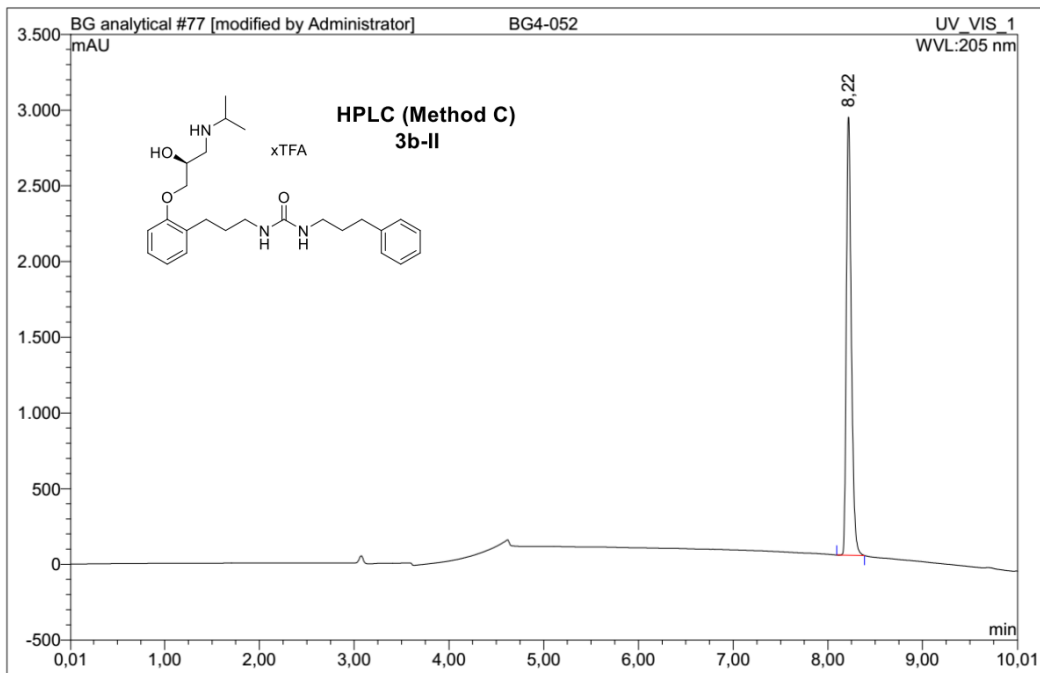
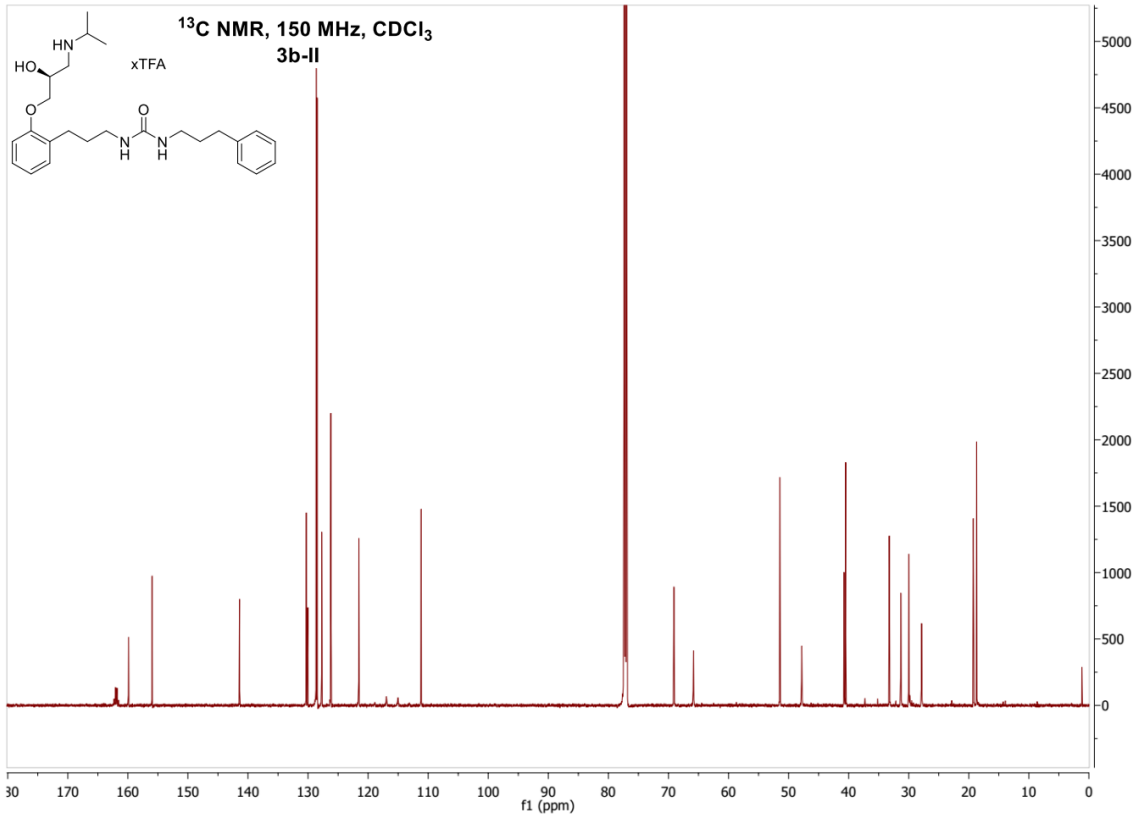
No.	Ret.Time min	Peak Name	Height mAU	Area mAU*min	Rel.Area %	Amount	Resolution(EP)
1	2,82	n.a.	3,528	0,215	0,42	n.a.	38,30
2	7,86	n.a.	1,757	0,173	0,34	n.a.	13,29
3	9,54	n.a.	0,480	0,000	0,00	n.a.	2,38
4	9,99	n.a.	0,214	0,015	0,03	n.a.	13,36
5	12,90	n.a.	489,829	50,469	98,80	n.a.	50,86
6	20,12	n.a.	2,569	0,208	0,41	n.a.	n.a.
Total:			498,376	51,082	100,00	0,000	



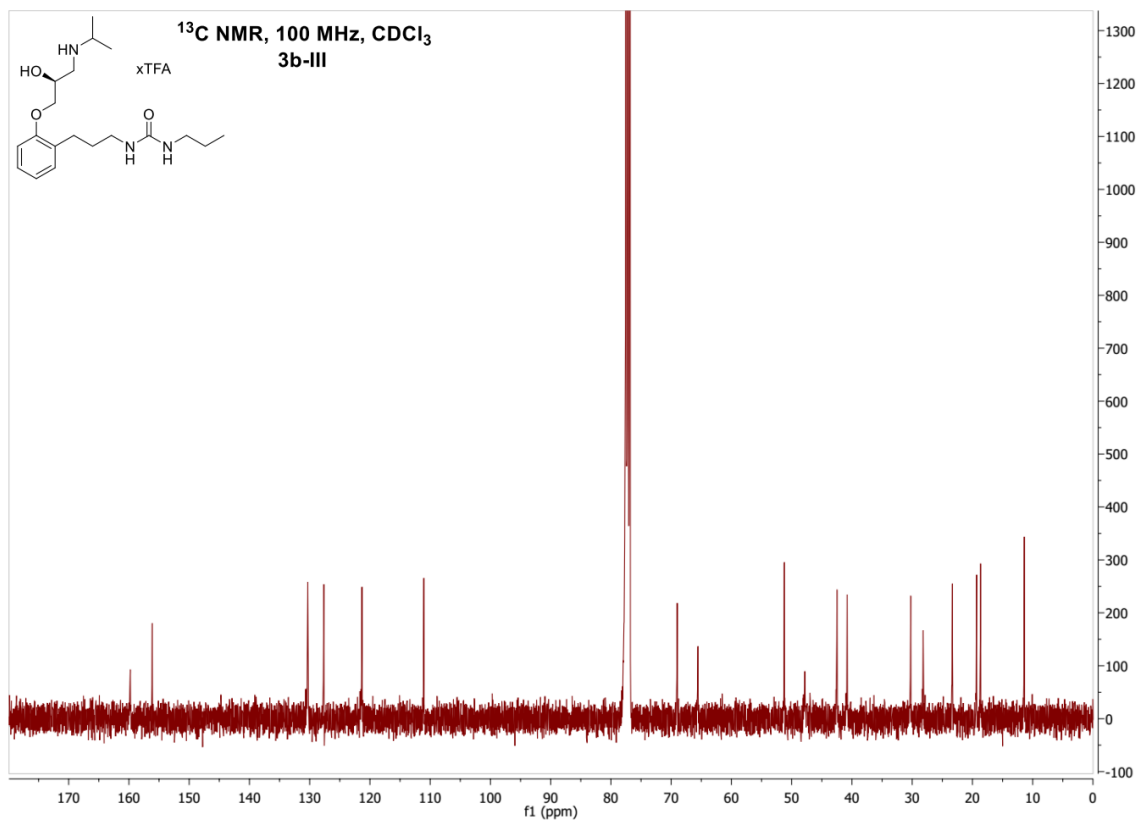
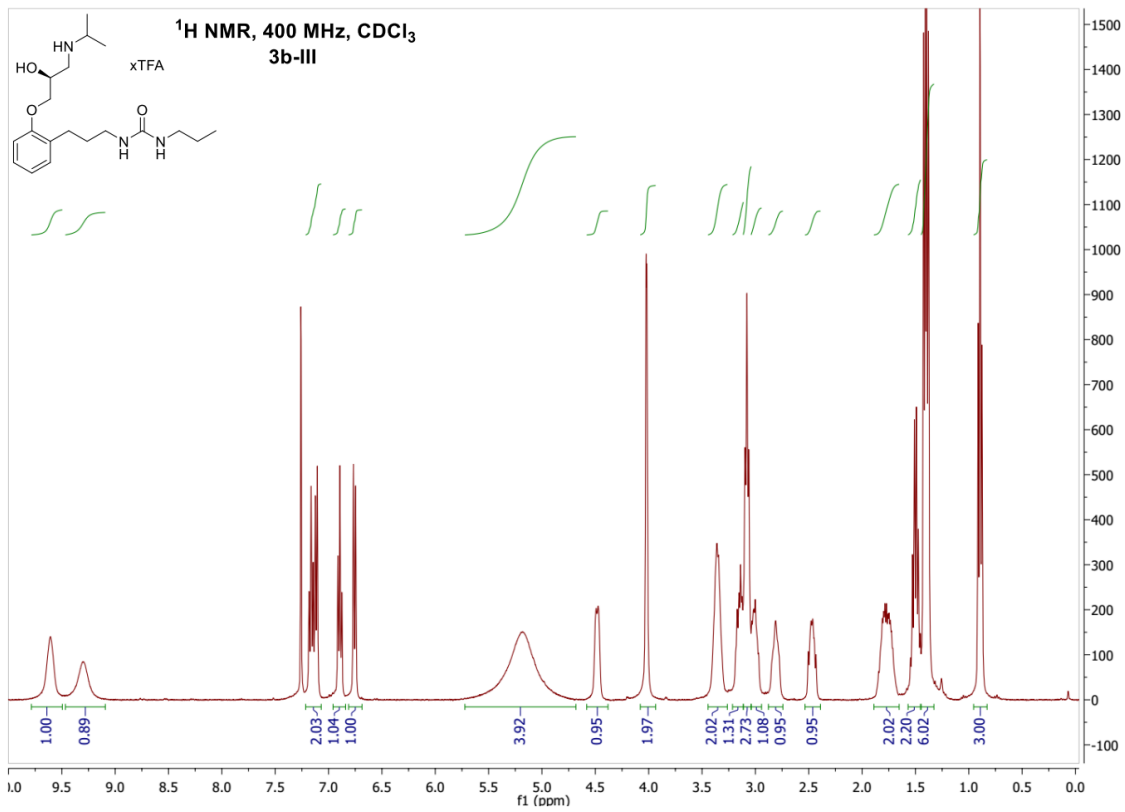


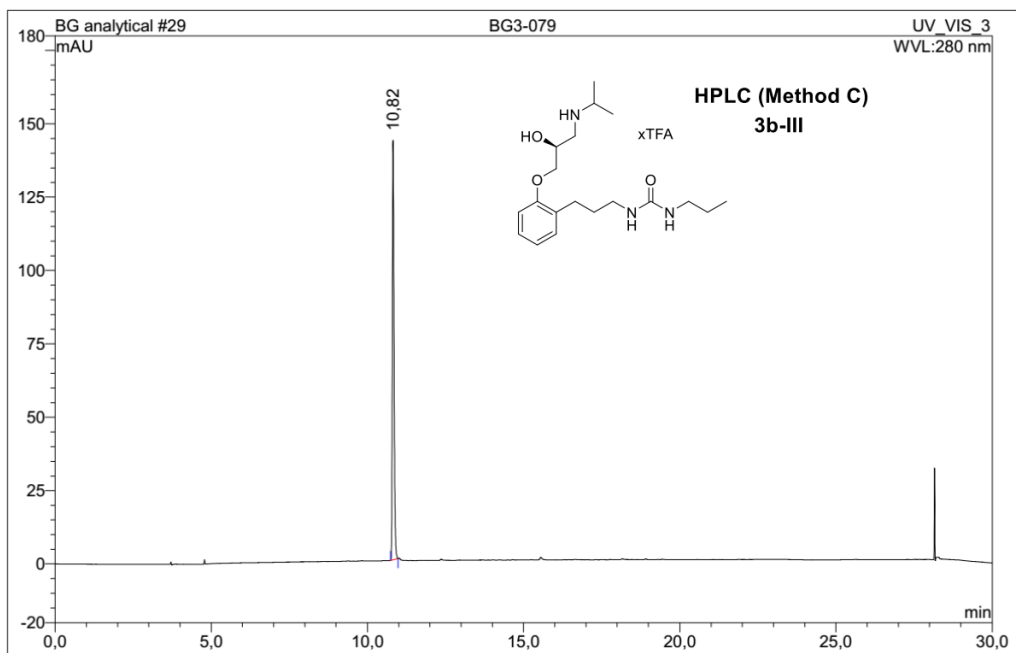
No.	Ret.Time min	Peak Name	Height mAU	Area mAU*min	Rel.Area %	Amount	Resolution(EP)
1	9,88	n.a.	21,188	12,119	5,24	n.a.	27,88
2	22,23	n.a.	2806,323	219,323	94,76	n.a.	n.a.
Total:			2827,511	231,442	100,00	0,000	



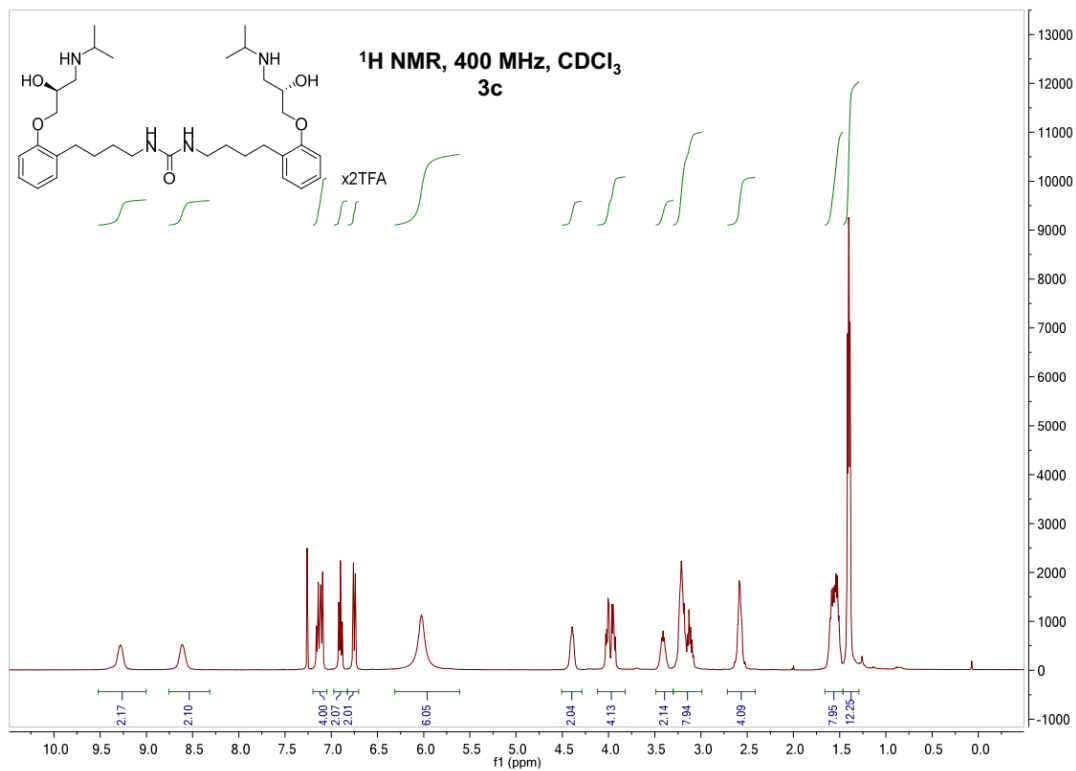


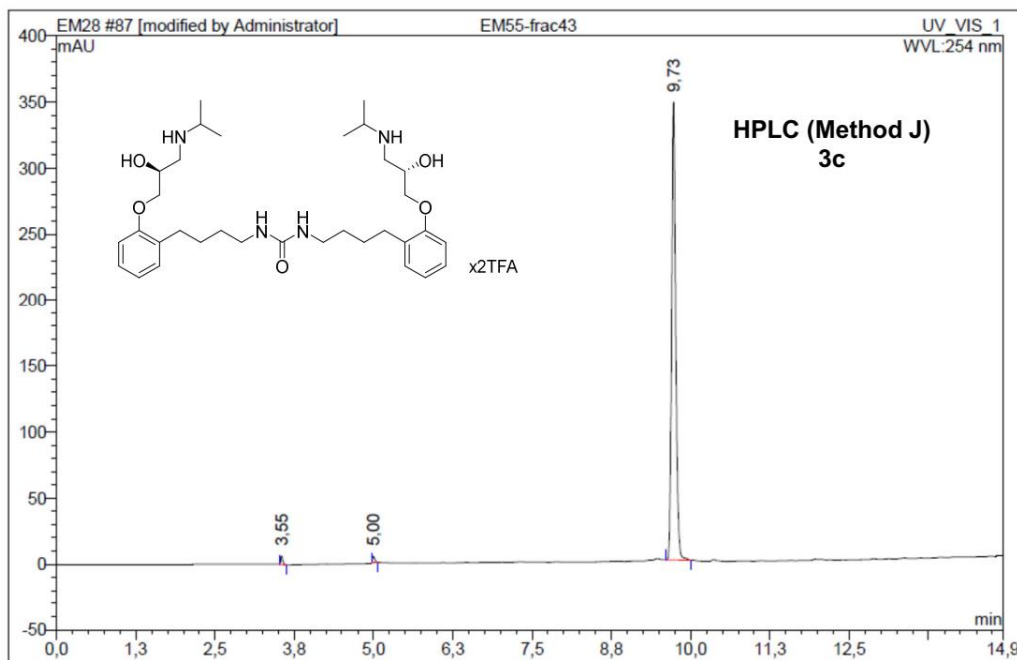
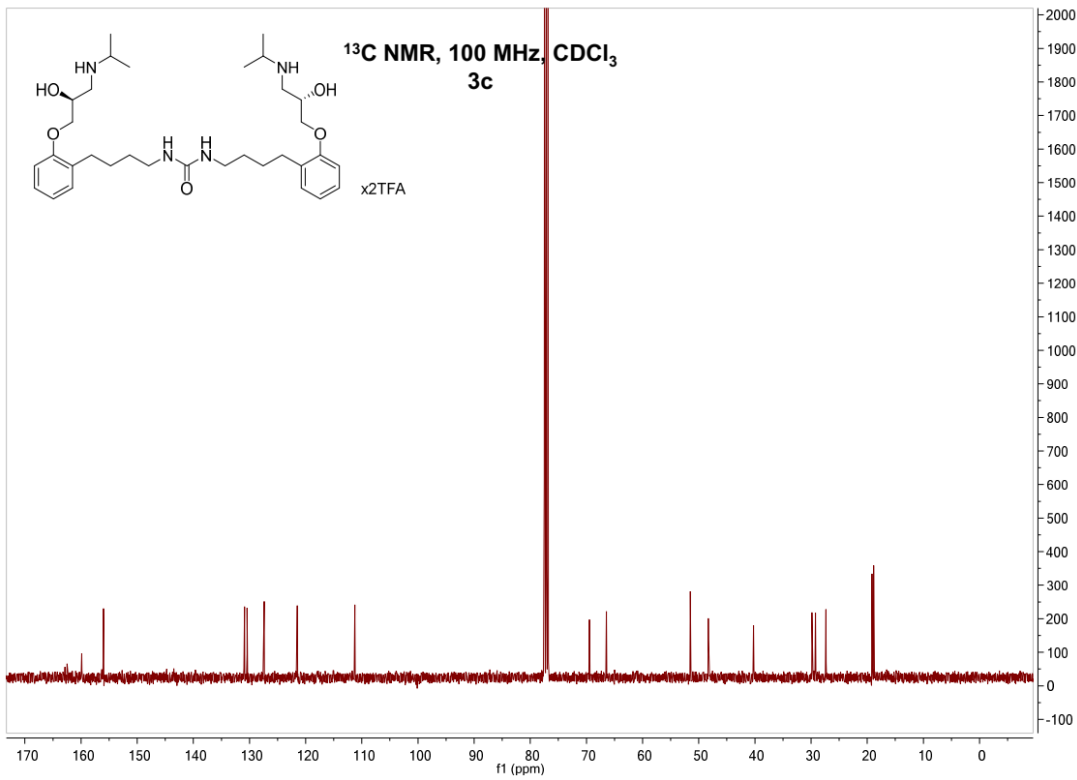
No.	Ret.Time min	Peak Name	Height mAU	Area mAU*min	Rel.Area %	Amount	Resolution(EP)
1	8,22	n.a.	2894,368	177,310	100,00	n.a.	n.a.
Total:			2894,368	177,310	100,00	0,000	



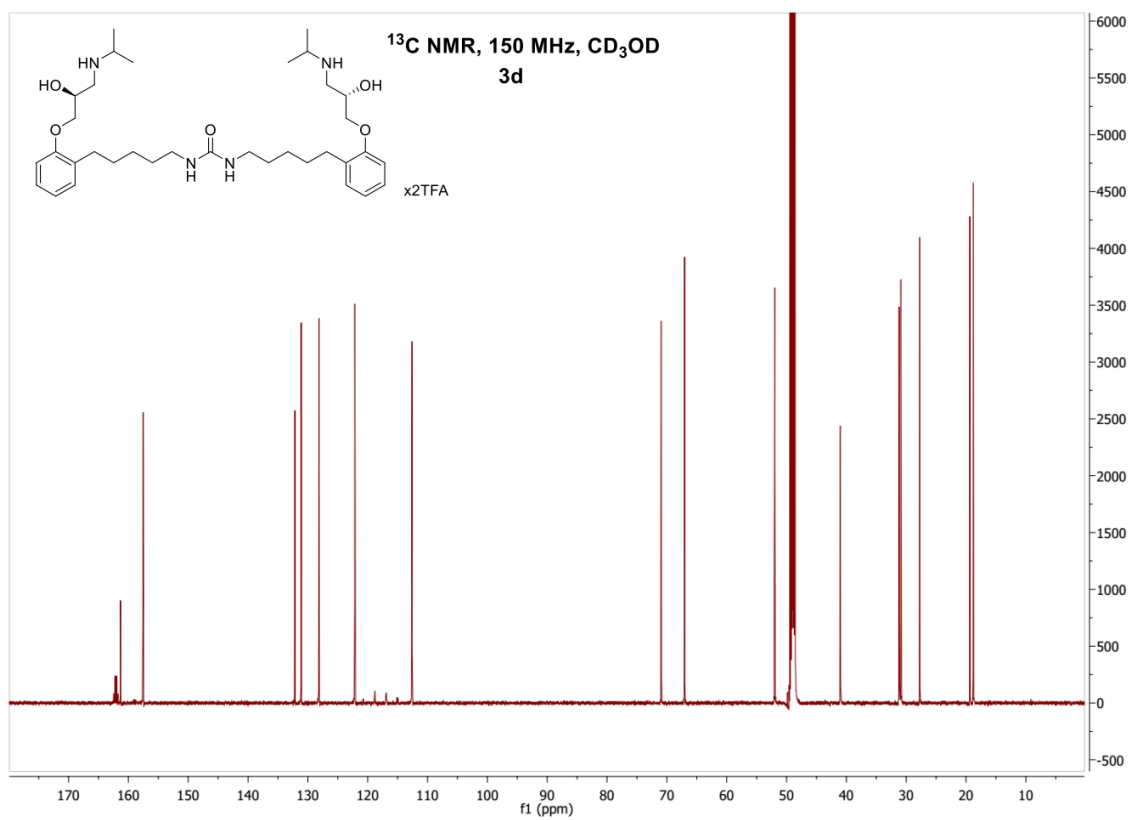
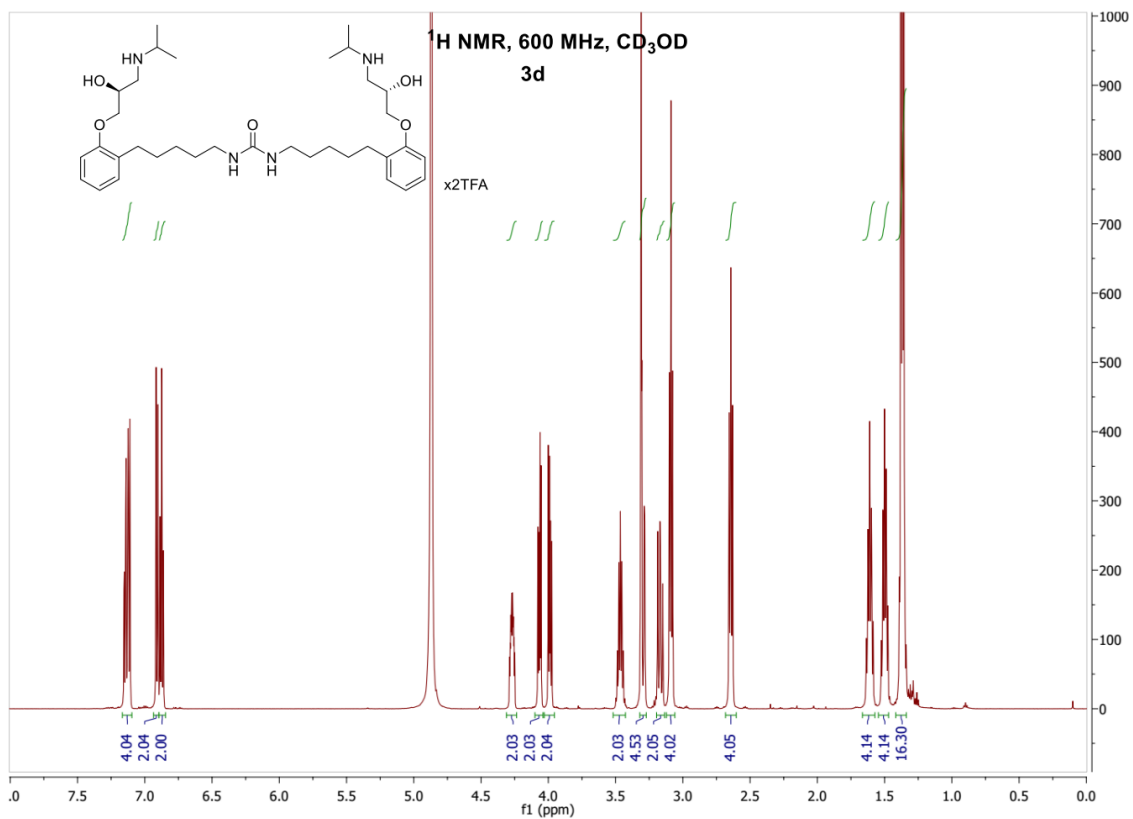


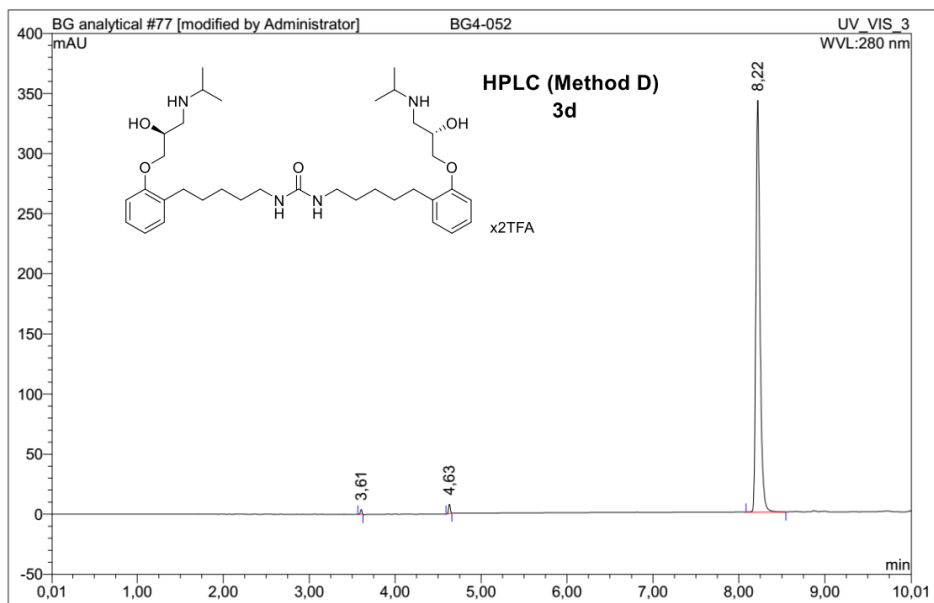
No.	Ret.Time min	Peak Name	Height mAU	Area mAU*min	Rel.Area %	Amount	Resolution(EP)
1	10,82	n.a.	143,015	9,135	100,00	n.a.	n.a.
Total:			143,015	9,135	100,00	0,000	



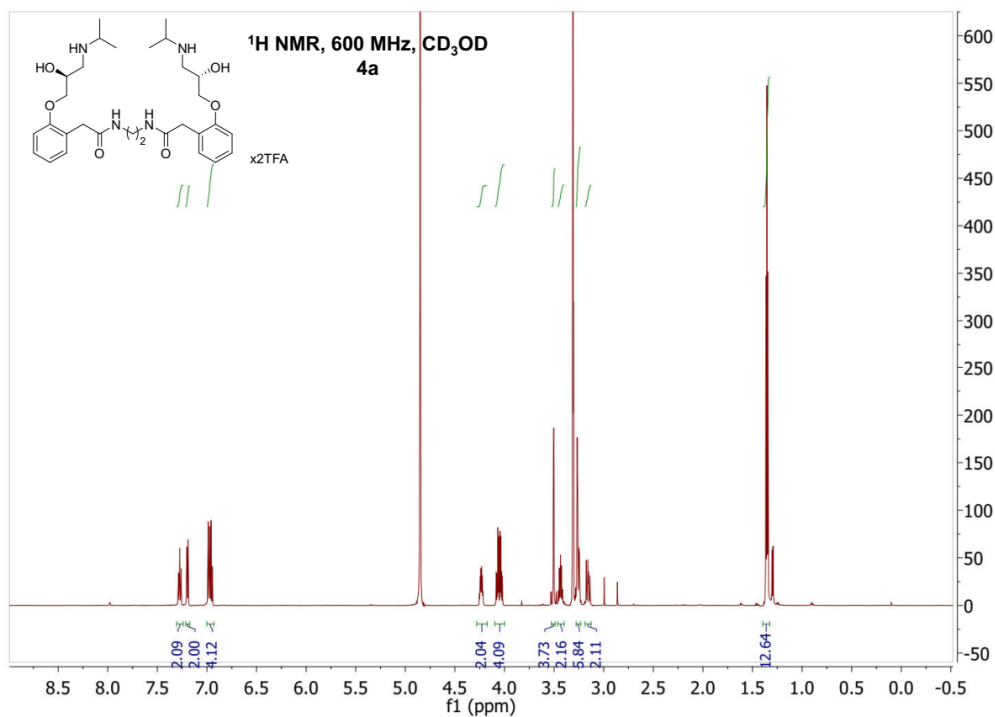


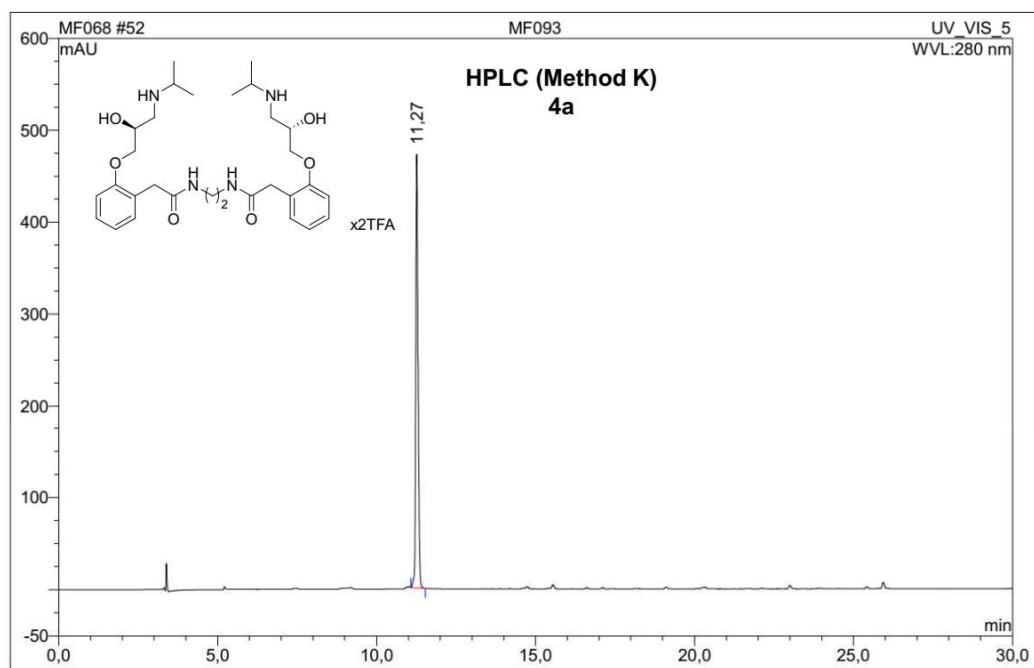
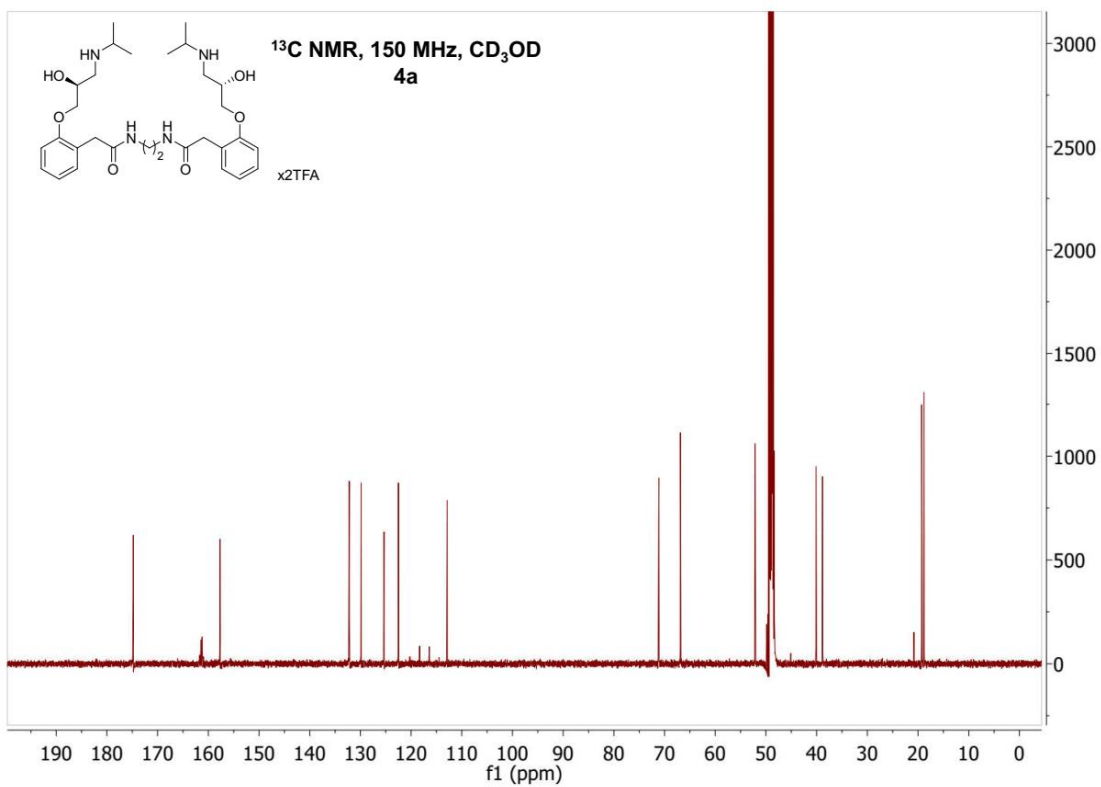
No.	Ret.Time min	Peak Name	Height mAU	Area mAU*min	Rel.Area %	Amount	Resolution(EP)
1	3,55	n.a.	6,472	0,231	0,89	n.a.	23,44
2	5,00	n.a.	4,784	0,198	0,76	n.a.	52,90
3	9,73	n.a.	346,670	25,639	98,36	n.a.	n.a.
Total:			357,926	26,068	100,00	0,000	



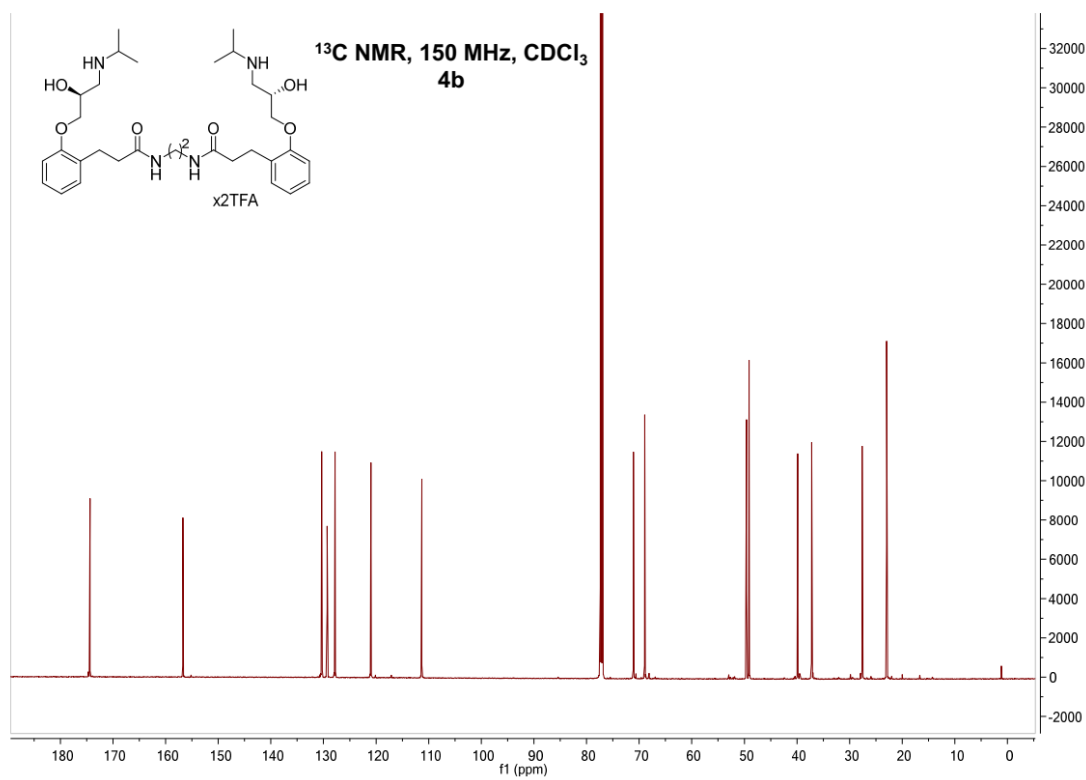
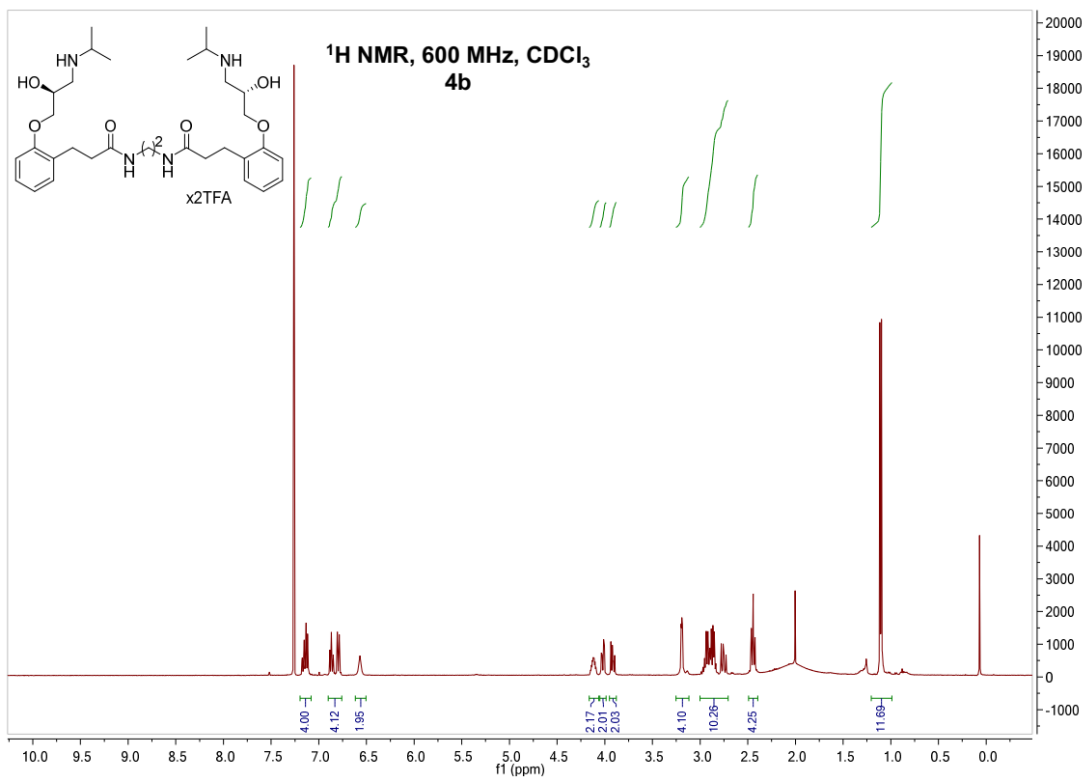


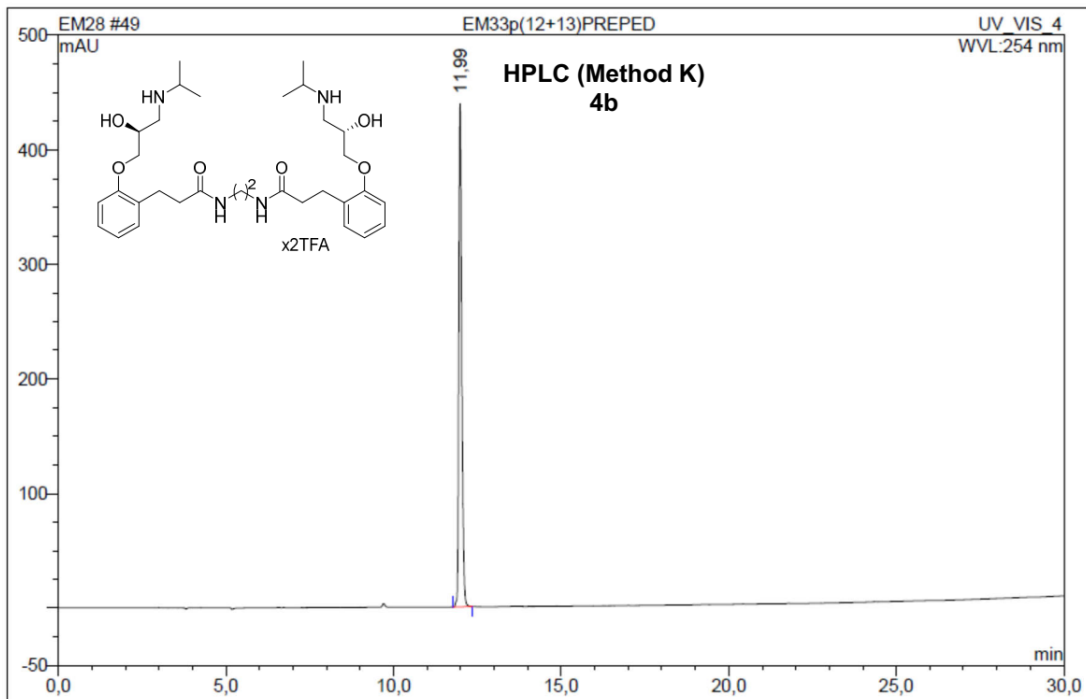
No.	Ret.Time min	Peak Name	Height mAU	Area mAU*min	Rel.Area %	Amount	Resolution(EP)
1	3,61	n.a.	3,885	0,087	0,44	n.a.	27,03
2	4,63	n.a.	7,699	0,182	0,92	n.a.	57,58
3	8,22	n.a.	342,614	19,454	98,63	n.a.	n.a.
Total:			354,198	19,724	100,00	0,000	



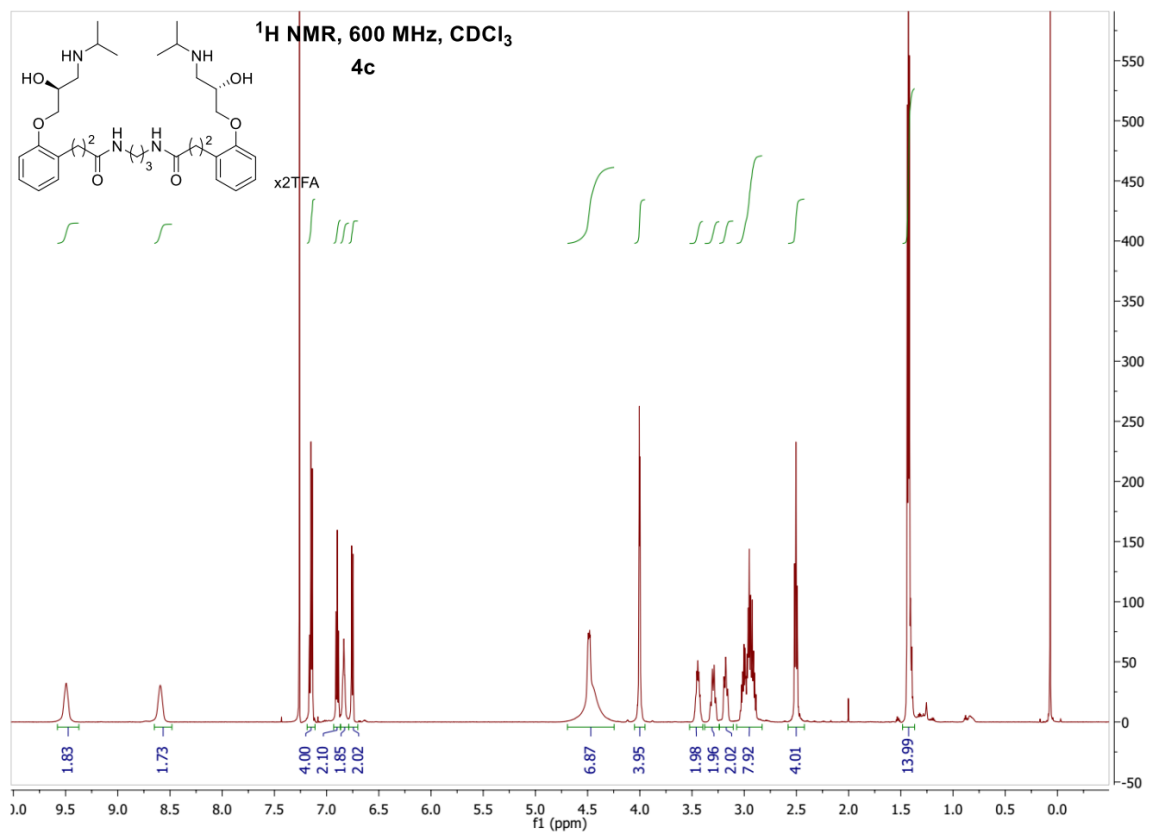


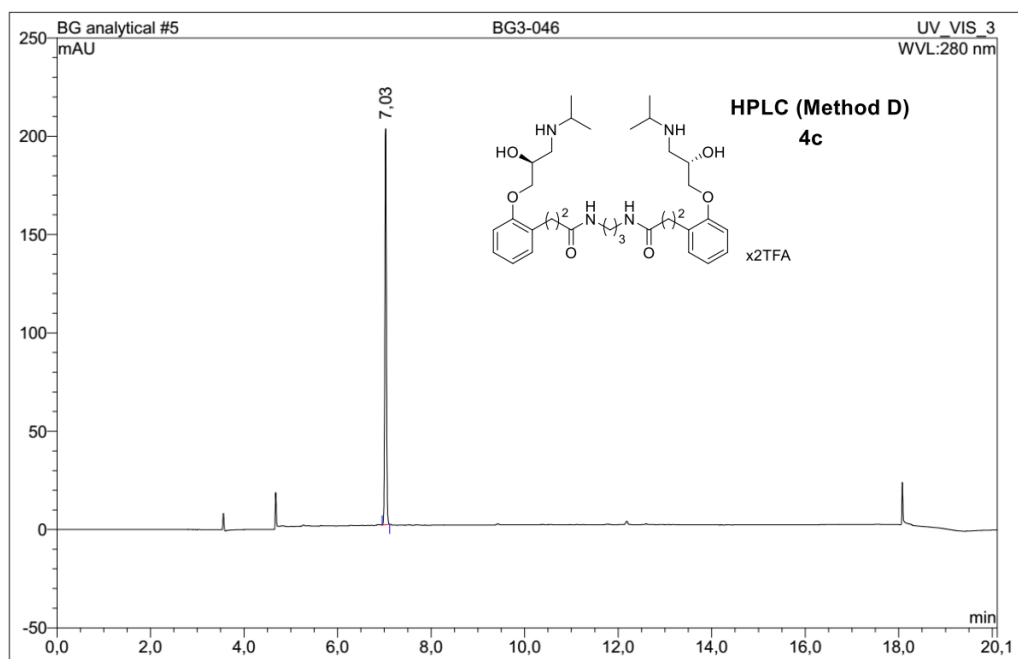
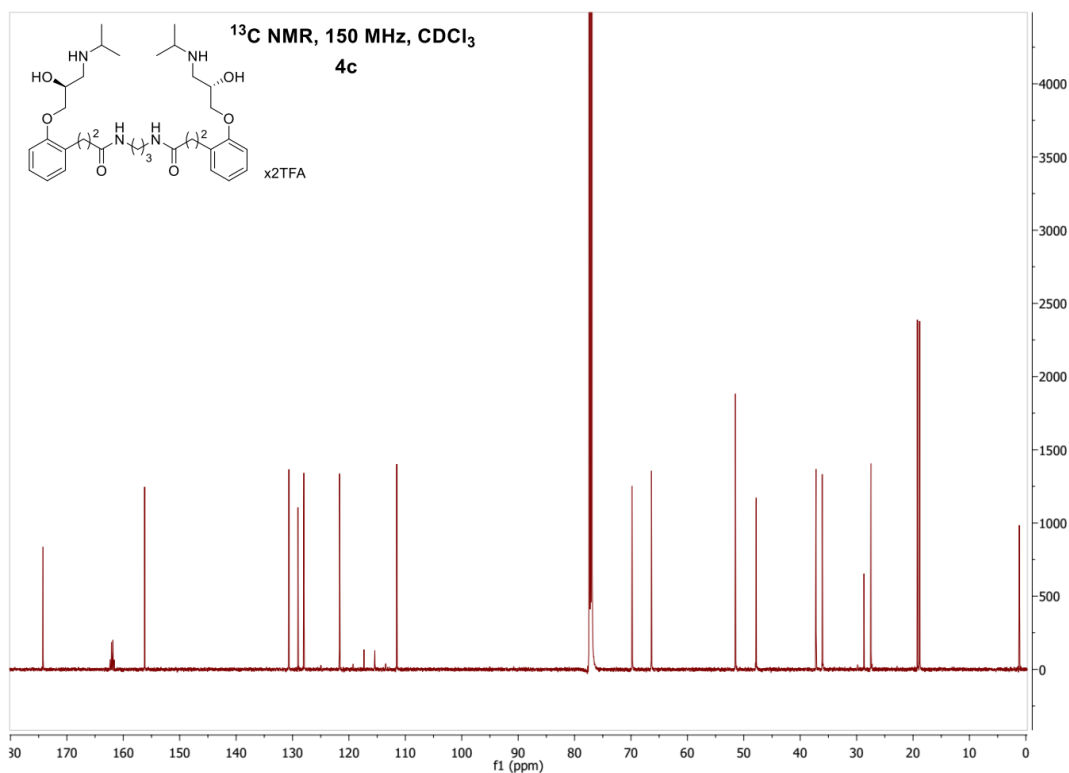
No.	Ret.Time min	Peak Name	Height mAU	Area mAU*min	Rel.Area %	Amount	Resolution(EP)
1	11,27	n.a.	472,116	38,600	100,00	n.a.	n.a.
Total:			472,116	38,600	100,00	0,000	



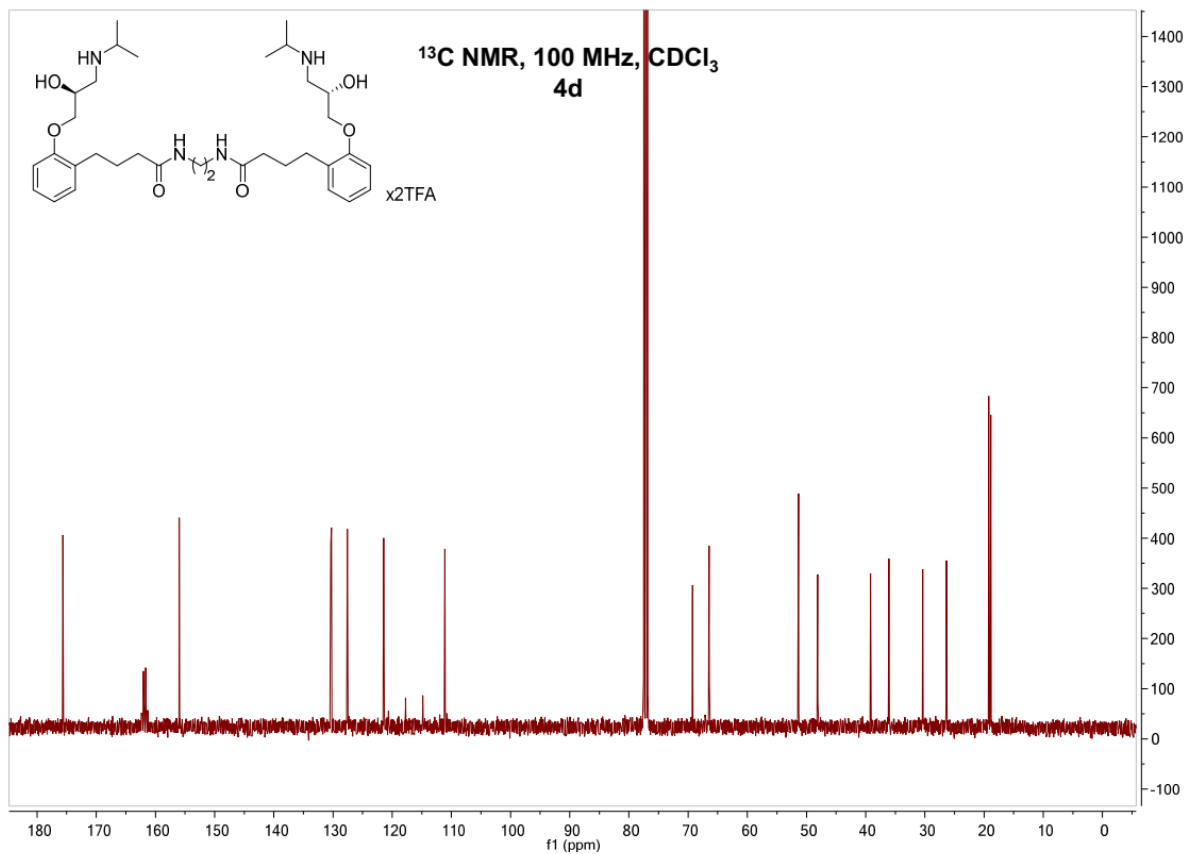
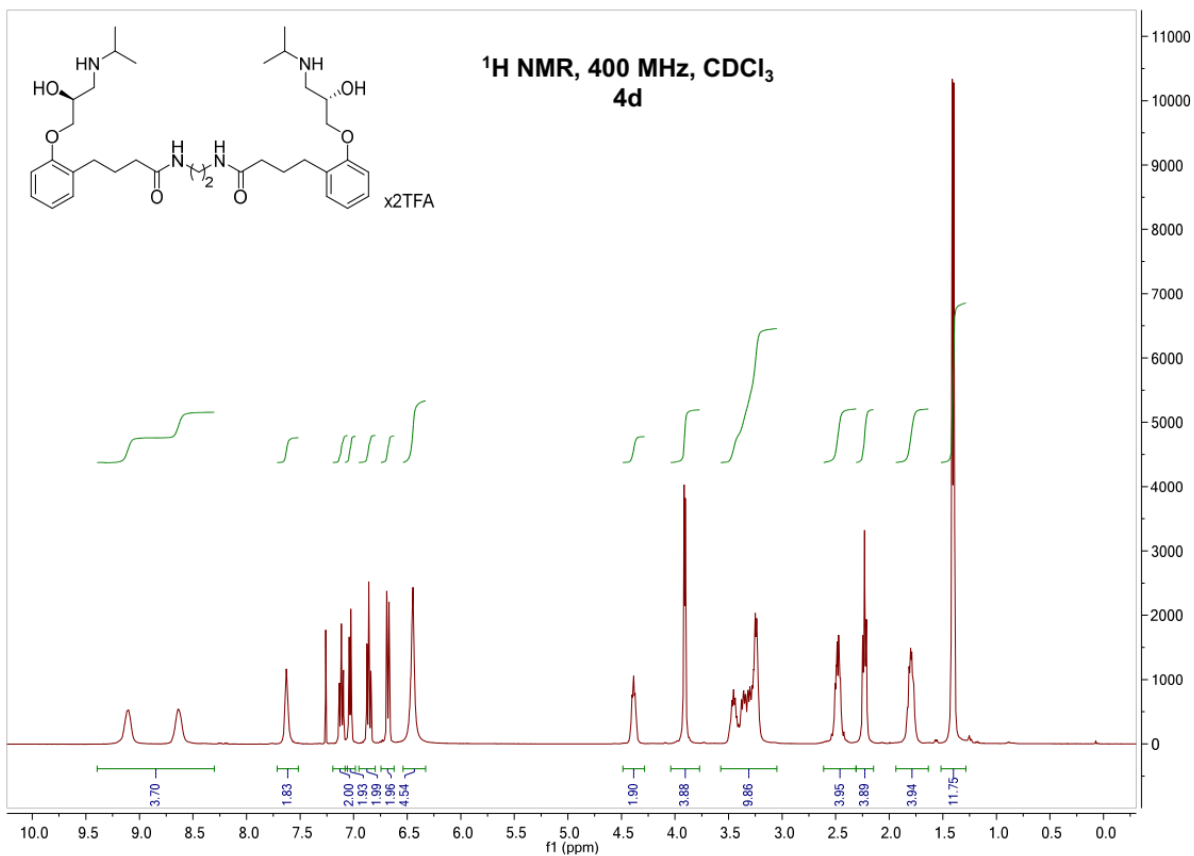


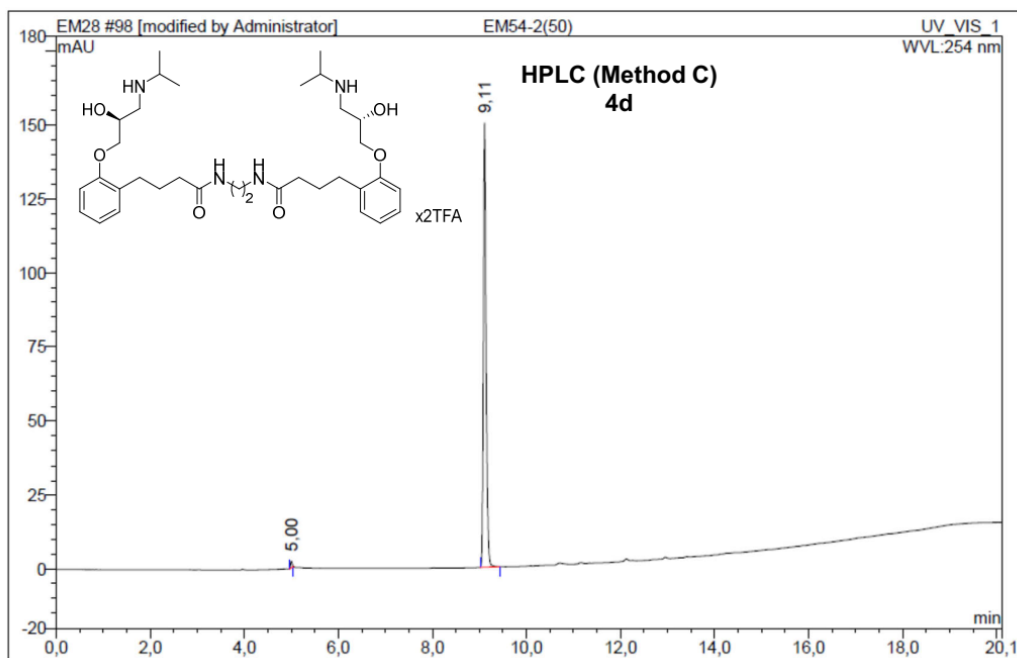
No.	Ret.Time min	Peak Name	Height mAU	Area mAU*min	Rel.Area %	Amount	Resolution(EP)
1	11,99	n.a.	439,439	43,786	100,00	n.a.	n.a.
Total:			439,439	43,786	100,00	0,000	



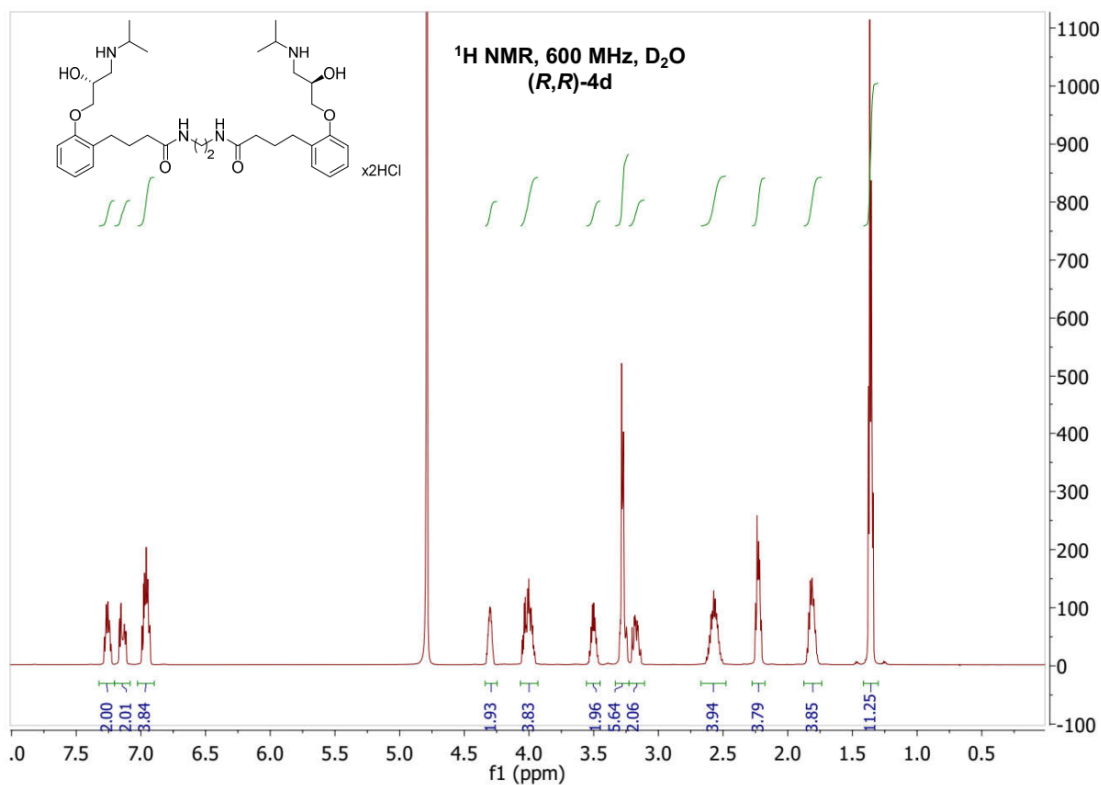


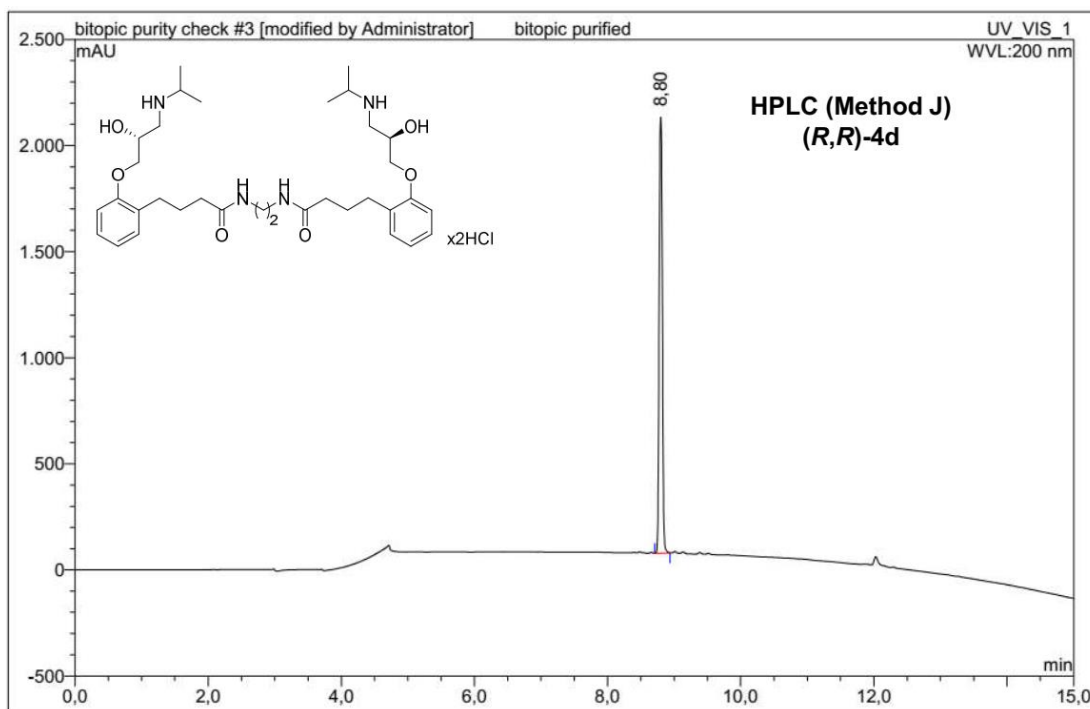
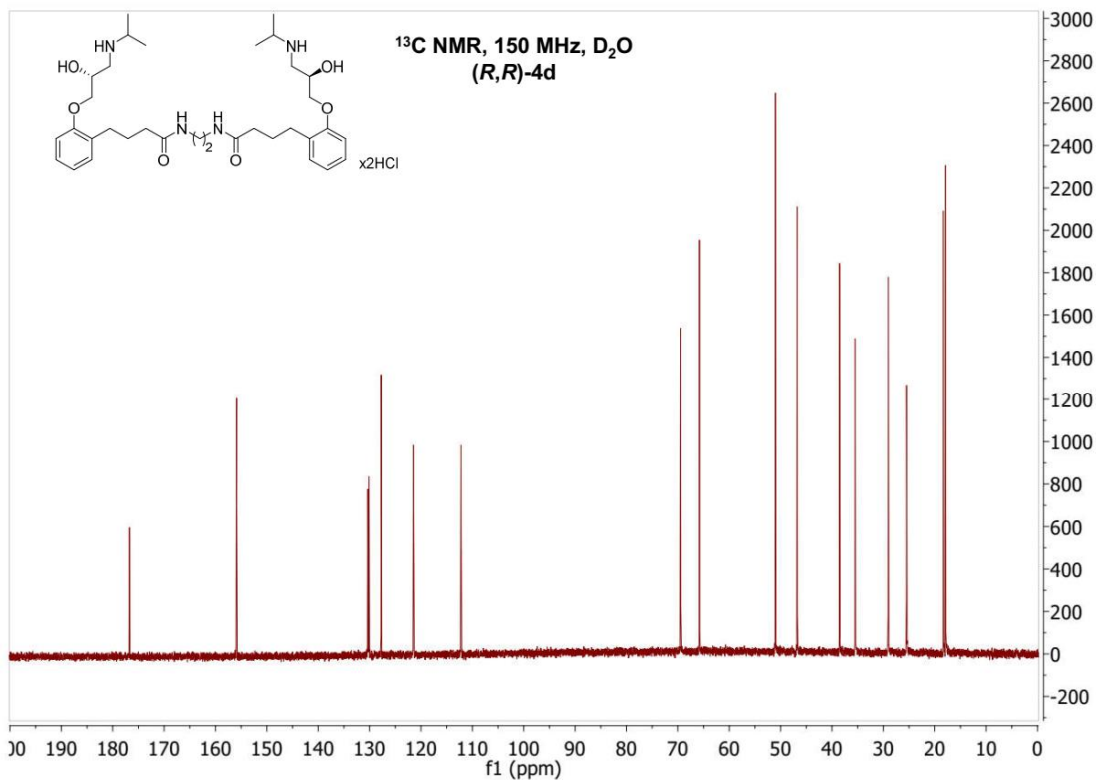
No.	Ret.Time min	Peak Name	Height mAU	Area mAU*min	Rel.Area %	Amount	Resolution(EP)
1	7,03	n.a.	201,411	7,972	100,00	n.a.	n.a.
Total:			201,411	7,972	100,00	0,000	



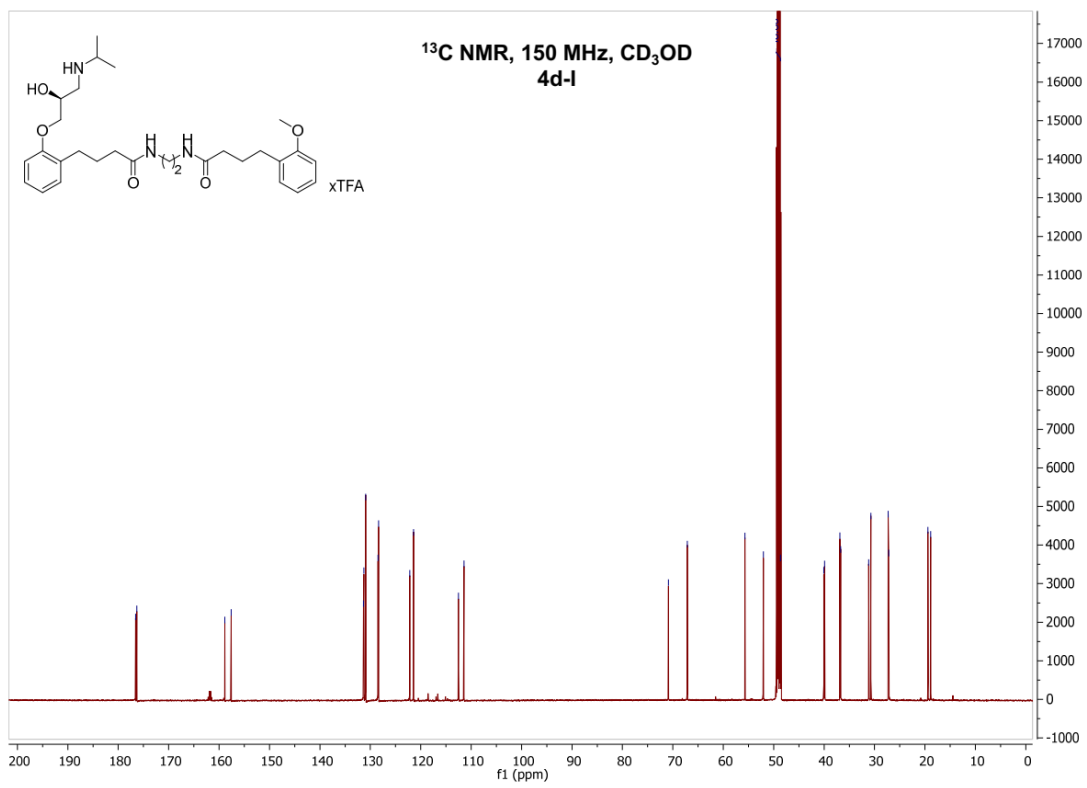
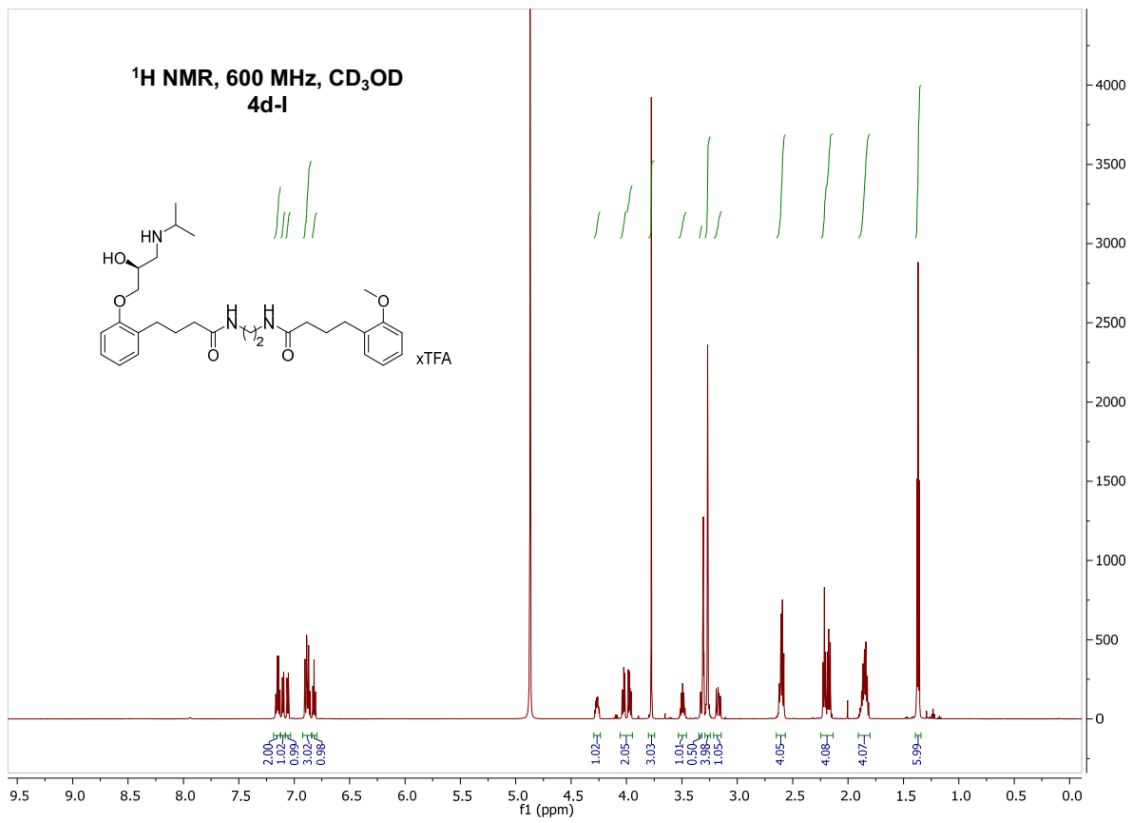


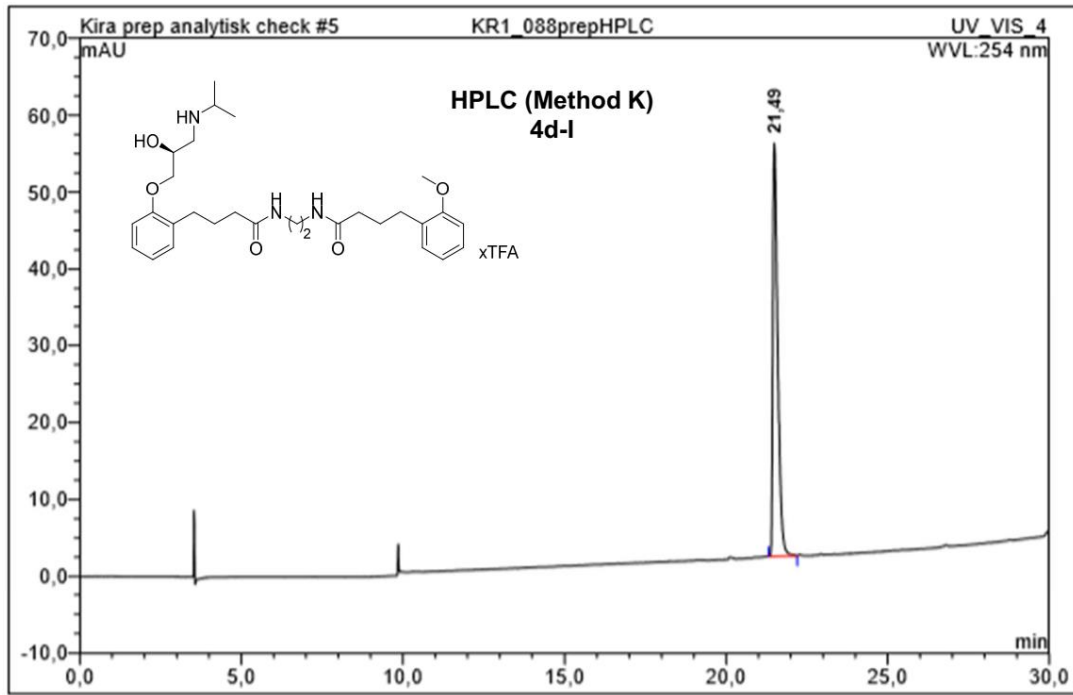
No.	Ret.Time min	Peak Name	Height mAU	Area mAU*min	Rel.Area %	Amount	Resolution(EP)
1	5,00	n.a.	2,271	0,088	0,87	n.a.	50,04
2	9,11	n.a.	149,956	10,038	99,13	n.a.	n.a.
Total:			152,227	10,126	100,00	0,000	



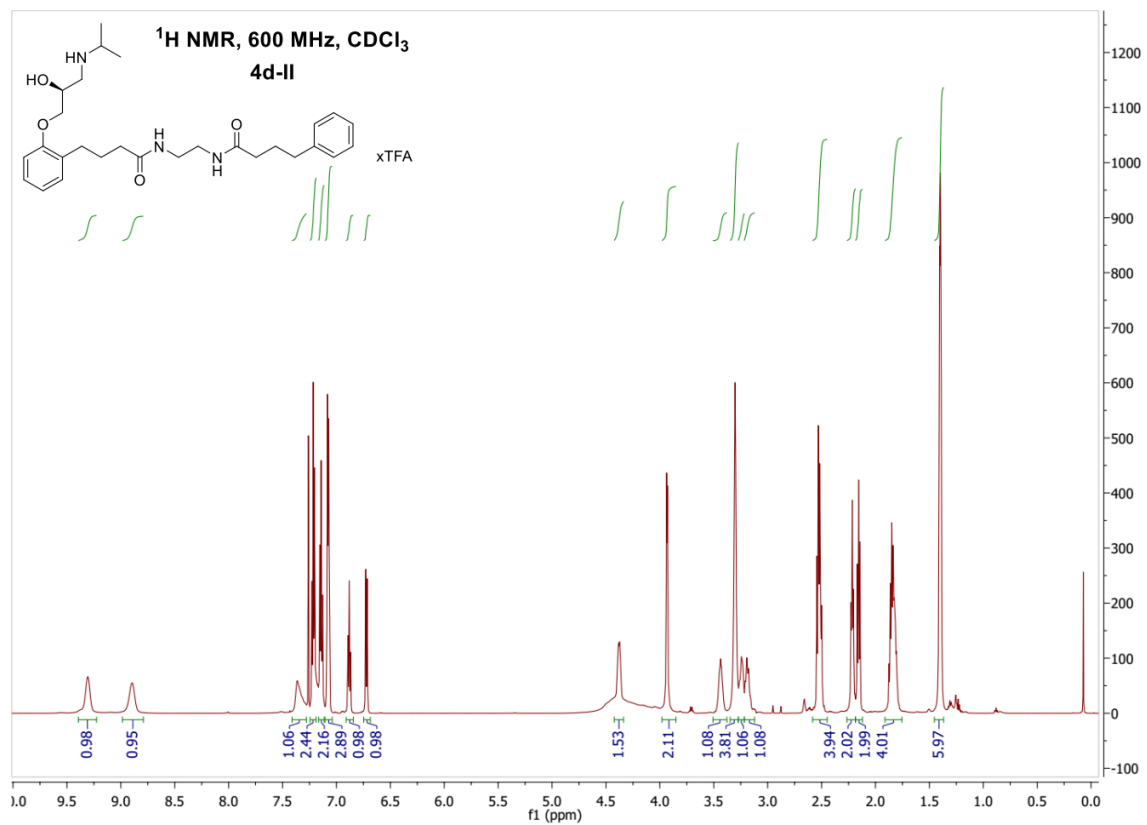


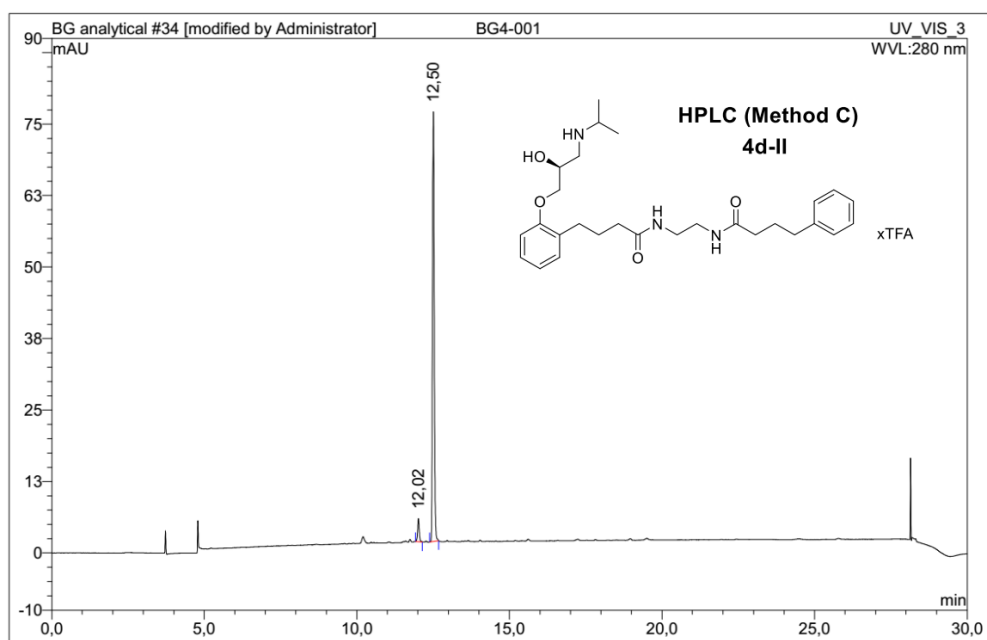
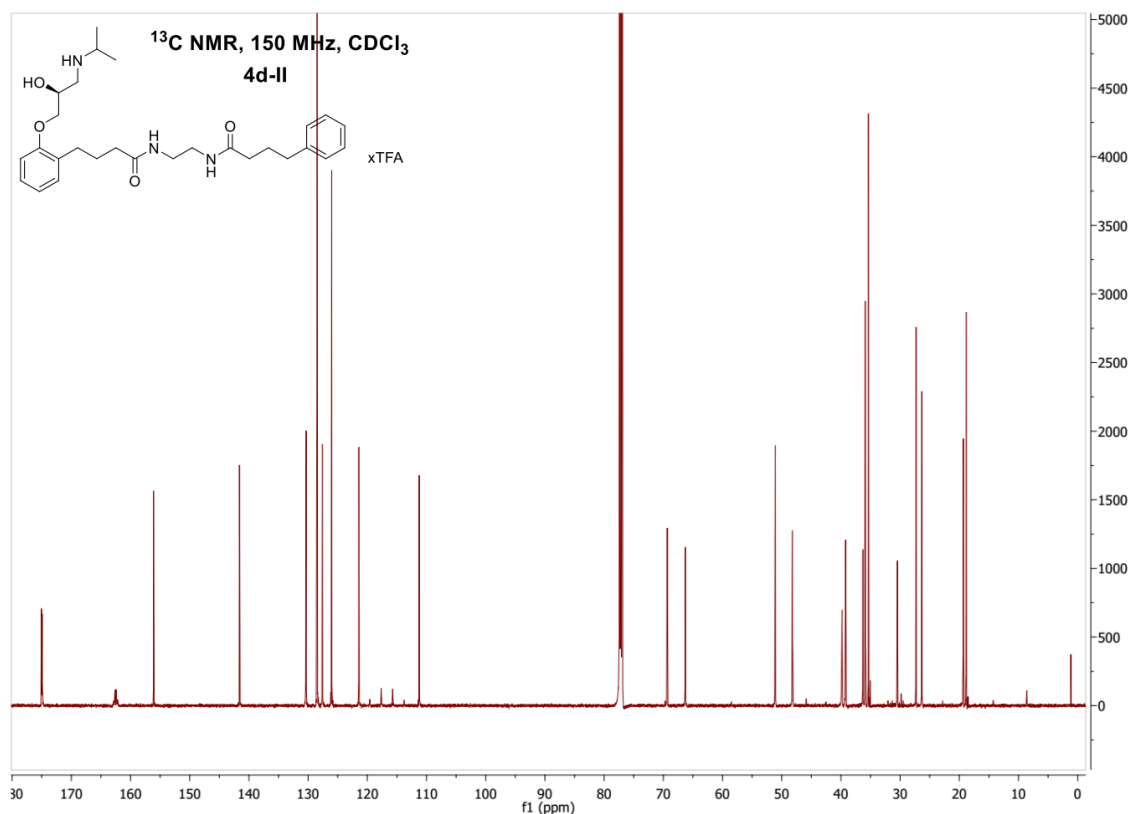
No.	Ret.Time min	Peak Name	Height mAU	Area mAU*min	Rel.Area %	Amount	Resolution(EP)
1	8,80	n.a.	2055,300	118,120	100,00	n.a.	n.a.
Total:			2055,300	118,120	100,00	0,000	



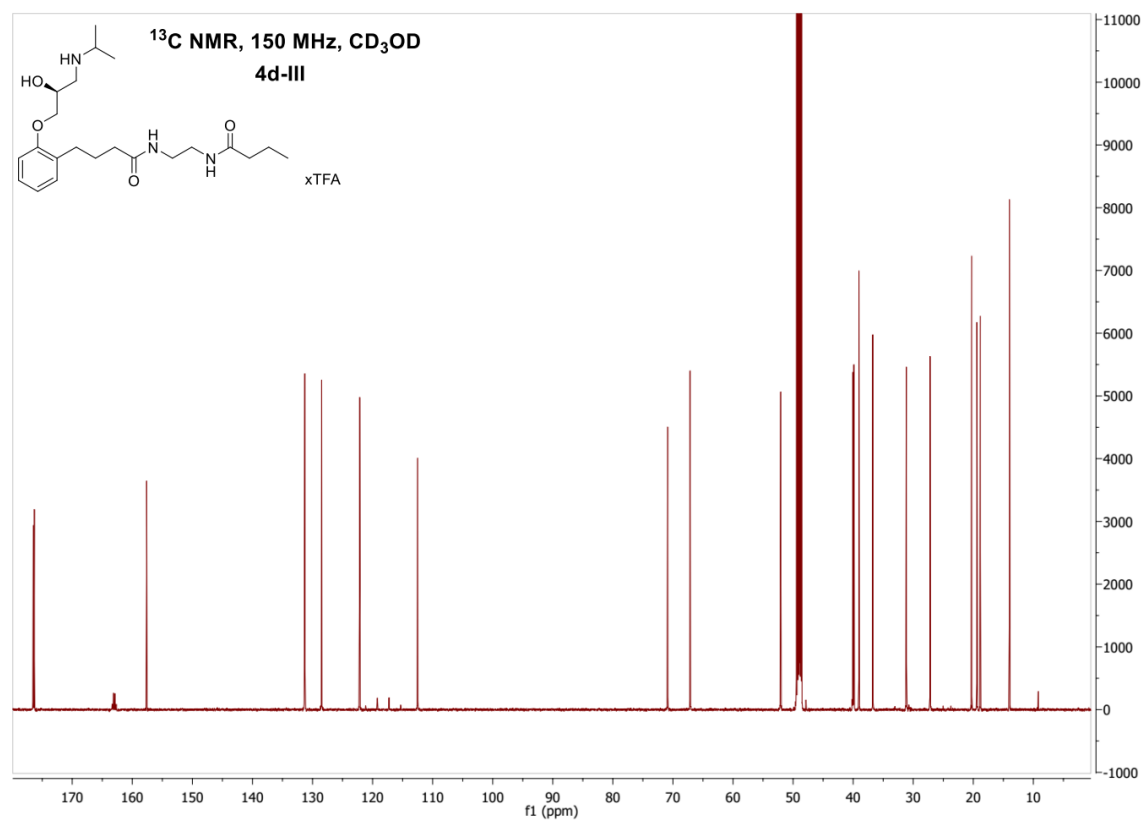
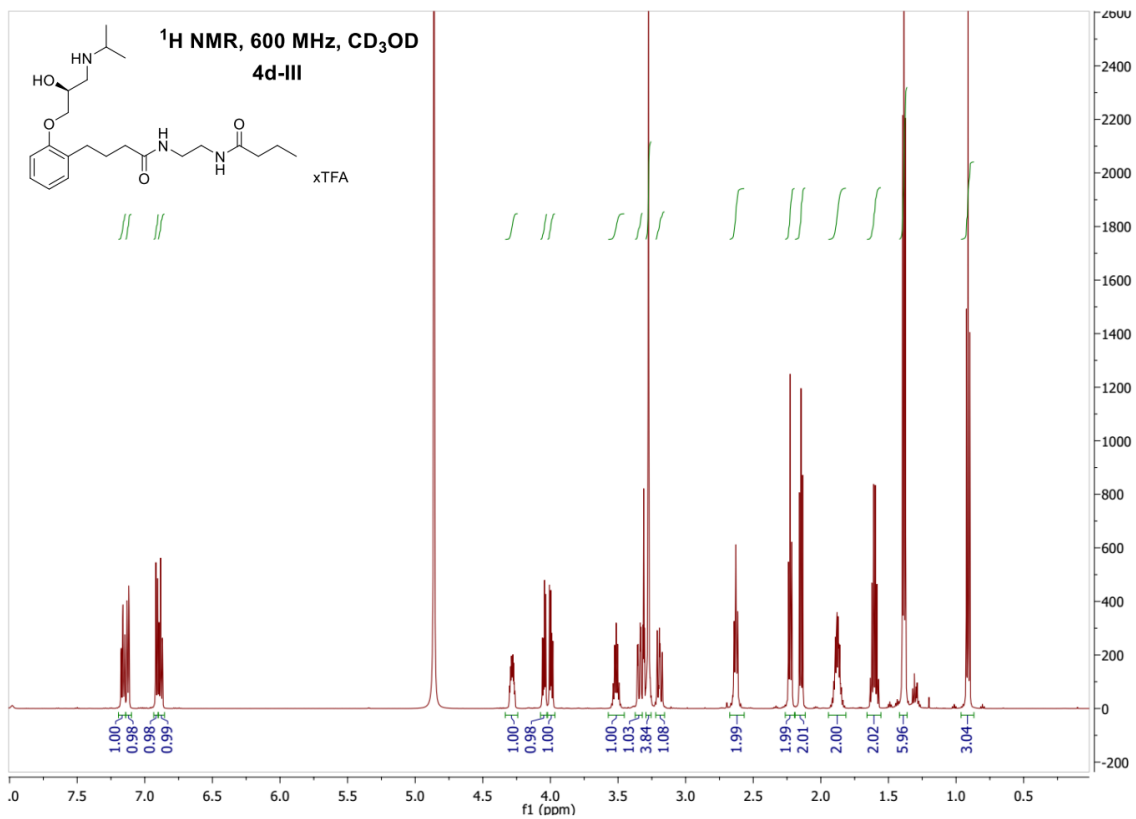


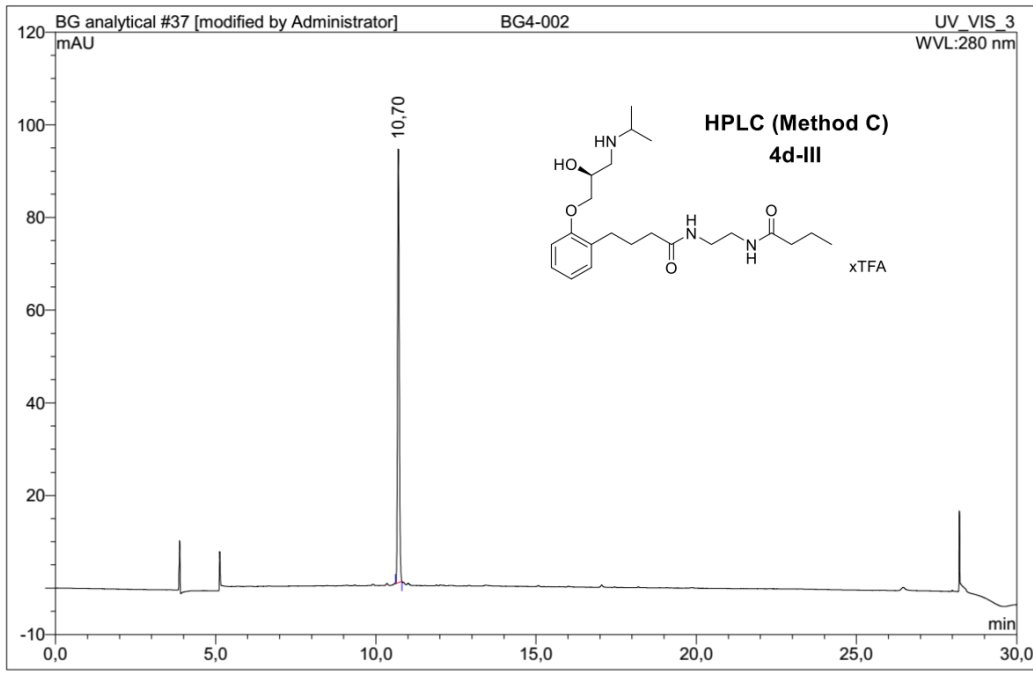
No.	Ret.Time min	Peak Name	Height mAU	Area mAU*min	Rel.Area %	Amount	Resolution(EP)
1	21.49	n.a.	53.732	9.434	100.00	n.a.	n.a.
Total:			53,732	9,434	100,00	0,000	



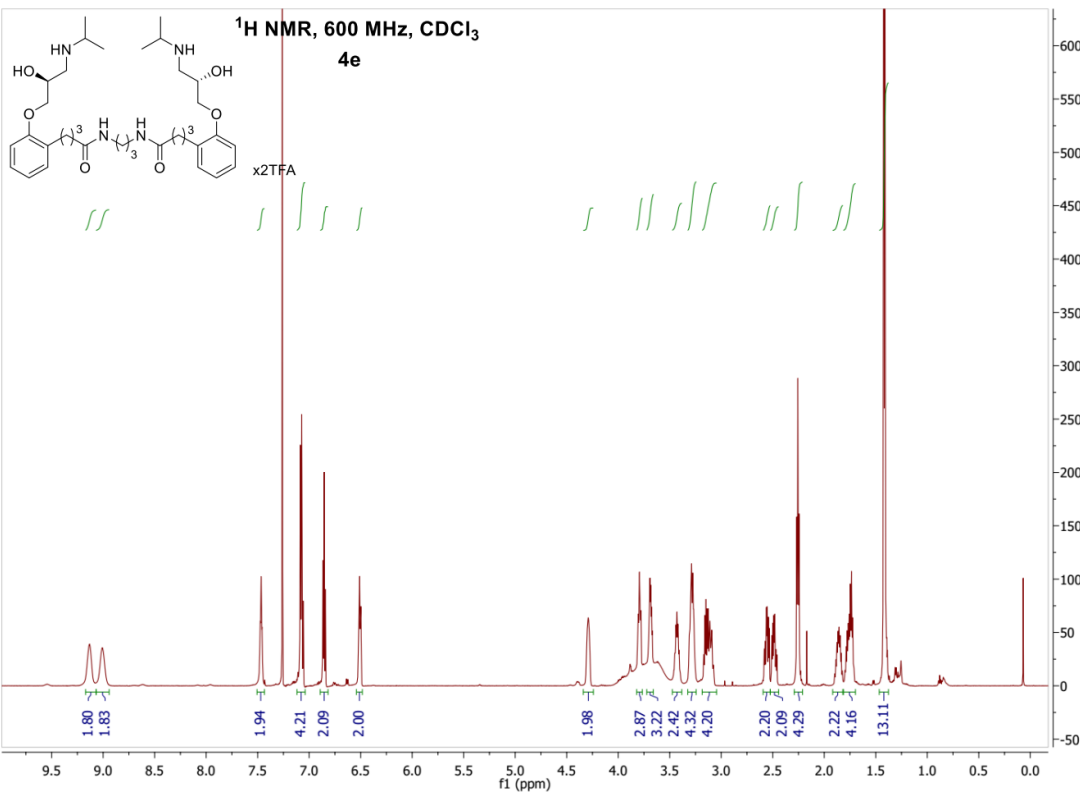


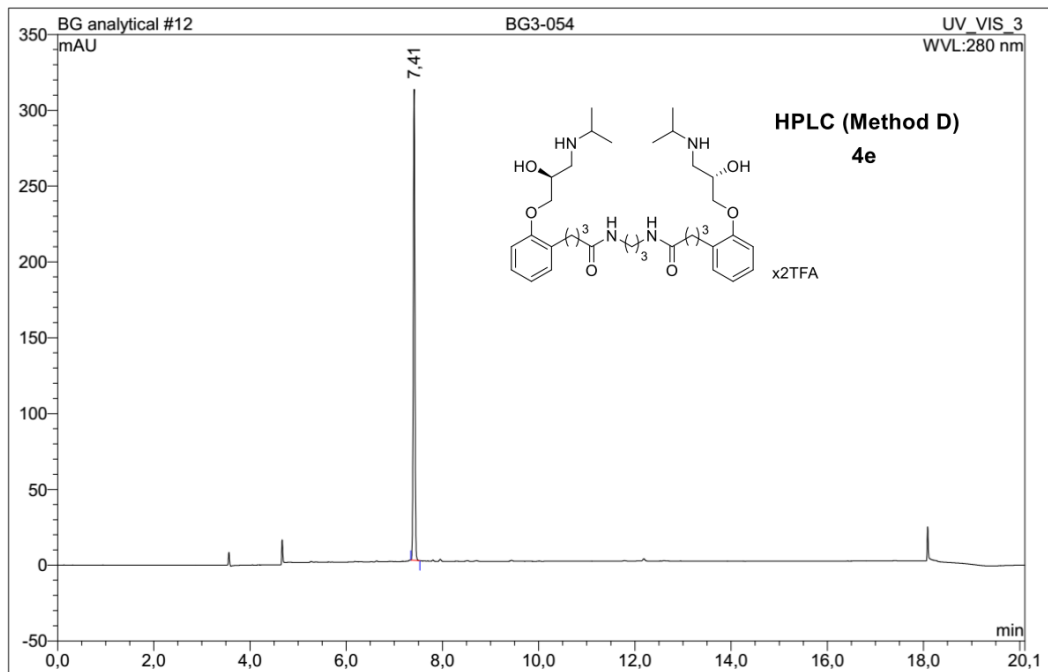
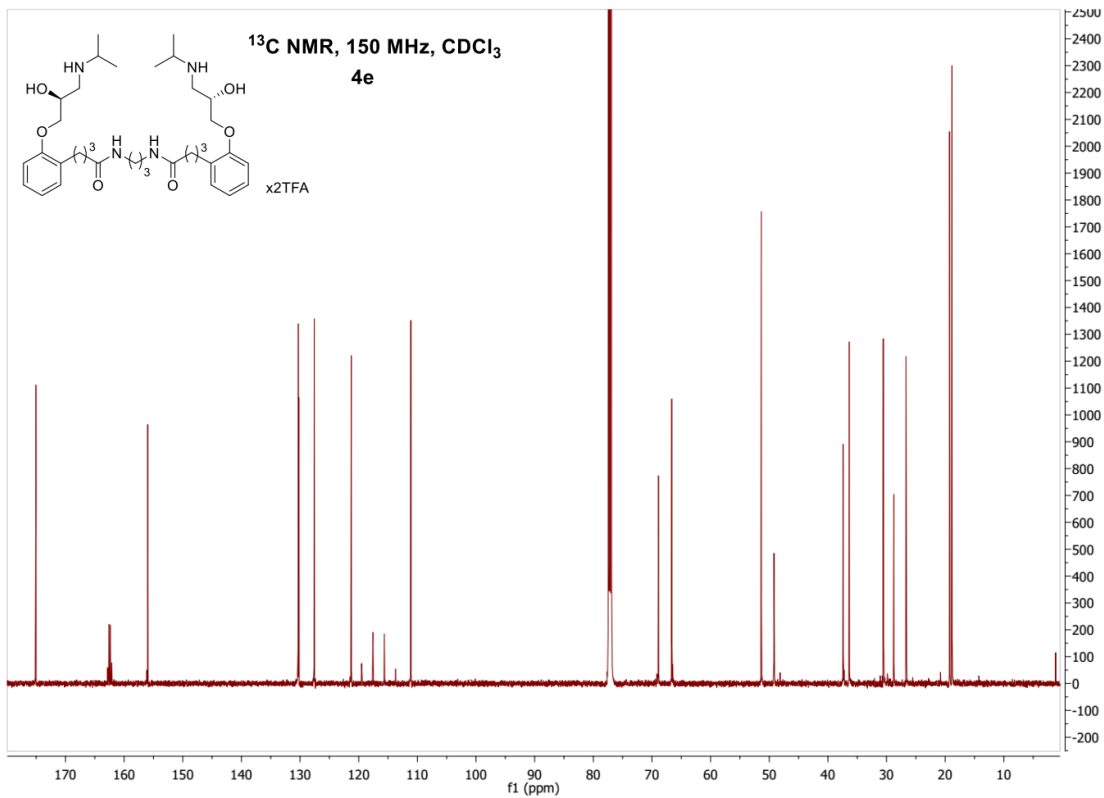
No.	Ret.Time min	Peak Name	Height mAU	Area mAU*min	Rel.Area %	Amount	Resolution(EP)
1	12,02	n.a.	4,019	0,255	5,27	n.a.	5,07
2	12,50	n.a.	75,159	4,592	94,73	n.a.	n.a.
Total:			79,178	4,847	100,00	0,000	



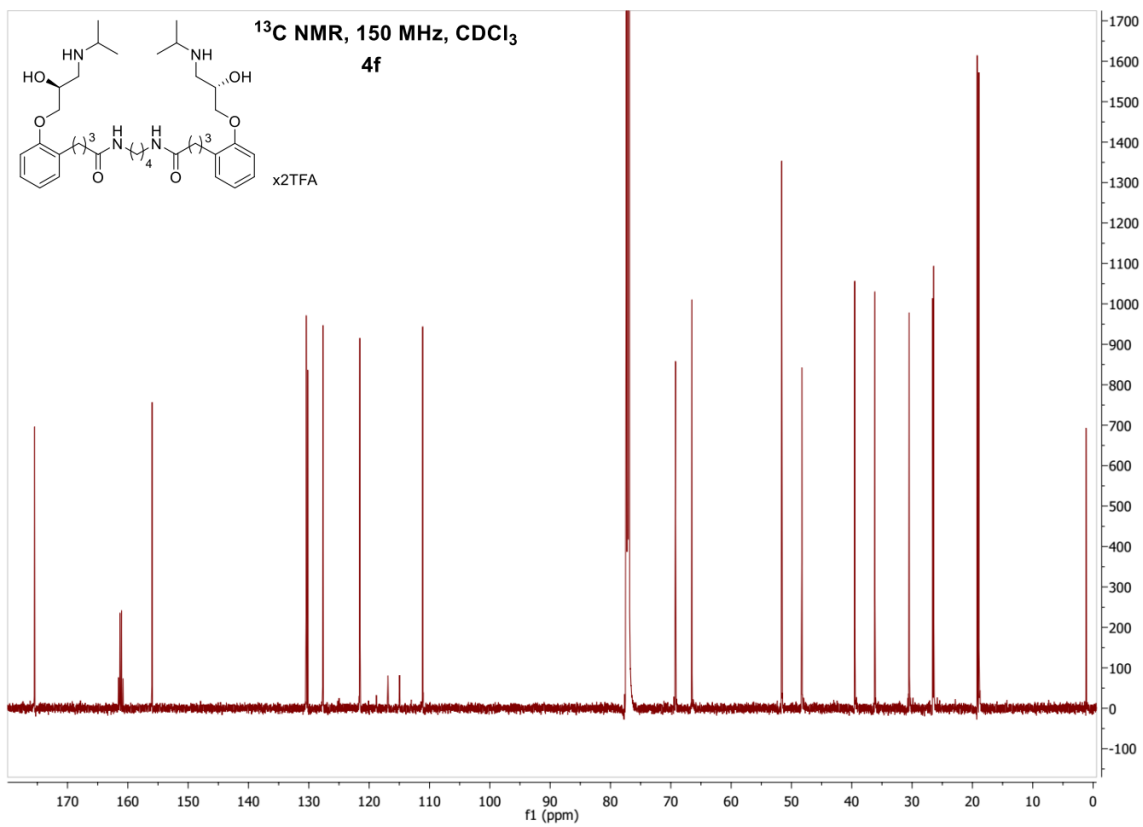
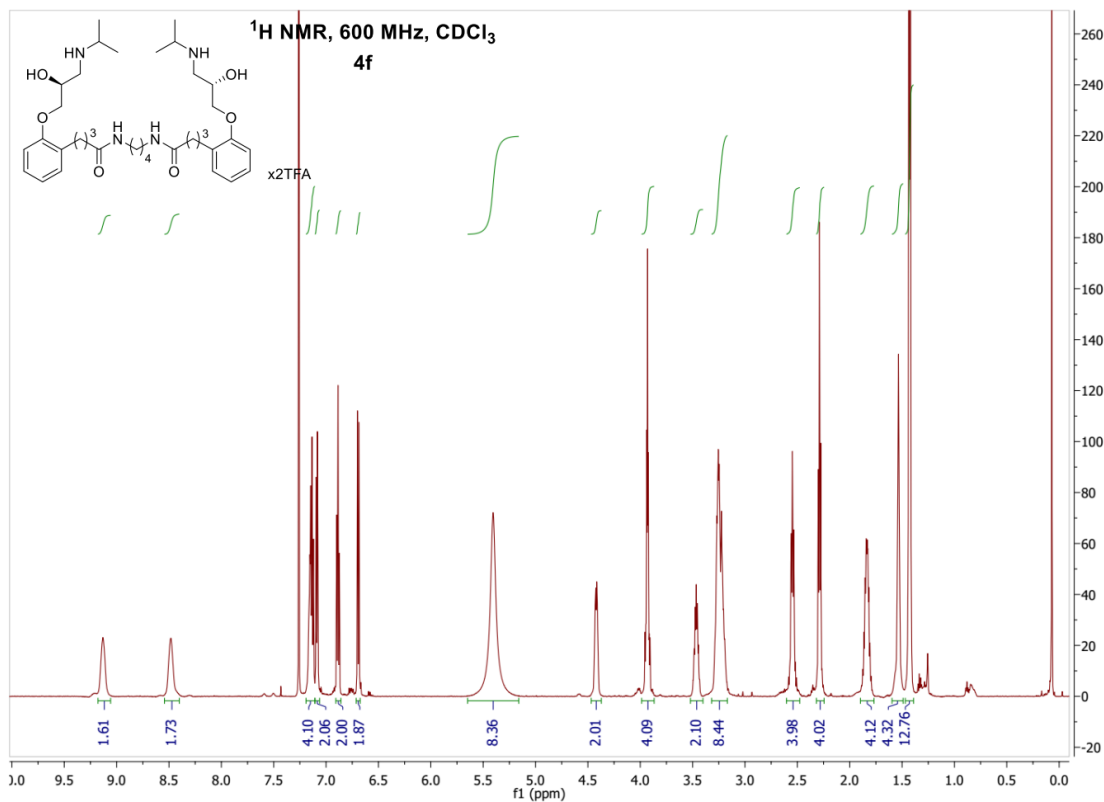


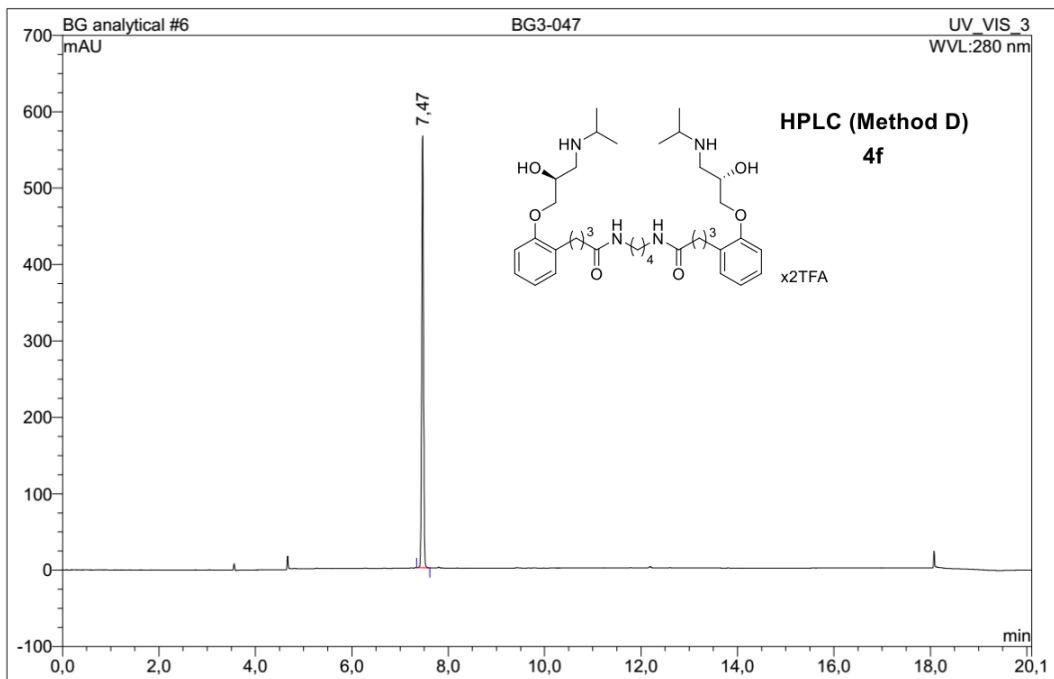
No.	Ret.Time min	Peak Name	Height mAU	Area mAU*min	Rel.Area %	Amount	Resolution(EP)
1	10,70	n.a.	93,617	5,773	100,00	n.a.	n.a.
Total:			93,617	5,773	100,00	0,000	



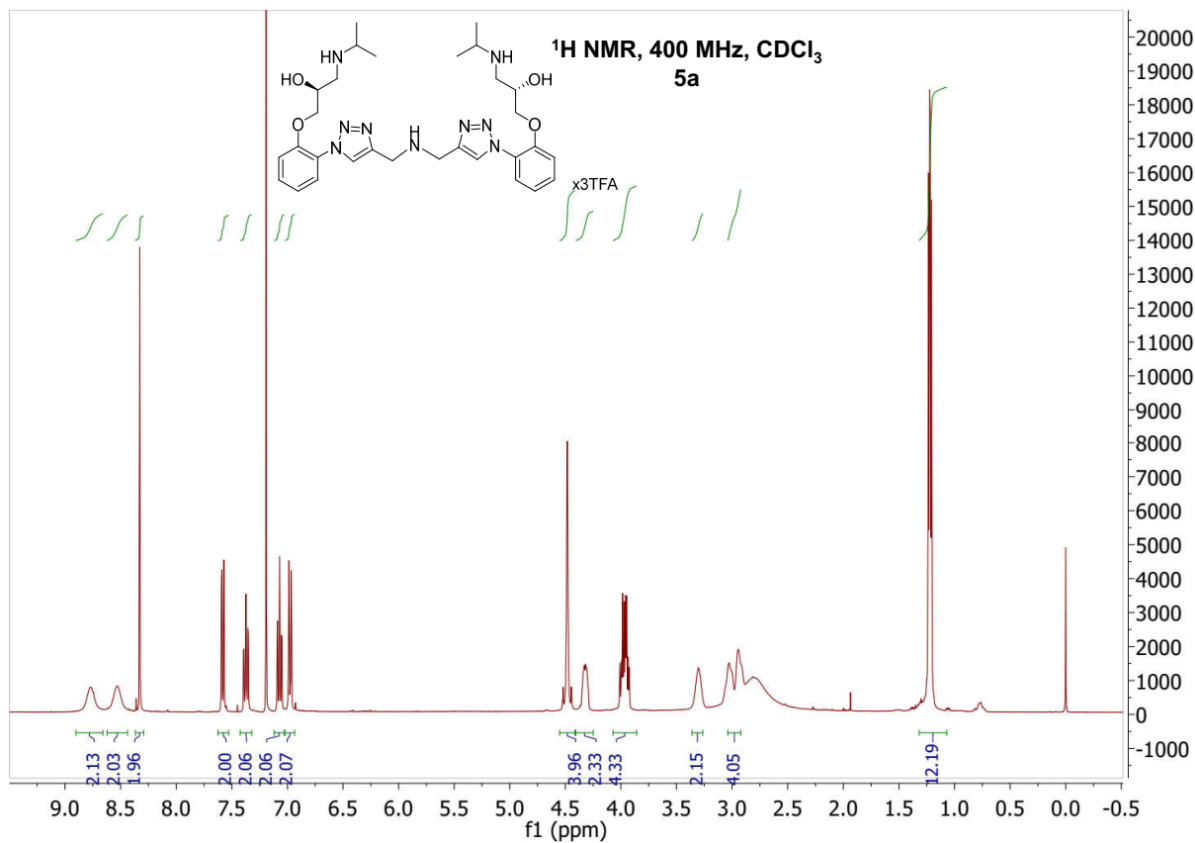


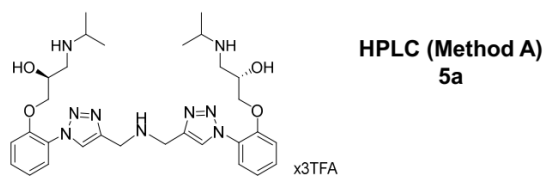
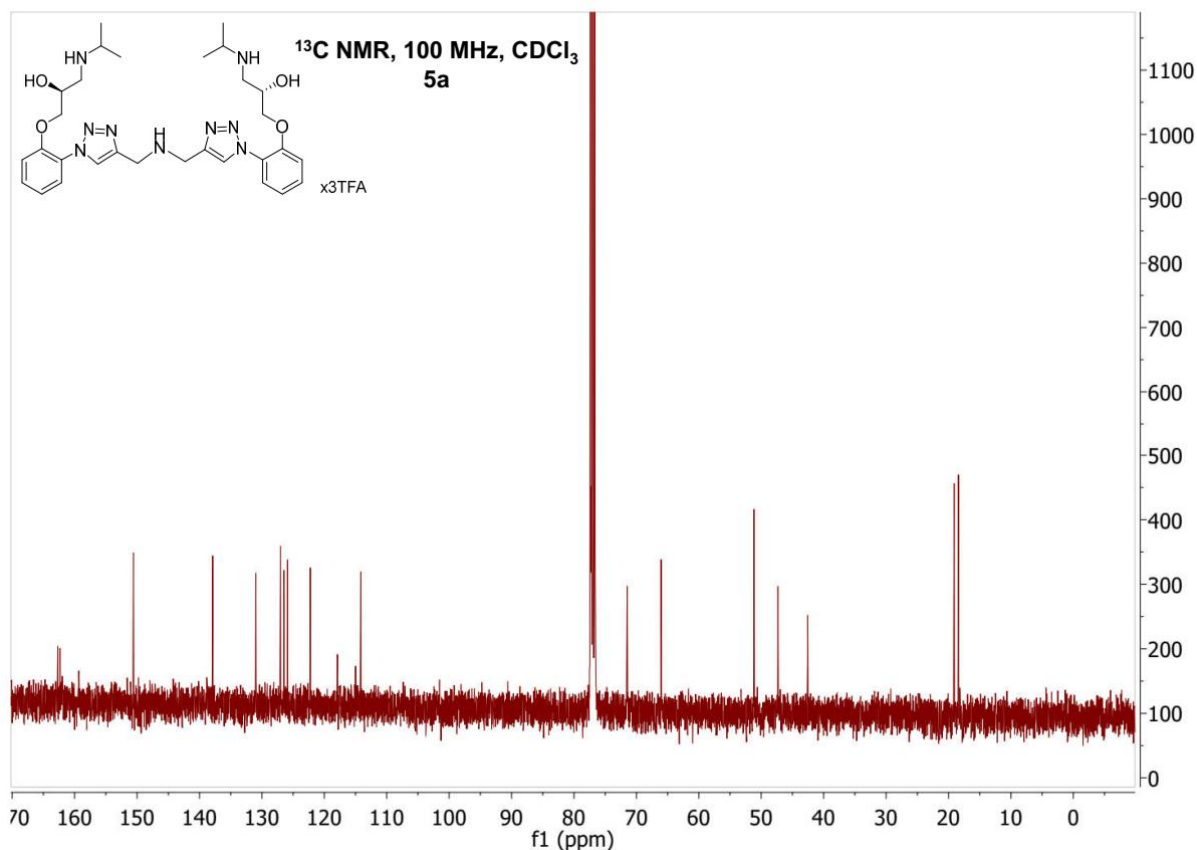
No.	Ret.Time min	Peak Name	Height mAU	Area mAU*min	Rel.Area %	Amount	Resolution(EP)
1	7,41	n.a.	310,700	12,217	100,00	n.a.	n.a.
Total:			310,700	12,217	100,00	0,000	





No.	Ret.Time min	Peak Name	Height mAU	Area mAU*min	Rel.Area %	Amount	Resolution(EP)
1	7,47	n.a.	565,798	23,633	100,00	n.a.	n.a.
Total:			565,798	23,633	100,00	0,000	

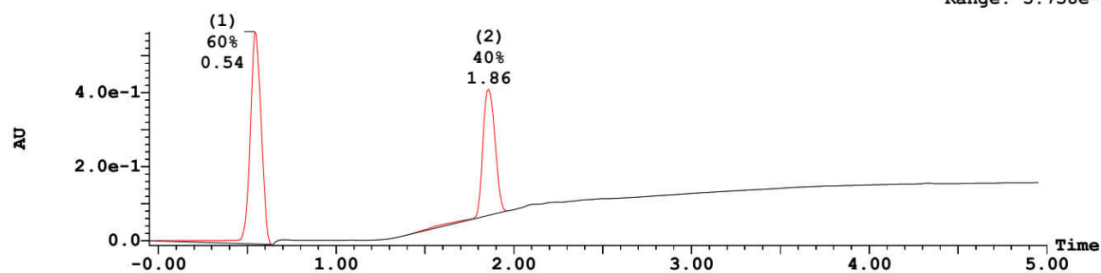




Sample 4 Vial 2:7 ID MCR_BG_151006_MF080T6prep File MCR_BG_151006_MF080T6prep Date 06-Oct-2015 Time 17:23:03 Descrip

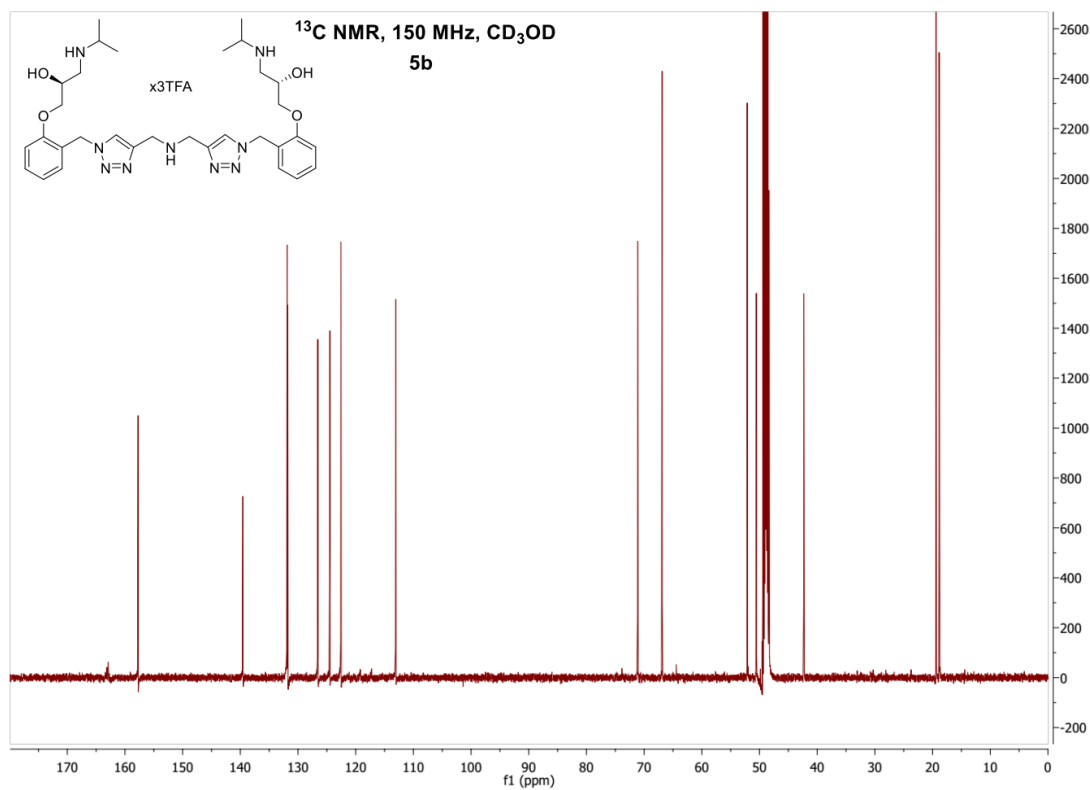
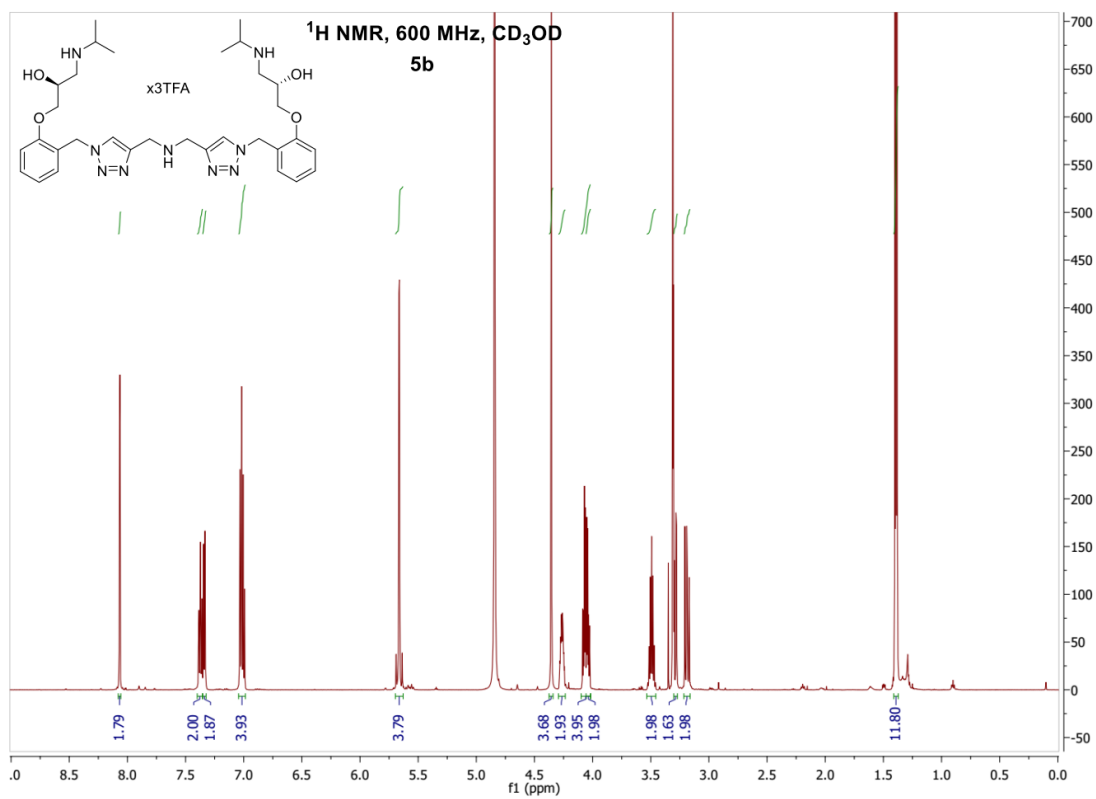
2: UV Detector: TAC :Wavelength Range: (215 - 254)

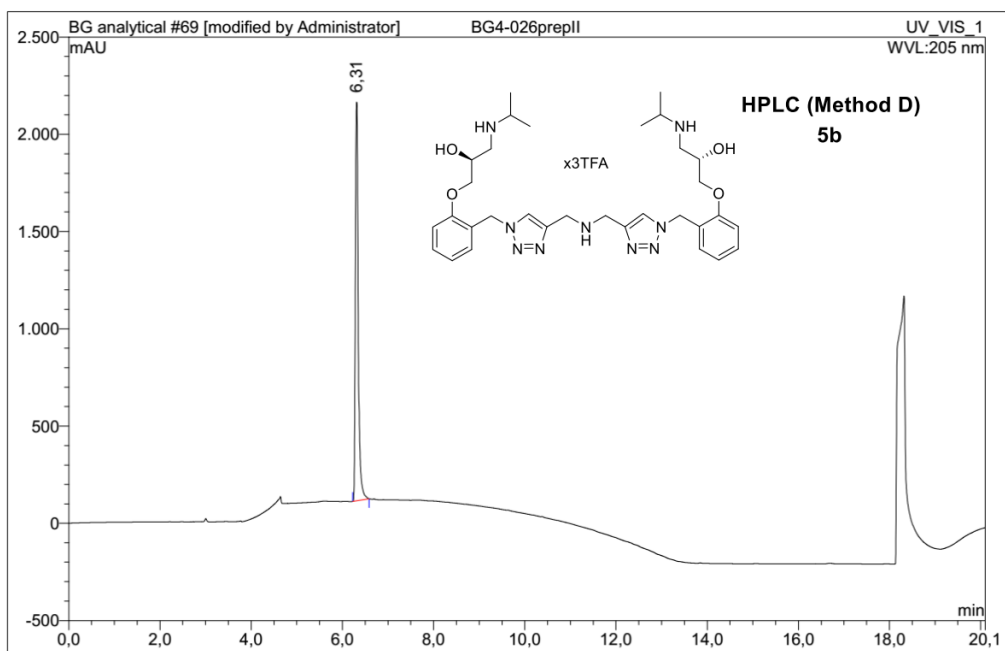
5.642e-1
Range: 5.758e-1



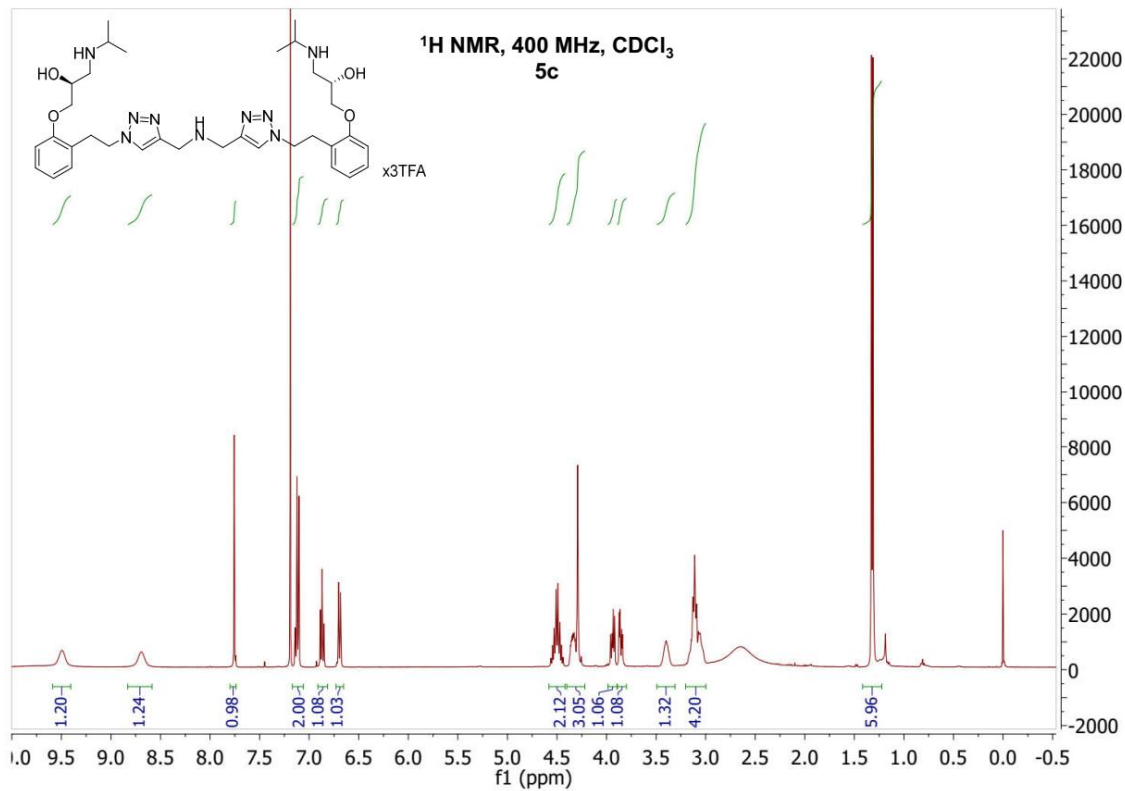
Peak Number	Compound	Time	AreaAbs	Area %Total	Width	Height	Mass Found
1		0.54	4e+004	60.23	1	6e+005	Not Found
2		1.86	3e+004	39.77	1	3e+005	Not Found

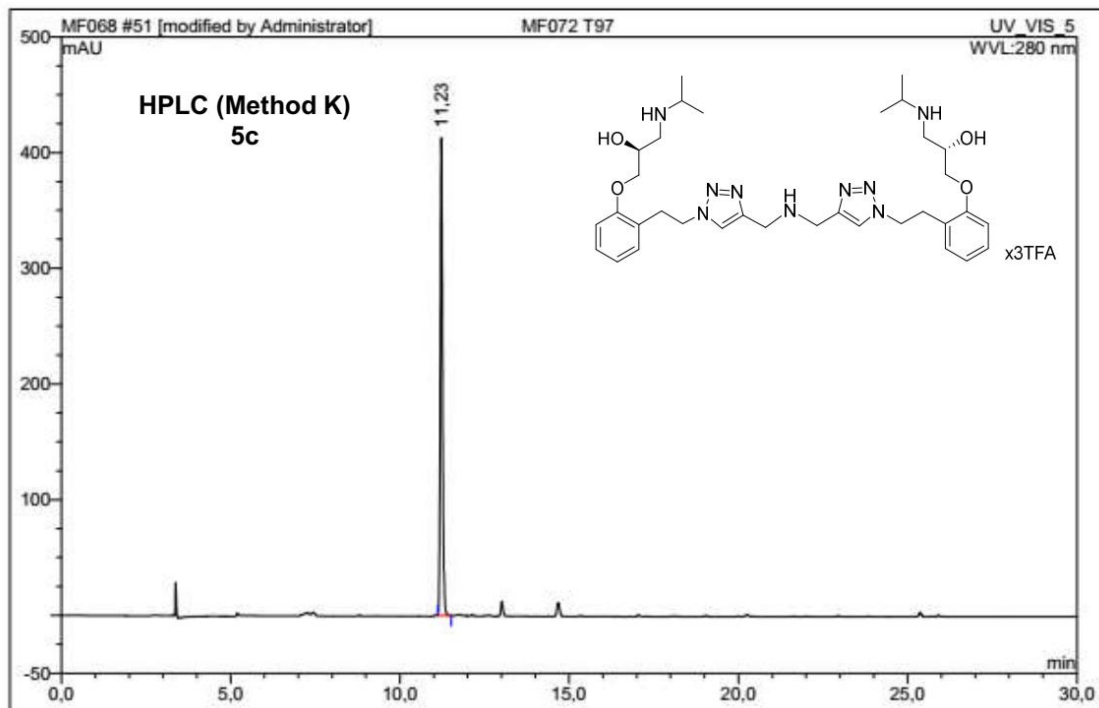
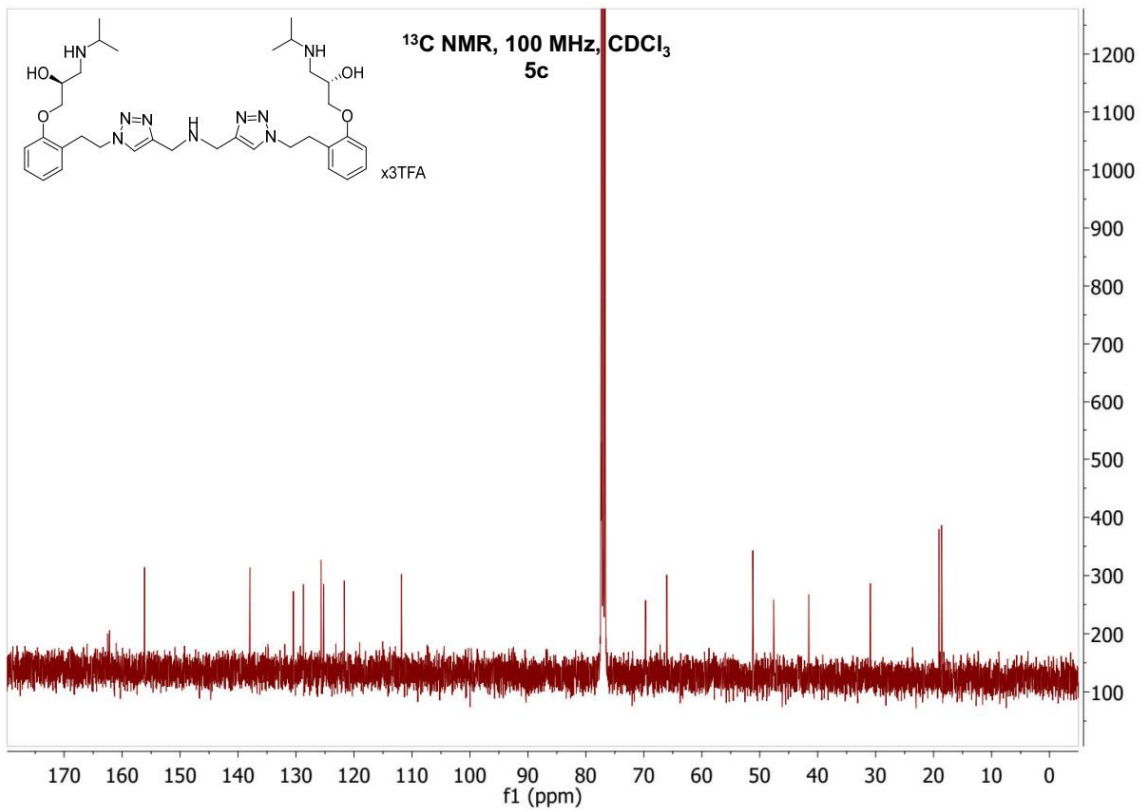
The peak at 0.54 min is caused by negligible amounts of the highly UV active sodium ascorbate.



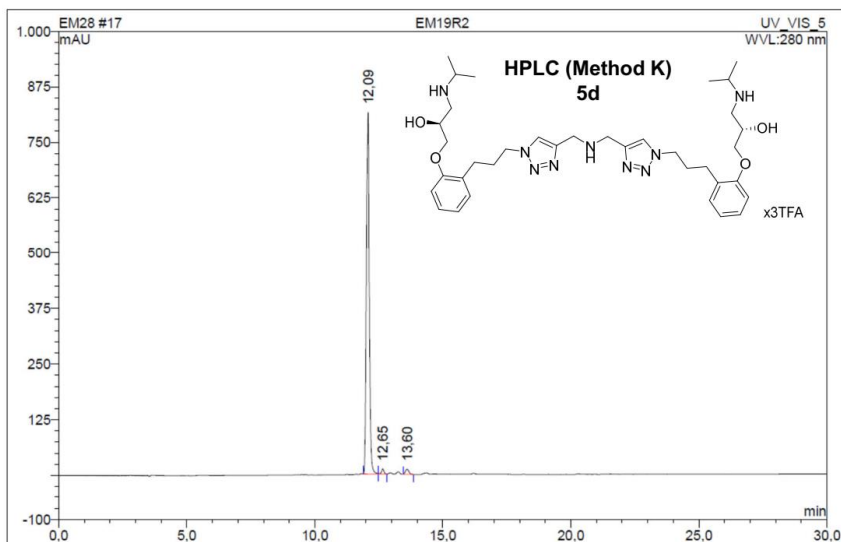


No.	Ret.Time min	Peak Name	Height mAU	Area mAU*min	Rel.Area %	Amount	Resolution(EP)
1	6,31	n.a.	2049,371	152,536	100,00	n.a.	n.a.
Total:			2049,371	152,536	100,00	0,000	



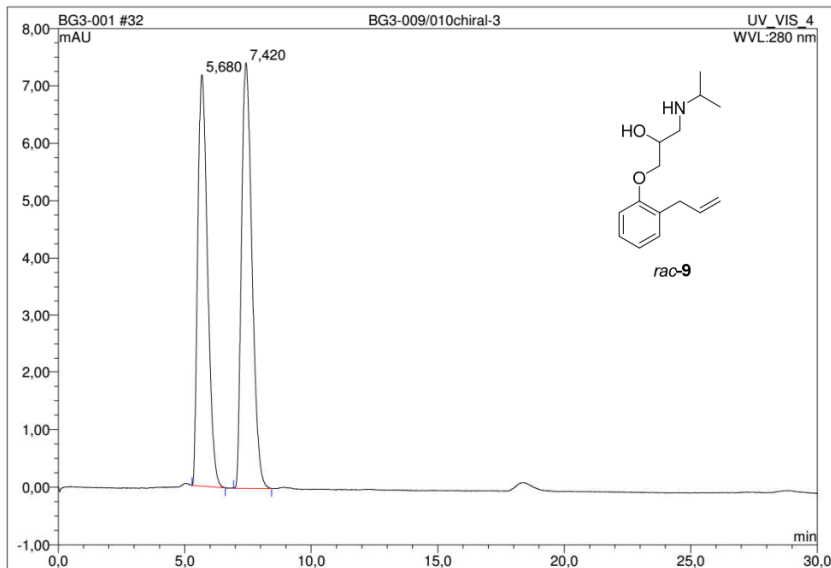


No.	Ret.Time min	Peak Name	Height mAU	Area mAU*min	Rel.Area %	Amount	Resolution(EP)
1	11,23	n.a.	412,750	31,797	100,00	n.a.	n.a.
Total:			412,750	31,797	100,00	0,000	

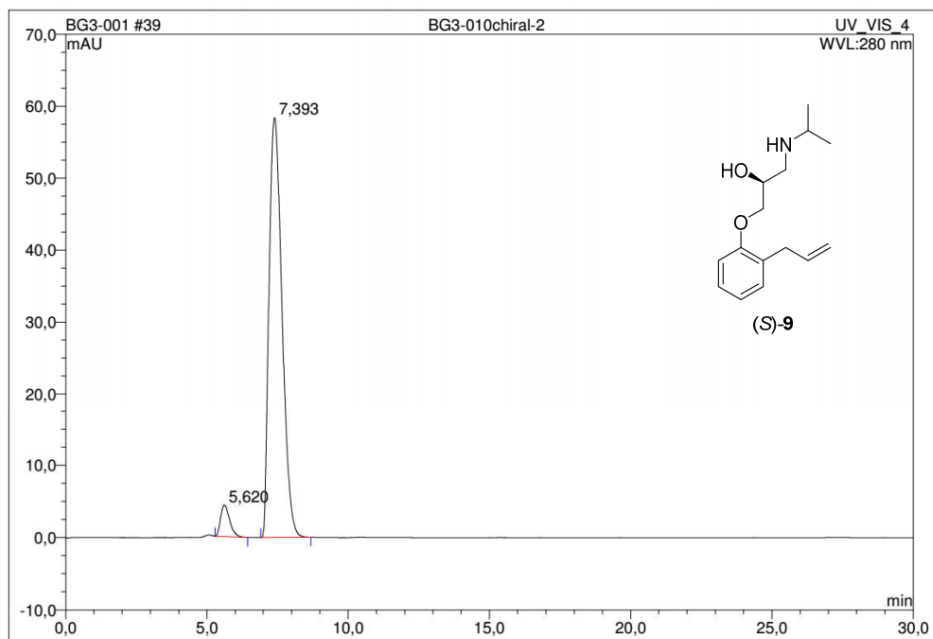


No.	Ret.Time min	Peak Name	Height mAU	Area mAU*min	Rel.Area %	Amount	Resolution(EP)
1	12,09	n.a.	814,120	107,241	97,16	n.a.	3,07
2	12,65	n.a.	12,121	1,375	1,25	n.a.	4,59
3	13,60	n.a.	11,269	1,757	1,59	n.a.	n.a.
Total:			837,510	110,372	100,00	0,000	

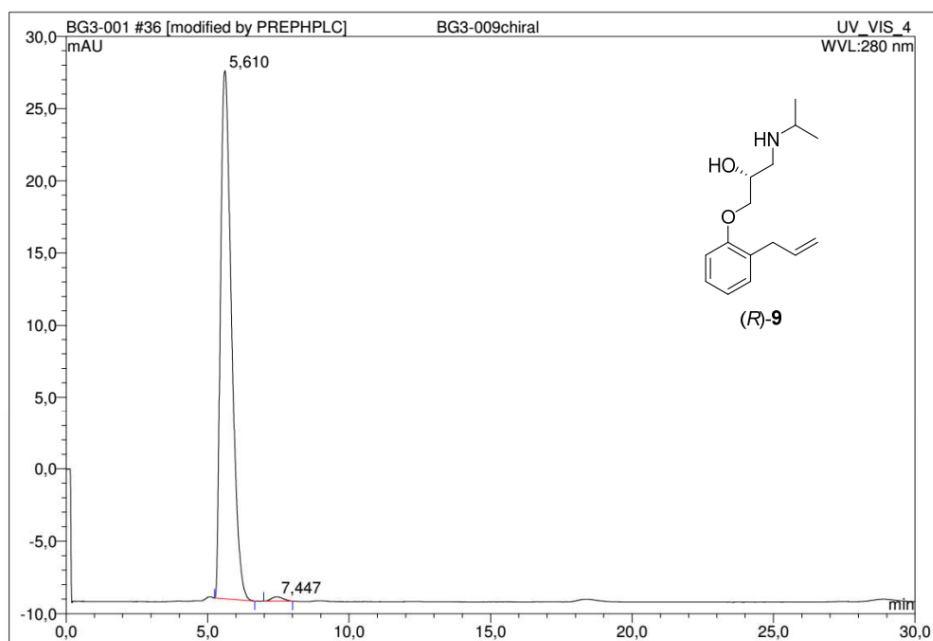
Chiral HPLC chromatograms of *rac*-**9**, (*S*)-**9** and (*R*)-**9** showing that the stereochemical information has been retained during construction of the propanolamine motif.



No.	Ret.Time min	Peak Name	Height mAU	Area mAU*min	Rel.Area %	Amount	Type
1	5,68	n.a.	7,176	3,220	47,42	n.a.	BMB
2	7,42	n.a.	7,425	3,571	52,58	n.a.	BMB
Total:			14,601	6,791	100,00	0,000	



No.	Ret.Time min	Peak Name	Height mAU	Area mAU*min	Rel.Area %	Amount	Type
1	5,62	n.a.	4,365	1,634	5,02	n.a.	BMB
2	7,39	n.a.	58,404	30,929	94,98	n.a.	BMB
Total:			62,769	32,563	100,00	0,000	



No.	Ret.Time min	Peak Name	Height mAU	Area mAU*min	Rel.Area %	Amount	Type
1	5,61	n.a.	36,609	16,441	99,14	n.a.	BMB
2	7,45	n.a.	0,296	0,143	0,86	n.a.	BMB*
Total:			36,906	16,583	100,00	0,000	

4 REFERENCES

- (1) Wacker, D.; Fenalti, G.; Brown, M. A.; Katritch, V.; Abagyan, R.; Cherezov, V.; Stevens, R. C. Conserved Binding Mode of Human β_2 Adrenergic Receptor Inverse Agonists and Antagonist Revealed by X-Ray Crystallography. *J. Am. Chem. Soc.* **2010**, *132* (33), 11443–11445.
- (2) Schrödinger Release 2015-1. Schrödinger Suite 2015-1 Protein Preparation Wizard; Epik, Schrödinger, LLC, New York, NY, 2015 2015.
- (3) Schrödinger Release 2015-1. Glide, Schrödinger, LLC, New York, NY, 2015.
- (4) Sejer Pedersen, D.; Rosenbohm, C. Dry Column Vacuum Chromatography. *Synthesis* **2001**, *16*, 2431–2434.
- (5) Gottlieb, H. E.; Kotlyar, V.; Nudelman, A. NMR Chemical Shifts of Common Laboratory Solvents as Trace Impurities. *J. Org. Chem.* **1997**, *62* (21), 7512–7515.
- (6) Marquis, R. W.; Lago, A. M.; Callahan, J. F.; Trout, R. E.; Gowen, M.; DelMar, E. G.; Van Wagenen, B. C.; Logan, S.; Shimizu, S.; Fox, J.; Nemeth, E. F.; Yang, Z.; Roethke, T.; Smith, B. R.; Ward, K. W.; Lee, J.; Keenan, R. M.; Bhatnagar, P. Antagonists of the Calcium Receptor I. Amino Alcohol-Based Parathyroid Hormone Secretagogues. *J. Med. Chem.* **2009**, *52* (13), 3982–3993.
- (7) Beckmann, H. S. G.; Nie, F.; Hagerman, C. E.; Johansson, H.; Tan, Y. S.; Wilcke, D.; Spring, D. R. A Strategy for the Diversity-Oriented Synthesis of Macrocyclic Scaffolds Using Multidimensional Coupling. *Nat. Chem.* **2013**, *5* (10), 861–867.
- (8) Rostovtsev, V. V.; Green, L. G.; Fokin, V. V.; Sharpless, K. B. A Stepwise Huisgen Cycloaddition Process: Copper(I)-Catalyzed Regioselective “Ligation” of Azides and Terminal Alkynes. *Angew. Chem. Int. Ed.* **2002**, *41* (14), 2596–2599.
- (9) Pohnert, G.; Boland, W. Highly Efficient One-Pot Double-Wittig Approach to Unsymmetrical (1Z, 4Z, 7Z)-Homoconjugated Trienes. *Eur. J. Org. Chem.* **2000**, *2000* (9), 1821–1826.
- (10) Lukin, K.; Kishore, V.; Gordon, T. Development of a Scalable Synthesis of Oxadiazole Based S1P1 Receptor Agonists. *Org. Process Res. Dev.* **2013**, *17* (4), 666–671.
- (11) Goddard-Borger, E. D.; Stick, R. V. An Efficient, Inexpensive, and Shelf-Stable Diazotransfer Reagent: Imidazole-1-Sulfonyl Azide Hydrochloride. *Org. Lett.* **2007**, *9* (19), 3797–3800.
- (12) Sminia, T. J.; Pedersen, D. S. Azide- and Alkyne-Functionalised α - and β -Amino Acids. *SYNLETT* **2012**, *23*, 2643–2646.
- (13) Johansson, H.; Sejer Pedersen, D. Azide- and Alkyne-Derivatised α -Amino Acids. *Eur. J. Org. Chem.* **2012**, *2012* (23), 4267–4281.
- (14) Klunder, J. M.; Onami, T.; Sharpless, K. B. Arenesulfonate Derivatives of Homochiral Glycidol: Versatile Chiral Building Blocks for Organic Synthesis. *J. Org. Chem.* **1989**, *54* (6), 1295–1304.
- (15) Baker, J. G.; Adams, L. A.; Salchow, K.; Mistry, S. N.; Middleton, R. J.; Hill, S. J.; Kellam, B. Synthesis and Characterization of High-Affinity 4,4-Difluoro-4-Bora-

- 3a,4a-Diaza-S-Indacene-Labeled Fluorescent Ligands for Human β -Adrenoceptors. *J. Med. Chem.* **2011**, *54* (19), 6874–6887.
- (16) Hojo, M.; Murakami, Y.; Aihara, H.; Sakuragi, R.; Baba, Y.; Hosomi, A. Iron-Catalyzed Regio- and Stereoselective Carbolithiation of Alkynes. *Angew. Chemie - Int. Ed.* **2001**, *113* (3), 641–643.
- (17) Ghiaci, M.; Sedaghat, M. E.; Kalbasi, R. J.; Abbaspur, A. Applications of Surfactant-Modified Clays to Synthetic Organic Chemistry. *Tetrahedron* **2005**, *61* (23), 5529–5534.
- (18) Heydenreuter, W.; Kunold, E.; Sieber, S. A. Alkynol Natural Products Target ALDH2 in Cancer Cells by Irreversible Binding to the Active Site. *Chem. Commun.* **2015**, *51* (87), 15784–15787.
- (19) He, Y.-T.; Yang, H.-N.; Yao, Z.-J. Sharpless AD Strategy towards the γ -Methyl Butenolide Unit of Acetogenins: Enantioselective Synthesis of Butenolide I and II with Mosquito Larvicidal Activity. *Tetrahedron* **2002**, *58*, 8805–8810.
- (20) Long, T. M.; Simmons, B. A.; McElhanon, J. R.; Kline, S. R.; Wheeler, D. R.; Loy, D. A.; Rahimian, K.; Zifer, T.; Jamison, G. M. Metathesis Depolymerization for Removable Surfactant Templates. *Langmuir* **2005**, *21* (20), 9365–9373.
- (21) Calcagno, P.; Kariuki, B. M.; Kitchin, S. J.; Robinson, J. M. A.; Philp, D.; Harris, K. D. M. Understanding the Structural Properties of a Homologous Series of Bis-Diphenylphosphine Oxides. *Chem. Eur. J.* **2000**, *6* (13), 2338–2349.
- (22) Ross, M. F.; Ros, T. D. A.; Blaikie, F. H.; Prime, T. A.; Porteous, C. M.; Severina, I. I.; Skulachev, V. P.; Kjaergaard, H. G.; Smith, R. A. J.; Murphy, M. P. Accumulation of Lipophilic Dications by Mitochondria and Cells. *Biochem. J.* **2006**, *400*, 199–208.
- (23) Youssefyeh, R. D.; Campbell, H. F.; Klein, S.; Airey, J. E.; Darkes, P.; Powers, M.; Schnapper, M.; Neuenschwander, K.; Fitzpatrick, L. R.; Pendley, C. E.; Martin, G. E. Development of High-Affinity 5-HT₃ Receptor Antagonists. 1. Initial Structure-Activity Relationship of Novel Benzamides. *J. Med. Chem.* **1992**, *35* (5), 895–903.
- (24) Bistrzycki, von A.; Schmutz, W. Einwirkung von Ortho- Und Peri-Diaminen Sowie von Äthylendiamin Auf γ -Lactone. *Justus Liebigs Ann. Chem.* **1917**, *415* (1), 1–28.
- (25) Ren, L.; Jiao, N. PdCl₂ Catalyzed Efficient Assembly of Organic Azides, CO, and Alcohols under Mild Conditions: A Direct Approach to Synthesize Carbamates. *Chem. Commun.* **2014**, *50* (28), 3706–3709.
- (26) Woods, M.; Sherry, A. D. Synthesis and Luminescence Studies of Aryl Substituted Tetraamide Complexes of Europium(III): A New Approach to pH Responsive Luminescent Europium Probes. *Inorg. Chem.* **2003**, *42* (14), 4401–4408.
- (27) Schwartz, M. A.; Zoda, M.; Vishnuvajjala, B.; Mami, I. A Convenient Synthesis of O- and P-Hydroxy Substituted Phenylacetone nitriles and Phenethylamines. *J. Org. Chem.* **1976**, *41* (14), 2502–2503.
- (28) Gogoi, P.; Bezboruah, P.; Gogoi, J.; Boruah, R. C. Ipso-Hydroxylation of Arylboronic Acids and Boronate Esters by Using Sodium Chlorite as an Oxidant in Water. *Eur. J. Org. Chem.* **2013**, *2013* (32), 7291–7294.
- (29) Hellal, M.; Singh, S.; Cuny, G. D. Monoligated Pd(0)-Catalyzed Intramolecular Ortho-

- and Para-Arylation of Phenols for the Synthesis of Aporphine Alkaloids. Synthesis of (-)-Lirinine. *Tetrahedron* **2012**, *68* (6), 1674–1681.
- (30) Veitch, G. E.; Bridgwood, K. L.; Ley, S. V. Magnesium Nitride as a Convenient Source of Ammonia: Preparation of Primary Amides. *Org. Lett.* **2008**, *10* (16), 3623–3625.
- (31) Gerpe, A.; Bollini, M.; González, M.; Cerecetto, H. Convenient Route to Primary (Z)-Allyl Amines and Homologs. *Synth. Commun.* **2009**, *39* (1), 29–47.
- (32) Awuah, E.; Ma, E.; Hoegl, A.; Vong, K.; Habib, E.; Auclair, K. Exploring Structural Motifs Necessary for Substrate Binding in the Active Site of Escherichia Coli Pantothenate Kinase. *Bioorg. Med. Chem.* **2014**, *22* (12), 3083–3090.
- (33) Vedel, L.; Bräuner-Osborne, H.; Mathiesen, J. M. A cAMP Biosensor-Based High-Throughput Screening Assay for Identification of Gs-Coupled GPCR Ligands and Phosphodiesterase Inhibitors. *J. Biomol. Screen.* **2015**, *20* (7), 849–857.
- (34) Mathiesen, J. M.; Vedel, L.; Bräuner-Osborne, H. cAMP Biosensors Applied in Molecular Pharmacological Studies of G Protein-Coupled Receptors. In *Methods in Enzymology*; 2013; Vol. 522, pp 191–207.
- (35) Motulsky, H. J.; Mahan, L. C. The Kinetics of Competitive Radioligand Binding Predicted by the Law of Mass Action. *Mol. Pharmacol.* **1984**, *25* (1), 1–9.
- (36) Contreras, M. L.; Wolfe, B. B.; Molinoff, P. B. Kinetic Analysis of the Interactions of Agonists and Antagonists with Beta Adrenergic Receptors. *J. Pharmacol. Exp. Ther.* **1986**, *239* (1), 136–143.
- (37) Sykes, D. A.; Parry, C.; Reilly, J.; Wright, P.; Fairhurst, R. A.; Charlton, S. J. Observed Drug-Receptor Association Rates Are Governed by Membrane Affinity: The Importance of Establishing “Micro-Pharmacokinetic/Pharmacodynamic Relationships” at the β 2-Adrenoceptor. *Mol. Pharmacol.* **2014**, *85* (4), 608–617.
- (38) Zawilska, J. B.; Zalewska-Kaszubska, J.; Marczak, G.; Górska, D.; Woldan-Tambor, A. Characterization of β -Adrenergic Receptors in Duck Cerebral Cortex. *Acta Neurobiol. Exp.* **2000**, *60*, 301–307.
- (39) Cheng, Y.-C.; Prusoff, W. H. Relationship between the Inhibition Constant (K_i) and the Concentration of Inhibitor Which Causes 50 per Cent Inhibition (I_{50}) of an Enzymatic Reaction. *Biochem. Pharmacol.* **1973**, *22* (23), 3099–3108.